

**GRAPH QUILTING:
GRAPHICAL MODEL SELECTION FROM
PARTIALLY OBSERVED COVARIANCES**

BY GIUSEPPE VINCI*, GAUTAM DASARATHY[†] AND GENEVERA I. ALLEN*

*Rice University**, *Arizona State University[†]*

We investigate the problem of conditional dependence graph estimation when several pairs of nodes have no joint observation. For these pairs even the simplest metric of covariability, the sample covariance, is unavailable. This problem arises, for instance, in calcium imaging recordings where the activities of a large population of neurons are typically observed by recording from smaller subsets of cells at once, and several pairs of cells are never recorded simultaneously. With no additional assumption, the unavailability of parts of the covariance matrix translates into the unidentifiability of the precision matrix that, in the Gaussian graphical model setting, specifies the graph. Recovering a conditional dependence graph in such settings is fundamentally an extremely hard challenge, because it requires to infer conditional dependences between network nodes with no empirical evidence of their covariability. We call this challenge the “graph quilting problem”. We demonstrate that, under mild conditions, it is possible to correctly identify not only the edges connecting the observed pairs of nodes, but also a superset of those connecting the variables that are never observed jointly. We propose an ℓ_1 regularized graph estimator based on a partially observed sample covariance matrix and establish its rates of convergence in high-dimensions. We finally present a simulation study and the analysis of calcium imaging data of ten thousand neurons in mouse visual cortex.

1. Introduction. Let $X = (X_1, \dots, X_p)^T$ be a p -dimensional random vector following a multivariate Gaussian distribution $N(\mu, \Sigma)$, where μ is the mean vector and $\Theta = \Sigma^{-1}$ is the $p \times p$ positive definite precision matrix. The nonzero entries of Θ identify conditional dependences, which can be depicted by an undirected graph $G = (V, E)$ where the vertices or nodes $V = \{1, \dots, p\}$ represent the p variables in X , and an edge in E connects two vertices (i, j) if and only if $\Theta_{ij} \neq 0$. Given n i.i.d. data samples $X^{(1)}, \dots, X^{(n)}$ of X , the precision matrix Θ , and thereby the conditional dependence graph G , are typically estimated via penalized maximum likelihood estimation, such as ℓ_1 -regularization (Yuan and Lin, 2007), which requires the sample covariance matrix $\hat{\Sigma}$ computed from $X^{(1)}, \dots, X^{(n)}$. Gaussian graphical

MSC 2010 subject classifications: Primary 60K35, 60K35; secondary 60K35

Keywords and phrases: calcium imaging, Gaussian graphical model, high-dimensionality, matrix completion, optimization, regularization, sparsity, sparsistency.

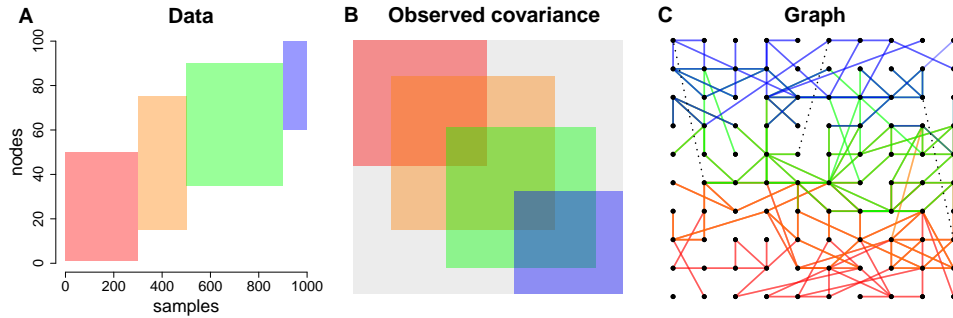


FIG 1. (A) Four different subsets of nodes are observed across a total of 1000 samples. (B) Observed empirical covariance. Grey entries have zero sample size. (C) Graph with edges colored in correspondence to the observed pairs of nodes. Dotted edges connect pairs of nodes that are never observed jointly.

models have been extensively used to infer neuronal functional connectivity (Yatsenko et al., 2015; Vinci et al., 2018a,b), gene expression networks (Allen and Liu, 2013; Dobra et al., 2004; Gallopin et al., 2013; Hartemink et al., 2000; Krämer et al., 2009), and metabolic networks (Krumsiek et al., 2011), and their theoretical properties have been largely studied in high-dimensions (Yuan, 2010; Ravikumar et al., 2011; Liu et al., 2012), where the sample size n can be small relatively to the number of nodes p .

1.1. *The graph quilting problem.* Suppose now that the vectors $X^{(1)}, \dots, X^{(n)}$ are not fully observed in a way that several pairs of the p variables are never observed jointly across the n samples. For instance, Figure 1 illustrates the case where four different subsets $V_1, V_2, V_3, V_4 \subset V$ of $p = 100$ nodes are observed across a total of $n = 1000$ data points but, although $\cup_k V_k = V$, many pairs of nodes are never observed jointly. Indeed, we only observe pairs in the set $O = \cup_k V_k \times V_k \subset V \times V$. These circumstances generate a fundamental problem: the sample covariances for the pairs of nodes in O^c that have no joint observation are infeasible. This situation brings us to pose several questions: Can we recover the precision matrix Θ from an incomplete covariance matrix? Can we estimate the precision matrix from an incomplete set of empirical covariances? It is certainly possible to recover or estimate a graph for any subset of the p nodes for which all pairs have been observed jointly, but such graph would represent the dependence structure of those nodes unconditionally on the others. Recovering the full conditional dependence graph of all p nodes in such settings is fundamentally extremely hard, because it requires to infer dependences between network nodes with no empirical evidence of their covariability. We call the challenging situation of recovering the precision matrix

and the graph from partially observed covariances the “graph quilting problem”. The name of this problem is evocative of the implicit task of recovering or estimating the graph by “quilting” together multiple graphical structures relative to the observed subsets of nodes.

1.2. *Graph quilting in applied contexts.* The graph quilting problem is not only a theoretical conundrum. It may arise in several applied contexts.

Neuroscience. Functional connectivity is the statistical dependence structure of neurons’ activities. Estimating functional connectivity from *in vivo* neuronal recordings helps us understand how neurons interact with one another while they process information under different stimuli and other experimental conditions (Vinci et al., 2016, 2018a,b; Yatsenko et al., 2015), and ultimately it enables us to understand the functions of neuronal circuits and the causes of their dysfunction characterizing various brain disorders (Baggio and Junqué, 2019; Engels et al., 2018; Cai et al., 2018). With the development of multiple-neuron recording technologies, such as multielectrode arrays (Kelly et al., 2007) and 2-photon calcium imaging (Pnevmatikakis et al., 2016), the study of neuronal dependence has progressed from the simple assessment of marginal pairwise neuronal dependences (Smith and Kohn, 2008; Smith and Sommer, 2013; Goris, Movshon, and Simoncelli, 2014; Vinci et al., 2016) to the more complex task of conditional dependence graph estimation (Vinci et al., 2018a,b; Yatsenko et al., 2015), where the strength of the relationship between two neurons is quantified taking into account the effects of the other neurons and input processes in the network. Gaussian graphical models have been successfully applied to several neuronal data recordings to infer the functional connectivity of hundreds of neurons (Vinci et al., 2018a,b; Yatsenko et al., 2015). However, the fast increase in the number of neurons that can be recorded simultaneously (Ahrens et al., 2015; Alivisatos et al., 2013; Kerr and Denk, 2008; Kipke et al., 2008) has posed new statistical challenges requiring new appropriate methodologies that can recover and explain the covariability structure of large neuronal networks (Shadlen and Newsome, 1998; Brown et al., 2004; Cunningham and Yu, 2014; Stevenson and Kording, 2011; Song et al., 2013; Yatsenko et al., 2015; Cohen and Maunsell, 2009; Cohen and Kohn, 2011; Efron et al., 2001; Kelly and Kass, 2012; Mitchell, Sundberg, and Reynolds, 2009; Vinci et al., 2016, 2018a,b).

New ambitious neuroscience projects involve the *in vivo* recording of the activities of tens-to-hundreds of thousands of neurons in 3-dimensional portions of brain via calcium imaging technology. One of the ultimate goals of these massive experiments is to understand the relationship between the functional connectivity of the full neuronal population and the structure of neuronal anatomical connections. A

fundamental trade-off between temporal and spatial resolution characterizes calcium imaging technologies: the more neurons we aim to record from simultaneously, the coarser the time resolution is. Since important neuronal activity patterns happen on very short time scales, it is often preferred to record the activities of a subset of neurons at once with a fine temporal resolution rather than recording the activities of the entire neuronal population simultaneously with a coarse time resolution (see Figure 6 in Section 6). Yet, on the other hand, if these subsets of the neuronal population are recorded *nonsimultaneously*, only a subset O of all possible pairs of neurons may have joint observations, while the rest (O^c) remain unobserved with no empirical covariance. Hence, the graph quilting problem arises.

Genetics. Since the advent of high-throughput measures of gene expression over twenty years ago, scientists have studied gene co-expression networks leading to discoveries of new genomic pathways, novel important disease genes or “hub” genes, and disrupted gene expression patterns and pathways in disease, among others (Stuart et al., 2003; Heng et al., 2008; Zhang and Horvath, 2005; Wang and Huang, 2014). Many have argued that graphical models based on conditional dependencies are particularly advantageous for modeling gene expression (Friedman, 2004; Dobra et al., 2004; Hartemink et al., 2000), and have applied these to estimate gene expression networks from microarrays (Friedman, 2004; Dobra et al., 2004; Krämer et al., 2009) and RNA-sequencing (RNAseq) (Allen and Liu, 2013; Gallopín et al., 2013).

However, there is much recent excitement about a fairly new genomic technology, single cell RNA-sequencing (scRNAseq), which can measure gene expression levels of each individual cell (Macosko et al., 2015; Klein et al., 2015). This technology along with the successes of studying gene expression networks prompts the scientific question: How do gene expression networks change across cell types? Answering this question would allow scientists to study the specific genomic changes that lead to cell-specific functions (e.g. individual immune cell functions) or dysfunctions associated with disease (e.g. changes that have developed in tumor cells) (Gerlinger et al., 2012). But, this scientific problem poses several major statistical challenges. Data quality of scRNAseq is much poorer than that of bulk RNAseq. This is in large part due to “dropouts”, a technical artifact where genes appear to have zero expression because scRNAseq technology can only capture a small fraction of the transcriptome of each cell, thus missing many genes which are indeed expressed (Gawad et al., 2016; Li and Li, 2018). Data from scRNAseq is highly sparse with “zeros” in the data either occurring for biological reasons (no expression) or due to technical artifacts (missing values = dropouts). Many have attempted to retrieve gene expression networks from scRNAseq by first

(i) aggressively filtering the genes down to those that are largely non-missing and by (ii) imputing the remaining missing values, for which many techniques have been developed (Li and Li, 2018; Gong et al., 2018; Zhang and Zhang, 2018). After these two preprocessing steps, several have gone on to estimate gene expression networks (van Dijk et al., 2017; Stegle et al., 2015). But, these preprocessing steps may create major biases in downstream analysis. First, restricting the analysis to genes largely non-missing leads to a limited set of genes to study in the network and also induces false positives in the estimated graph structure because other genes in the system are removed and not conditioned on (Chandrasekaran et al., 2012). Second, many have noted challenges with existing imputation methods for scRNAseq (Kiselev et al., 2019) that are likely to be exacerbated and cause errors in graph estimation, as they are designed to impute the data and not directly for the task of graph estimation. Thus, the inference of gene expression networks from scRNAseq data is still an unsolved problem falling within the graph quilting problem.

Other fields. The graph quilting problem may also arise in the analysis of *medical records*, since different physiological characteristics may be recorded across patients, although it would be of interest to study the dependence structure of all medical variables ever surveyed across patients. In *proteomics*, we aim at finding relationships among proteomes, which differ from cell to cell and from time to time, as distinct genes are expressed in different cell types. In *finance*, it is of interest to study the dependence structure of the several financial risks that companies may face, although companies are exposed to different sets of risks.

1.3. *Related literature.* The graph quilting problem is fundamentally different from a typical missing-data problem (Candès and Recht, 2009; Candès and Plan, 2010; Loh and Wainwright, 2012; Kolar and Xing, 2012; Städler and Bühlmann, 2012; Soudry et al., 2015), where missingness is usually assumed to be at random in such a way that all pairs of variables are observed jointly at least once or twice with high-probability – in Figure 1 we would have $O^c = \emptyset$ with high-probability, whereas in our case $O^c \neq \emptyset$. The problem we deal with is instead strictly related to covariance matrix completion, for which several approaches exist: positive definite matrix completions (Dempster, 1972; Grone et al., 1984; Bakonyi and Woerdeman, 1995; Vandenberghe et al., 1998; Laurent, 2009), methods that assume the covariance matrix to be low-rank (Pfau et al., 2013; Bishop and Yu, 2014), and statistical models for neural data (Wohrer et al., 2010; Turaga et al., 2013). Yet, most of the existing literature does not deal with the quality of retrieval of a conditional dependence graph, which, in the Gaussian framework, is given by the nonzero structure of the inverse covariance matrix – covariance matrix completion does not guarantee

the accurate recovery of the graphical structure of the inverse covariance matrix.

The graph quilting problem is therefore an unsolved, largely unexplored problem, especially in the finite sample case, where a partially observed empirical covariance matrix is to be used and it is not even guaranteed to enjoy the algebraic properties required by matrix completion methods. The problem is undoubtedly substantially magnified in high-dimensions, where the sample size n can be small relatively to the number of nodes p .

1.4. *Main contributions.* We now outline our main contributions.

Characterization of the graph quilting problem. We define the graph quilting problem as the problem of retrieving Θ and G given the partially observed covariance matrix $\Sigma_O = \{\Sigma_{ij} : (i, j) \in O\}$, or the estimation of Θ and G from an incomplete set of empirical covariances $\widehat{\Sigma}_O$. As we show in Section 2, with no additional assumptions, the answers to these problems are strikingly disheartening: the precision matrix Θ and the conditional dependence graph G are impossible to be uniquely recovered from Σ_O alone. This is because no one-to-one mapping may be established between Σ_O and Θ – not even between Σ_O and Θ_O – and this problem is inherited at the estimation level where Σ_O is replaced by an empirical estimate $\widehat{\Sigma}_O$. However, in Section 3 we show that the assumption $\Theta_{O^c} = 0$ lets us obtain $\tilde{\Theta}$, an approximation of Θ given Σ_O that can be very close to Θ . For instance if $\|\Theta_{O^c}\|_\infty$ is relatively small, that is the edges in O^c are relatively weak, then the distortion $\Theta - \tilde{\Theta}$ can also be very small, and some thresholding strategies may be implemented to eliminate just the spurious edges produced in $\tilde{\Theta}$. If $\Theta_{O^c} = 0$ truly, then $\tilde{\Theta} = \Theta$. We call the approximation $\tilde{\Theta}$ **MAD_{GQ}** because of its relationship with the maximum determinant problem (Dempster, 1972). By exploiting the distortions identified in $\tilde{\Theta}_O$, it is also possible to construct a minimal superset \mathcal{S} of the edges in O^c via a novel algorithm, the Recursive Complement (RECO), which we propose in this paper.

Graph recovery in high-dimensions. To recover Θ and G given an incomplete empirical covariance matrix $\widehat{\Sigma}_O$, in Section 4 we propose the **MAD_{GQlasso}**, an ℓ_1 regularized estimator given by

$$\widehat{\Theta} = \underset{\Theta > 0, \Theta_{O^c} = 0}{\operatorname{argmax}} \log \det \Theta - \sum_{(i,j) \in O} \Theta_{ij} \widehat{\Sigma}_{ij} - \|\Lambda \circ \Theta\|_{1,\text{off}},$$

where Λ is a matrix of nonnegative penalties, and the constraint $\Theta_{O^c} = 0$ rules out the dependence of the likelihood function on the unobserved empirical covariances $\widehat{\Sigma}_{O^c}$. We prove the following main results:

MAIN RESULT 1 - GRAPH RECOVERY IN O . Under appropriate conditions, there exists a threshold τ such that the graph estimate $\widehat{E} = \{(i, j) : |\widehat{\Theta}_{ij}| > \tau\}$ satisfies

$$\widehat{E}_O = E_O := \{(i, j) \in O : \Theta_{ij} \neq 0\}$$

with high probability.

MAIN RESULT 2 - GRAPH RECOVERY IN O^c . Under appropriate conditions, we can obtain a set-valued function $\widehat{\mathcal{F}}$ of $\widehat{\Theta}$ such that, for a sufficiently large sample size,

$$\widehat{\mathcal{F}} = \mathcal{S} \supseteq E_{O^c} := \{(i, j) \in O^c : \Theta_{ij} \neq 0\}$$

with high probability. Alternatively, under weaker conditions we can obtain another set-valued function $\widehat{\mathcal{U}}$ of $\widehat{\Theta}$ that, for sufficiently large sample size, contains a minimal number of edges in O^c with high probability.

The first result exploits the fact that the estimator $\widehat{\Theta}$ converges in ℓ_∞ norm to the population quantity $\widetilde{\Theta}$, that is the MAD_{GQ} reconstruction of Θ given Σ_O . If $\widetilde{\Theta}$ is sufficiently close to Θ , then $\widehat{\Theta}$ can be appropriately thresholded to perfectly recover the graphical structure of Θ . The proof involves several lemmas exploiting the Fixed Point Theorem, Union bound, Berge's Maximum Theorem, and several results on matrix concentration inequalities. The rate at which $\widehat{\Theta}$ converges to $\widetilde{\Theta}$ is derived in a setting similar to the one used in Ravikumar et al. (2011) for the graphical lasso in the full data case (no missingness). Our second main result also relies on the fact that the estimator $\widehat{\Theta}$ converges to $\widetilde{\Theta}$, but further exploits the Recursive-Complement algorithm for the detection of edges in the set O^c . We illustrate the properties of our graph estimators in simulations (Section 5) and the analysis of calcium imaging data (Section 6).

2. The graph quilting problem. Let $\Theta = \Sigma^{-1}$ be a $p \times p$ positive definite precision matrix whose support induces the graph $G = (V, E)$, where $V = \{1, \dots, p\}$ is the set of vertices representing p random variables X_1, \dots, X_p , and $E = \{(i, j) : \Theta_{ij} \neq 0\}$ is the set of vertex pairs connected by an edge. If $X = (X_1, \dots, X_p)^T \sim N(\mu, \Sigma)$, then the p random variables are said to form a Gaussian graphical model with conditional dependence structure given by G : two variables X_i, X_j are independent conditionally on the other $p - 2$ variables if and only if $\Theta_{ij} = 0$. By uniqueness of the matrix inverse operator, also Σ identifies G – the converse is not true, since E only specifies the support of Θ . Given n data vectors $X^{(1)}, \dots, X^{(n)} \stackrel{i.i.d.}{\sim} N(\mu, \Sigma)$, the

precision matrix Θ may be estimated via maximum likelihood estimation (MLE)

$$(2.1) \quad \hat{\Theta} = \operatorname{argmax}_{\Theta} \log \det \Theta - \sum_{i,j=1}^p \Theta_{ij} \hat{\Sigma}_{ij},$$

where $\hat{\Sigma} = \frac{1}{n} \sum_{r=1}^n (X^{(r)} - \bar{X})(X^{(r)} - \bar{X})^T$ is the sample covariance matrix, and $\bar{X} = \frac{1}{n} \sum_{r=1}^n X^{(r)}$ is the sample mean vector. When $p < n$, the solution to Equation (2.1) is $\hat{\Theta} = \hat{\Sigma}^{-1}$. However, the MLE contains no zero entries almost surely, that is $\hat{\Theta}$ in Equation (2.1) does not readily provide an estimate of G . Moreover, when p is large the MLE performs poorly, and when $p \geq n$, $\hat{\Sigma}$ is singular. To achieve graphical structure and better statistical efficiency, Θ and thereby the graph G are typically estimated via penalized likelihood maximization

$$(2.2) \quad \hat{\Theta} = \operatorname{argmax}_{\Theta > 0} \log \det \Theta - \sum_{i,j=1}^p \Theta_{ij} \hat{\Sigma}_{ij} - \text{PENALTY}(\Theta),$$

where $\Theta > 0$ constrains Θ to be in the cone of $p \times p$ positive definite matrices, and the component $\text{PENALTY}(\Theta)$ is often designed to enforce sparsity in $\hat{\Theta}$. A notable example is the graphical lasso estimator (Yuan and Lin, 2007; Yuan, 2010; Ravikumar et al., 2011), where $\text{PENALTY}(\Theta) = \lambda \|\Theta\|_{1,\text{off}} = \lambda \sum_{i \neq j} |\Theta_{ij}|$, and $\lambda > 0$. In the last decade, the graphical lasso has been applied to very disparate research fields and several extensions have been proposed (Fan et al., 2009; Chandrasekaran et al., 2012; Banerjee and Ghosal, 2015; Vinci et al., 2018a,b; Dobra et al., 2004; Krämer et al., 2009; Krumsiek et al., 2011; Yin and Li, 2011; Yatsenko et al., 2015).

2.1. Partially observed covariances. Maximum likelihood estimation and penalized maximum likelihood estimation (Equations (2.1) and (2.2)) rely on the availability of the empirical covariance matrix $\hat{\Sigma}$. Suppose now that none of the vectors $X^{(1)}, \dots, X^{(n)}$ is fully observed although all p variables are individually observed across some of the n samples. Specifically, suppose we observe multiple datasets $\mathbf{X}_1, \dots, \mathbf{X}_K$, where $\mathbf{X}_k \in \mathbb{R}^{n_k \times |V_k|}$ contains $n_k > 1$ samples of vectors of nodes $V_k \subset V$, implying $|V_k| < p, \forall k$, and with $V_k \neq V_h, \forall k \neq h, \cup_k V_k = V$, and $\sum_{k=1}^K n_k = n$. The set of jointly observed pairs of nodes across the n samples is given by

$$(2.3) \quad O = \bigcup_{k=1}^K V_k \times V_k,$$

where O is a subset of $V \times V$. If $O \subset V \times V$, then several pairs of the p variables – the pairs in $O^c \neq \emptyset$ – are never observed jointly across the n samples. This situation is fundamentally different from a typical missing-data problem (Cand

and Recht, 2009; Candès and Plan, 2010; Loh and Wainwright, 2012; Kolar and Xing, 2012; Städler and Bühlmann, 2012; Soudry et al., 2015), where missingness is usually assumed to be at random and/or in such a way that all pairs of variables are observed jointly at least once or twice with high-probability; that is, such methods assume $O = V \times V$ with high probability. As discussed in Section 1.2, the case $O^c \neq \emptyset$ is likely to happen in many applied contexts due to technology limitations constraining $|V_k| < p, \forall k$, or simply because an optimal observational scheme guaranteeing $O^c = \emptyset$ could not be planned prior data collection or was too expensive to implement. For instance, if $|V_k| \leq 2 < p, \forall k$, due to technology limitations, then we would need to observe data about $K = \binom{p}{2}$ node subsets V_1, \dots, V_K , which could be prohibitive to implement when p is large. Figure 1 illustrates (A) the case where we observe four datasets about subsets $V_1, V_2, V_3, V_4 \subset V$ of $p = 100$ nodes across a total of $n = 1000$ data points. Although $\cup_k V_k = V$, many pairs of nodes are never observed jointly. The four datasets are combined together to produce one incomplete sample covariance matrix (B),

$$(2.4) \quad \widehat{\Sigma}_O = \{\widehat{\Sigma}_{ij} : (i, j) \in O\},$$

where each entry $\widehat{\Sigma}_{ij}$ is computed using all available joint observations $(X_i^{(r)}, X_j^{(r)})$ across the n samples (Definition 4.1, Section 4.1). Differently colored portions of the observed empirical covariance matrix have different sample sizes. In particular, the grey portions have zero sample size, so the pairs of nodes falling in those regions have no covariance estimate. The true underlying graph is displayed (C) with edges colored to match the observed pairs. Dotted edges connect pairs of nodes that are never observed jointly.

2.2. The graph quilting problem. The situation described above brings us to pose several questions. Can we estimate Θ and G from an incomplete empirical covariance matrix $\widehat{\Sigma}_O$? Or even in the apparently easier situation where we observe $\Sigma_O = \{\Sigma_{ij} : (i, j) \in O\}$, a portion of the true covariance matrix Σ : Can we recover Θ from Σ_O ? Can we recover G from Σ_O ? We define the “graph quilting problem” as the problem of retrieving Θ and G given the partially observed covariance matrix Σ_O , or the estimation of Θ and G from an incomplete set of empirical covariances $\widehat{\Sigma}_O$. The term “quilting” is evocative of the implicit task of recovering or estimating the graph by “quilting” together multiple graphical structures relative to the observed subsets of nodes.

Recovering the full conditional dependence graph of all p nodes given partially observed covariances is fundamentally an extremely hard problem, because it requires to infer a multiplicity of conditional dependence statements among network

nodes, even for those node pairs with no empirical evidence of their covariability. In the Gaussian framework, to verify the conditional independence statement $X \perp Y \mid Z$ we need to observe each pair (X, Y) , (X, Z) , and (Y, Z) jointly to infer their covariances, but in our situation at least one of these pairs would be unobserved. In a conditional graphical model with p nodes we have to verify the conditional statement $X_i \perp X_j \mid \{X_k\}_{k \in V \setminus \{i, j\}}$ for each pair $(i, j) \in V \times V$, which requires to observe all possible pairs (X_i, X_j) , whereas in our case all pairs in O^c are not observed; indeed we only observe Σ_O , or its empirical estimate $\widehat{\Sigma}_O$.

It is certainly possible to estimate a graph for any subset of the p nodes for which all pairs have been observed (e.g. any set V_k in Equation (2.3)), but such graph would represent the dependence structure of those nodes unconditionally on the remaining nodes. Indeed, for any set $A \subset V$, the Schur complement gives $\Sigma_{AA}^{-1} = \Theta_{AA} - \Theta_{AA^c} \Theta_{A^c A^c}^{-1} \Theta_{A^c A}$, so in general $\Sigma_{AA}^{-1} \neq \Theta_{AA}$. Hence, neither the intersection nor the union of marginally recovered subgraphs in O are guaranteed to be good approximations of the graph in O . Furthermore, we also would like to recover the graph in O^c , which is clearly excluded from the intersection or union of marginal subgraphs in O . Alternatively, we could attempt to assign values to the entries of Σ_{O^c} or $\widehat{\Sigma}_{O^c}$, to obtain a full covariance matrix. But, what values? Assigning arbitrary values to the covariances in O^c would produce an inverse covariance matrix with a correspondingly arbitrary graphical structure. For instance, the simple choice $\Sigma_{O^c} = 0$ is not even guaranteed to yield a positive definite matrix.

With no additional assumptions, the answers to the questions we posed above, and that are the foundations of the graph quilting problem, are strikingly disheartening: the precision matrix Θ and the conditional dependence graph G are impossible to be uniquely recovered from Σ_O alone. This is because no one-to-one mapping may be established between Σ_O and Θ , and this problem is inherited at the estimation level where Σ_O is replaced by an empirical estimate $\widehat{\Sigma}_O$.

However, in this paper we show that *with sufficient additional assumptions* it is possible to recover, either fully or partially, Θ and G from partially observed covariances. First of all, consider the following theorem which describes the ideal, although unlikely, scenario where Θ can be fully retrieved from a partially observed covariance matrix Σ_O :

THEOREM 2.1 (Complete Identifiability). *If $E \subseteq O$, then Θ and G can be fully recovered from Σ_O .*

The proof of Theorem 2.1 is in Appendix A. Theorem 2.1 exploits the fact that the solution of Equation (2.1) when $\widehat{\Sigma}$ is replaced by Σ is exactly Θ . If $E \subseteq O$, then $\Theta_{O^c} = 0$ so that the optimization problem in Equation (2.1) no longer depends

on the unknown covariances Σ_{O^c} , while the solution is still Θ . For illustration, suppose A, B, C is a partition of V , and $O^c = (A \times C) \cup (C \times A)$. Then Theorem 2.1 implies that Θ and G can be completely recovered from Σ_O , for instance, if B is a separator of A and C , or if there is no path between A and B while each node in B has a path to every node in C . Yet, the condition $E \subseteq O$ is unlikely satisfied in practice, and reconstructing Θ under this assumption when it is incorrect can produce inaccurate graphs. For instance, consider a chain graph of $p = 10$ nodes, where, under appropriate ordering of the nodes' indices in V , we have $\Theta_{ij} \neq 0 \Leftrightarrow |i - j| \leq 1$. In this case all p nodes are connected to each other through some path, although each node connects directly with at most two nodes. Suppose $O^c = \{(5, 6), (6, 5)\}$. Assuming $\Theta_{5,6} = 0$ would break the chain, but the covariances in Σ_O would still carry information about the existence of paths connecting nodes $i \leq 5$ and $j \geq 6$. Indeed, the recovered precision matrix via Equation (2.1) with constrain $\Theta_{5,6} = 0$ will present several nonzero entries for $|i - j| > 1$ to reflect the dependence pathways expressed by Σ_O .

The graph quilting problem is strictly related to covariance matrix completion – recovery of Σ_{O^c} given Σ_O – for which several approaches exist. These approaches include positive definite completions (Dempster, 1972; Grone et al., 1984; Bakonyi and Woerdeman, 1995; Vandenberghe et al., 1998), methods that assume the covariance matrix to be low-rank (Pfau et al., 2013; Bishop and Yu, 2014), and statistical models for neural data (Wohrer et al., 2010; Turaga et al., 2013). Yet, most of the existing literature does not focus on the quality of retrieval of a conditional dependence graphical structure. Indeed, the graph quilting problem is more subtle and challenging than covariance matrix completion in which accuracy of reconstruction is focused on retrieving Σ_{O^c} , and typically it does not involve the problem of recovering exact zeros in the inverse of Σ . In the Gaussian framework the inverse of the covariance matrix specifies the graphical dependence structure of the random vector X , and, as a butterfly effect, little perturbations in the recovery of Σ_{O^c} can propagate over any entry of the reconstructed inverse covariance matrix, thereby providing a very inaccurate graph recovery. The gravity of the problem is even more amplified at the estimation level, when an estimate of Σ_O is to be used to recover Θ .

2.3. *How we tackle the problem.* We identify two broad families of solutions to the graph quilting problem:

- (a) *Two-step or plug-in methods*, which first perform covariance matrix completion on Σ_O or $\hat{\Sigma}_O$, and then retrieve the precision matrix through Equations (2.1) or (2.2);

- (b) *Observed likelihood methods*, which reconstruct the precision matrix from Σ_O or $\hat{\Sigma}_O$ directly by maximizing the observed part of the log likelihood function $L(\Theta, \Sigma_O) = \log \det \Theta - \sum_{(i,j) \in O} \Theta_{ij} \Sigma_{ij}$ with specific constraints on Θ_{O^c} .

These two approaches are strictly interrelated since reconstructing Σ or Θ also provides a reconstruction of their respective inverses. However, approaches of type (b) may be more suitable for a more targeted and accurate reconstruction of Θ and the graph G , which is the ultimate goal of this paper. Therefore, we follow strategy (b), which we characterize in the form of the constrained optimization problem

$$(2.5) \quad \tilde{\Theta} = \underset{\Theta > 0, \Theta_{O^c} \in \mathcal{C}}{\operatorname{argmax}} \log \det \Theta - \sum_{(i,j) \in O} \Theta_{ij} \Sigma_{ij},$$

where \mathcal{C} is a set of admissible values of Θ_{O^c} , and the objective function is the observed log likelihood function that does not depend on the unobserved covariances of the set O^c . Note that without an appropriate constraint $\Theta_{O^c} \in \mathcal{C}$ the optimization problem would not have any solution. The approach (b) that we investigate in this paper is very straightforward for the recovery of Θ from Σ_O , or the estimation of Θ given partially observed sample covariances $\hat{\Sigma}_O$. However, the study of the properties of the methodologies based on (b) will prove to be very challenging, although highly rewarding. We do not exclude the possibility of approaching the graph quilting problem in the frameworks of CLIME (Cai et al., 2011), Dantzig selector (Candas & Tao, 2007; Bickel et al., 2009), or nodewise lasso regression (Meinshausen and Buhlmann, 2006), but leave this investigation for future research.

2.4. *The MAD_{GQ} solution.* In this paper we focus on a specific instance of Equation (2.5) called MAD_{GQ} :

DEFINITION 2.1 (MAD_{GQ}). *Let Σ be a positive definite covariance matrix, and let $O \subseteq V \times V$ be a symmetric set of node pairs, with $(i, i) \in O, \forall i \in V$. The MAD_{GQ} approximation of $\Theta = \Sigma^{-1}$ given Σ_O is*

$$(2.6) \quad \tilde{\Theta} = \underset{\Theta > 0, \Theta_{O^c} = 0}{\operatorname{argmax}} \log \det \Theta - \sum_{(i,j) \in O} \Theta_{ij} \Sigma_{ij} \quad (\text{MAD}_{GQ})$$

We call this solution MAD_{GQ} because of its relationship with the maximum determinant positive definite covariance matrix completion:

LEMMA 2.1. *Equation (2.6) is equivalent to the max determinant problem*

$$(2.7) \quad \tilde{\Theta}^{-1} := \tilde{\Sigma} = \underset{S > 0, S_O = \Sigma_O}{\operatorname{argmax}} \det S,$$

which has a unique solution as long as all available principal minors in Σ_O are positive, i.e. as long as Σ_O is completable to a positive definite matrix.

The optimization problem in Equation (2.7) is discussed in Dempster (1972), Grone et al. (1984), and Bakonyi and Woerdeman (1995) as a covariance matrix completion methodology. Equation (2.7) and thereby Equation (2.6) enjoy several desirable statistical properties. Most notably, their solution corresponds to the maximum entropy distribution with covariance constraints over the set O . The representation in Equation (2.6) further reveals that the MAD_{GQ} maximizes the expected Gaussian log density under the constraint $\Theta_{O^c} = 0$, which rules out the dependence of the objective function on the unobserved Σ_{O^c} by assuming no edges among the unobserved pairs of nodes. Lemma 2.1 also demonstrates that $[\tilde{\Theta}^{-1}]_O = \Sigma_O$, that is the MAD_{GQ} solution preserves the observed portion Σ_O while inducing a covariance matrix completion over O^c . Note that the simple alternate completion Σ^* where $\Sigma_O^* = \Sigma_O$ and $\Sigma_{O^c}^* = 0$ is not as desirable as Equation (2.7), fundamentally because Σ^* is not guaranteed to be positive definite. The optimization problems in Equations (2.6) and (2.7) can be solved algorithmically (Grone et al., 1984) or with closed formulae when the graph or O^c are of special kinds (Smith, 2008). In Equation (C.6) of Appendix C we derive a closed formula for $\tilde{\Theta}$ (Equation (2.6)) in the case where $O^c = (A \times C) \cup (C \times A)$ with $A, C \subset V$, $A \cap C = \emptyset$ (see Section 3.2.4).

Although Equation (2.7) has been investigated as a covariance completion approach, the reliability of the retrieved conditional dependence graph given by $\tilde{\Theta}$ is largely unexplored. If the assumption $E \subseteq O$ of the Complete Identifiability Theorem (Theorem 2.1) is correct, then the reconstructed MAD_{GQ} matrix $\tilde{\Theta}$ matches Θ exactly, and thereby the graph G is perfectly recovered. If $E \not\subseteq O$, then, in general, $\tilde{\Theta} \neq \Theta$, so that the graphical structure of $\tilde{\Theta}$ will not match G . Indeed, as discussed earlier with an example of chain graph, erroneously assuming that one or more pairs of nodes are conditionally independent within a network of p nodes would force the rest of the recovered network to adjust in order to reflect the dependence pathways expressed by Σ_O . For instance, if two nodes i and j are dependent only through a node k , and we assume (i, k) to be conditionally independent, then it is likely that (i, j) will be connected by an edge (or a new path through other nodes) in the recovered graph given the observed covariances. Moreover, other unexplored problems are: Can we recover any information about the graph in O^c ? How do we deal with the finite sample case where Σ_O is replaced by an empirical estimate $\hat{\Sigma}_O$ that is not guaranteed to be completable to a positive definite matrix as required by Lemma 2.1? In this paper we try to answer all such questions.

We first investigate the graph quilting problem at the population level, where we aim at reconstructing Θ and the graph G from Σ_O , a portion of the true covariance

matrix (Section 3). We show that the MAD_{GQ} solution (Equation (2.6)) contains no false negatives in O almost everywhere and further give conditions and strategies to manipulate the MAD_{GQ} solution to perfectly recover the graph in O . Furthermore, for the purpose of identifying all potential edges in O^c based on distortions found in $\tilde{\Theta}_O$, we devise the Recursive-Complement (RECO), a powerful algorithm which allows us to identify edges connecting the variables that are never observed jointly. In Section 4 we deal with the estimation of Θ and G given an empirical estimate $\hat{\Sigma}_O$. We propose the $\text{MAD}_{GQ\text{lasso}}$, an ℓ_1 -regularized variant of MAD_{GQ} that enjoys all properties of MAD_{GQ} with high-probability whenever the sample size is sufficiently large relatively to the number of nodes. Based on the $\text{MAD}_{GQ\text{lasso}}$, we construct graph estimators and assess their graph recovery performance in high-dimensions. In Section 5 we report an extensive simulation study, and in Section 6 we apply the methods to neuronal functional connectivity graph estimation from nonsimultaneous calcium imaging recordings of ten thousand neurons in mouse visual cortex.

3. Graph recovery: population analysis. In this section we investigate the graph quilting problem at the population level, where we aim at reconstructing Θ and the graph G from Σ_O , a portion of the true covariance matrix. In the next two sections we investigate the recovery of the graph in O and in O^c by virtue of the MAD_{GQ} solution (Equation (2.6)).

3.1. *Graph recovery in O .* We state two important theorems about the recovery of the graph in O ,

$$(3.1) \quad E_O = \{(i, j) \in O : \Theta_{ij} \neq 0\},$$

by virtue of the MAD_{GQ} solution $\tilde{\Theta}$ in Equation (2.6) given Σ_O : Theorem 3.1 proves the theoretical negligibility of the cases where the graph induced by $\tilde{\Theta}$ contains any false negatives in O , i.e. cases where $\tilde{\Theta}$ is zero over some pair $(i, j) \in O$, whereas $\Theta_{ij} \neq 0$; and Theorem 3.2 states conditions under which it is possible to perfectly retrieve the graph in O by appropriately thresholding $\tilde{\Theta}$. These two theorems are proved in Appendix A and exploit Lemma B.4 in Appendix B, which shows that $\tilde{\Theta}$ is a continuous function of $\Sigma_O > 0$ and, given Θ_O , it is a continuous function of Θ_{O^c} , as long as $\Theta > 0$. The lemma uses Berge's Maximum Theorem for which $\tilde{\Theta}$ is an upper hemicontinuous correspondence of Σ_O and, for fixed Θ_O , of Θ_{O^c} . The uniqueness of the solution $\tilde{\Theta}$ further guarantees that $\tilde{\Theta}$ is a single-valued correspondence, hence a function.

We now move on to the statement of the first theorem:

THEOREM 3.1 (MAIN RESULT - NO FALSE NEGATIVES IN O). *Let $\tilde{E} = \{(i, j) : \tilde{\Theta}_{ij} \neq 0\}$ be the edge set induced by the MAD_{GQ} solution $\tilde{\Theta}$ in Equation (2.1). Then $E_O \subseteq \tilde{E}_O$ almost everywhere, since $\tilde{\Theta}_O$ is sparser than Θ_O only in situations that are Lebesgue measure negligible.*

This result is very strong and reassuring as it guarantees that it is theoretically negligible to incur into a situation where the MAD_{GQ} reconstruction misses any edge in O . Thus, the recovered graph in O is a superset of the true graph in O almost everywhere. To get intuition about Theorem 3.1, suppose Σ is any point of the cone of $p \times p$ positive definite matrices, and let $\Delta_{ij} = \tilde{\Theta}_{ij} - \Theta_{ij}$. Having a false negative in (i, j) would require $\Theta_{ij} = -\Delta_{ij}$. The set of matrices that exactly satisfy the latter equality constitutes a lower dimensional manifold which occupies zero volume in the positive definite cone.

For the second theorem, let

$$(3.2) \quad \delta = \max_{(i,j) \in O, i \neq j} |\Theta_{ij} - \tilde{\Theta}_{ij}|$$

denote the maximum distortion between the off-diagonals of Θ_O and $\tilde{\Theta}_O$, and let

$$(3.3) \quad \nu = \min_{(i,j) \in O, i \neq j, \Theta_{ij} \neq 0} |\Theta_{ij}|$$

be the smallest nonzero magnitude of the off-diagonals of Θ_O . We assume that at least one edge is in O , so that ν exists and is positive.

THEOREM 3.2 (MAIN RESULT - EXACT GRAPH RECOVERY IN O). *If $\delta < \nu/2$, then the true graph structure E_O can be perfectly recovered from $\tilde{\Theta}_O$ by assigning edges wherever $|\tilde{\Theta}_{ij}| > \nu/2$, that is*

$$(3.4) \quad E_O^{\nu/2}(\tilde{\Theta}) := \{(i, j) : |\tilde{\Theta}_{ij}| > \nu/2\} = E_O$$

Specifically, $|\tilde{\Theta}_{ij}| > \nu/2 \Leftrightarrow \Theta_{ij} \neq 0$ with $\text{sign}(\tilde{\Theta}_{ij}) = \text{sign}(\Theta_{ij})$, $\forall (i, j) \in O, i \neq j$. A sufficient condition for $\delta < \nu/2$ is $\|\Theta_{O^c}\|_\infty$ to be sufficiently small with $0 \in \mathcal{D}_{\Theta_O}$, where $\mathcal{D}_{M_O} = \{M_{O^c} : M > 0\}$.

Theorem 3.2 states that it is possible to perfectly recover the graph and the signs of the entries of the precision matrix in O from Σ_O as long as $\delta < \nu/2$, because this condition lets us appropriately eliminate all false positives in $\tilde{\Theta}_O$ without producing any false negatives. A sufficient condition for $\delta < \nu/2$ is $\|\Theta_{O^c}\|_\infty$ to be sufficiently small with $0 \in \mathcal{D}_{\Theta_O}$. This is due to the continuity of $\tilde{\Theta}$ as a function of Θ_{O^c} about $\Theta_{O^c} = 0$ when Θ_O is kept constant (Lemma B.4). Indeed, whenever $\|\Theta_{O^c}\|_\infty \approx 0$, we

have $\|\Theta - \tilde{\Theta}\|_\infty \approx 0$ because $\Theta_{O^c} = 0$ implies $\tilde{\Theta} = \Theta$, as guaranteed by the Complete Identifiability Theorem (Theorem 2.1). Theorem 3.2 can also be restated in terms of partial correlations. Let

$$(3.5) \quad \delta_{\text{pcor}} = \max_{(i,j) \in O, i \neq j} |R_{ij} - \tilde{R}_{ij}| \quad \text{and} \quad \nu_{\text{pcor}} = \min_{(i,j) \in O, i \neq j, R_{ij} \neq 0} |R_{ij}|,$$

where $R_{ij} = -\Theta_{ij}(\Theta_{ii}\Theta_{jj})^{-1/2}$ is the partial correlation of nodes (i, j) , and $\tilde{R}_{ij} = -\tilde{\Theta}_{ij}(\tilde{\Theta}_{ii}\tilde{\Theta}_{jj})^{-1/2}$ is its MAD_{GQ} recovery: if $\delta_{\text{pcor}} < \nu_{\text{pcor}}/2$, then E_O can be recovered perfectly by assigning edges wherever $|\tilde{R}_{ij}| > \nu_{\text{pcor}}/2$.

In Figure 2 we present an example where the precision matrix Θ displayed in (A) contains several edges in O^c (grey set of unobserved covariances shown in (B)). We designed Θ to have $\gamma := \|\Theta_{O^c}\|_\infty = 0.0125$ to be sufficiently small so that the condition $\delta < \nu/2$ of Theorem 3.2 is satisfied. The condition $\delta < \nu/2$ would still hold also if we slightly deviate from the specific value $\gamma = 0.0125$. To show this, we compute

$$(3.6) \quad \bar{\delta}(\gamma) = \max_{\substack{\Theta^* > 0 \\ \text{s.t. } \Theta_O^* = \Theta_O, \|\Theta_{O^c}^*\|_\infty = \gamma, E_{O^c}^* = E_{O^c}}} \delta(\Theta^*),$$

where $\delta(\Theta^*)$ is given by Equation (3.2) with $\Theta = \Theta^*$ and $\Sigma_O = [\Theta^{*-1}]_O$. The quantity $\bar{\delta}(\gamma)$ is the worst possible distortion given Θ_O , E_{O^c} , and as a function of γ . In Figure 2(C) we show that the distortion $\bar{\delta}(\gamma)$ increases with γ , goes to zero as $\gamma \rightarrow 0^+$, and for any value of γ in a neighborhood of $\gamma = 0.0125$ it stays well below $\nu/2$; in all such cases, Theorem 3.2 would successfully apply. In Figure 2(D) we show the support of the MAD_{GQ} solution $\tilde{\Theta}$, which contains several false positives in O , false negatives in O^c , but no false negatives are in O , in agreement with Theorem 3.1. After thresholding the entries of $\tilde{\Theta}$ at $\nu/2$ (i.e. removing all edges (i, j) where $|\tilde{\Theta}_{ij}| \leq \nu/2$) we perfectly recover the graph in O (Figure 2(E)) as per Theorem 3.2. Figure 3 illustrates another example analogous to Figure 2 where the observed sets V_1, \dots, V_K are random, demonstrating that, indeed, Theorem 3.2 does not require the sets V_1, \dots, V_K to be ‘‘chained’’ as in Figure 2. The edge identification in O^c (Figures 2(E)-(F) and 3(E)-(F)) is described in Section 3.2.

3.1.1. *Special case $K = 2$.* To provide more insight into Theorem 3.2, consider the simple case with $K = 2$ in Equation (2.3), which can be defined by $V_1 = A \cup B$ and $V_2 = B \cup C$, where A, B, C is a partition of V so that

$$(3.7) \quad O^c = (A \times C) \cup (C \times A).$$

The next theorem illustrates the dependence of the distortion $\Theta - \tilde{\Theta}$ on the features of Θ explicitly:

THEOREM 3.3 (Recovery guarantees in $O(K=2)$). *Suppose Equation (3.7) holds. For any node sets $E, F \subseteq V$, define $\gamma_{EF} = \|\Theta_{EF}\|_\infty$, $\tilde{\gamma}_{EE} = \|\Theta_{EE}^{-1}\|_\infty$, and $\text{rd}_{EF} = \max_{i \in E} \|\Theta_{iF}\|_0$. Let $\gamma = \gamma_{AC}$ and $\kappa = \|\Theta_{AC}\|_0$. Then*

$$(3.8) \quad \|\Theta_{AA} - \tilde{\Theta}_{AA}\|_\infty \leq \text{rd}_{AC}^2 \tilde{\gamma}_{CC} \gamma^2$$

$$(3.9) \quad \|\Theta_{CC} - \tilde{\Theta}_{CC}\|_\infty \leq \text{rd}_{CA}^2 \tilde{\gamma}_{AA} \gamma^2$$

$$(3.10) \quad \|\Theta_{AB} - \tilde{\Theta}_{AB}\|_\infty \leq \text{rd}_{AC} \text{rd}_{BC} \tilde{\gamma}_{CC} \gamma_{BC} \gamma$$

$$(3.11) \quad \|\Theta_{BC} - \tilde{\Theta}_{BC}\|_\infty \leq \text{rd}_{BA} \text{rd}_{CA} \tilde{\gamma}_{AA} \gamma_{AB} \gamma$$

An expression of the bound for $\|\Theta_{BB} - \tilde{\Theta}_{BB}\|_\infty$ together with bounds on the ℓ_0 distortion are in Lemma B.6 in Appendix B. For fixed Θ_O , there exist nonnegative constants a_1, a_2, b_0, b_1, b_2 such that

$$(3.12) \quad \|\Theta_O - \tilde{\Theta}_O\|_\infty \leq a_1 \gamma + a_2 \gamma^2$$

$$(3.13) \quad \|\Theta_O - \tilde{\Theta}_O\|_0 \leq b_0 I(\kappa > 0) + b_1 \kappa + b_2 \kappa^2.$$

Theorem 3.3, proved in Appendix A, displays the dependence of the distortion in O on the largest magnitude γ in Θ_{AC} , on the number of edges κ in AC , and on other graphical features of Θ in terms of row degrees over different portions of Θ . For instance, we can see that the smaller rd_{AC} and rd_{CA} , the smaller the impact of γ over the distortions across $\tilde{\Theta}$. Moreover, Equations (3.12) and (3.13) remark the quadratic forms of the bounds on the ℓ_∞ and ℓ_0 distortions as functions of γ and κ . We can see that, assuming $0 \in \mathcal{D}_{\Theta_O}$, $\gamma \rightarrow 0^+$ implies $\delta \leq \|\Theta_O - \tilde{\Theta}_O\|_\infty \rightarrow 0^+$, thereby allowing the condition $\delta < \nu/2$ of Theorem 3.2 to hold.

Case $B = \emptyset$ and the latent variable graphical model. In this paragraph we illustrate the relationship between the problem of estimating the conditional dependence graph of a set of nodes in the presence of latent variables, and graph quilting in the case $K=2$ with $B = \emptyset$. Suppose nodes $V = A \sqcup C$ and $O = A \times A$ while nodes C are hidden. It is known that

$$(3.14) \quad \Sigma_{AA}^{-1} = \Theta_{AA} - \Theta_{AC} \Theta_{CC}^{-1} \Theta_{CA},$$

where Θ_{AA} is the AA portion of the precision matrix Θ whose nonzero structure identifies the dependence structure of nodes A conditionally on C , while the second term of the right-hand-side has rank no larger than $|A|$, and accounts for the network

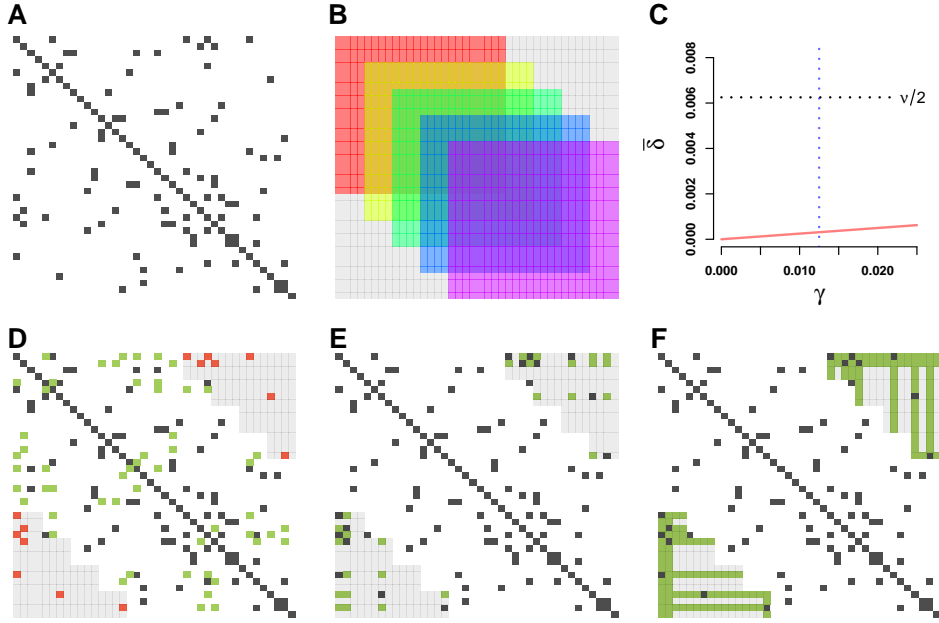


FIG 2. *Example of graph structure recovery. (A) Support of Θ , $p = 40$. (B) Observed pair set $O = \cup_k (V_k \times V_k)$ (colored areas), and O^c (grey area). (C) Exact graph recovery in O can be achieved when $\delta < \nu/2$, as per Theorem 3.2. The case considered here satisfies this condition. Indeed, the maximum possible distortion $\tilde{\delta}$ (Equation (3.6)) is smaller than $\nu/2$ at the true value of $\gamma = 0.0125$. Thus, the condition $\delta < \nu/2$ would still hold also if we slightly deviate from the specific value $\gamma = 0.0125$. (D) Support of the MAD_{GQ} solution $\hat{\Theta}$. Green entries are false positives, and red entries are false negatives. (E) Recovered graph after thresholding and superset identification via Theorems 3.2 and 3.4. All false positives in $\hat{\Theta}_O$ have been eliminated, and the superset of edges in O^c (black and green) contains all true edges. (F) Recovered graph via Theorem 3.2 and Proposition 3.1.*

effects of the hidden nodes in C . Based on this fact, Chandrasekaran et al. (2012) proposed to estimate E_{AA} – the AA subgraph of the full conditional dependence graph of all nodes V – by first estimating the inverse covariance matrix of A as the difference of a sparse matrix S and a low rank matrix L ,

$$\widehat{\Sigma}_{AA}^{-1} = \widehat{S} - \widehat{L},$$

and then taking the support of \widehat{S} as an estimate of E_{AA} . Suppose now that $O = (A \times A) \cup (C \times C)$, that is we are in a graph quilting situation where $V_1 = A$, and $V_2 = C$. Then, $O^c = (A \times C) \cup (C \times A)$ and the MAD_{GQ} solution would be equal to

$$(3.15) \quad \tilde{\Theta} = \begin{bmatrix} \Sigma_{AA}^{-1} & 0 \\ 0 & \Sigma_{CC}^{-1} \end{bmatrix}$$

Theorem 3.2 guarantees that if $\delta < \nu/2$ then E_O can be perfectly recovered from $\tilde{\Theta}_O$ by assigning edges wherever $|\tilde{\Theta}_{ij}| > \nu/2$. But since $\tilde{\Theta}_{AA}$ is not a function of Σ_{CC} , this thresholding is valid even if $O = A \times A$, that is even if nodes C are unobserved! The following corollary summarizes this result:

COROLLARY 3.1 (Latent variable graphical model). *Suppose $O = A \times A$, and $C = V \setminus A \neq \emptyset$. If $\delta < \nu/2$, then*

$$(3.16) \quad \{(i, j) \in A \times A : |[\Sigma_{AA}^{-1}]_{ij}| > \nu/2\} = E_{AA}$$

This corollary states that, under appropriate conditions, the subgraph connecting the nodes A within the full conditional dependence graph of $V = A \sqcup C$ can be retrieved from $\Sigma_O = \Sigma_{AA}$ without recovering the sparse and the low-rank components S and L , but by just appropriately thresholding the entries of the inverse of Σ_{AA} . Consequently, at the estimation level, it may be possible to avoid estimating the components S and L of the decomposition, but rather just obtain a good estimate of Σ_{AA}^{-1} to threshold. Such procedure may be more appealing than the sparse and low rank approach because it would involve the estimation of a much smaller number of parameters.

3.2. Graph recovery in O^c . In the previous section we demonstrated how it is possible to perfectly recover the graph in O from a partially observed covariance matrix Σ_O under certain conditions. We now consider the far more challenging problem of recovering the graph in O^c .

Recovering the graph in O^c based on a partially observed covariance matrix Σ_O is a seemingly impossible task because it requires to retrieve conditional dependence statements about pairs of variables for which even their marginal correlation is unobserved. Although under standard conditions marginal covariation is necessary to infer conditional dependence, we show that with some assumptions it is actually possible to retrieve substantial information about the graph in O^c even without knowledge about Σ_{O^c} . As described in the previous section, the MAD_{GQ} Equation (2.6) produces a precision matrix $\tilde{\Theta}$, where $\tilde{\Theta}_{O^c} = 0$ and $\tilde{\Theta}_O \neq \Theta_O$ whenever $\Theta_{O^c} \neq 0$. The distortions in $\tilde{\Theta}_O$, however, have a pattern which depends on the edge structure in O^c . Specifically, not all entries of $\tilde{\Theta}_O$ differ from the corresponding ones in Θ_O , and a specific pattern of distortions in O can be caused only by specific graphical structures in O^c . Hence, identifying distortions in $\tilde{\Theta}_O$ can let us triangulate the possible graphical structures in O^c , thereby discarding all those edges that may not have contributed to the origin of the observed distortions in $\tilde{\Theta}_O$.

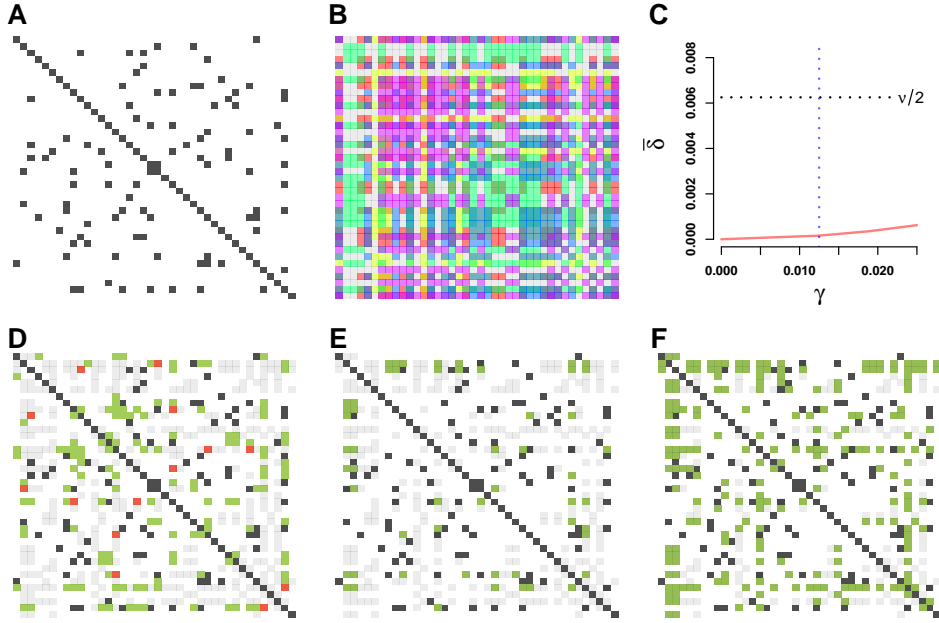


FIG 3. *Example of graph structure recovery. (A) Support of Θ , $p = 40$. (B) Observed pair set $O = \cup_k (V_k \times V_k)$ (colored areas), and O^c (grey area). (C) Exact graph recovery in O can be achieved when $\delta < \nu/2$, as per Theorem 3.2. The case considered here satisfies this condition. Indeed, the maximum possible distortion $\bar{\delta}$ (Equation (3.6)) is smaller than $\nu/2$ at the true value of $\gamma = 0.0125$. Thus, the condition $\delta < \nu/2$ would still hold also if we slightly deviate from the specific value $\gamma = 0.0125$ (D) Support of the MAD_{GQ} solution $\tilde{\Theta}$. Green entries are false positives, and red entries are false negatives. (E) Recovered graph after thresholding and superset identification via Theorems 3.2 and 3.4. All false positives in $\tilde{\Theta}_O$ have been eliminated, and the superset of edges in O^c (black and green) contains all true edges. (F) Recovered graph via Theorem 3.2 and Proposition 3.1.*

For the purpose of identifying edges in O^c based on distortions found in $\tilde{\Theta}_O$, we devise the Recursive-Complement (**RECO**), a novel algorithm which allows us to identify the potential graphical structures in O^c that may have induced the observed distortions in the MAD_{GQ} reconstruction $\tilde{\Theta}_O$. The RECO algorithm builds upon a fundamental property that entangles $\tilde{\Theta}$ with Θ through Σ by virtue of the Schur complement:

LEMMA 3.1 (**MAD_{GQ} ENTANGLEMENT**). *Let $\tilde{\Theta}$ be the MAD_{GQ} solution in Equation (2.6) based on the observed covariance matrix Σ_O . For any $U \subset V$ such that $U \times U \subseteq O$,*

$$(3.17) \quad \tilde{\Theta}_{UU} - \tilde{\Theta}_{UU^c} \tilde{\Theta}_{U^c U^c}^{-1} \tilde{\Theta}_{U^c U} = \Sigma_{UU}^{-1} = \Theta_{UU} - \Theta_{UU^c} \Theta_{U^c U^c}^{-1} \Theta_{U^c U}.$$

The proof of this lemma uses the fact that $[\tilde{\Theta}^{-1}]_O \equiv \Sigma_O \equiv [\Theta^{-1}]_O$ (Lemma 2.1),

which creates a channel of correspondences between $\tilde{\Theta}$ and Θ via Schur complements. We propose two versions of the RECO algorithm: (a) one that assumes $\text{diag}(\Theta)$ to be known and produces a superset \mathcal{S} of all edges in O^c (Algorithm 3.1), and (b) one that identifies a minimum number of true edges in O^c but without assuming $\text{diag}(\Theta)$ known (Algorithm 3.2). For each case, we will see the important role played by Lemma 3.1.

3.2.1. *Assuming $\text{diag}(\Theta)$ known.* In Equation (3.17), if a diagonal entry (i, i) of $\tilde{\Theta}_{UU} - \tilde{\Theta}_{UU^c} \tilde{\Theta}_{U^c U^c}^{-1} \tilde{\Theta}_{U^c U}$ is smaller than the corresponding diagonal entry of Θ_{UU} , then $\Theta_{UU^c} \Theta_{U^c U^c}^{-1} \Theta_{U^c U}$ must be nonzero on the same diagonal position. Since $\Theta_{U^c U^c}$ is positive definite we also conclude that Θ_{UU^c} is nonzero in row i . This fact is relevant if $(U \times U^c) \cap O^c \neq \emptyset$, as it indicates the possible presence of an edge in O^c . The RECO procedure summarized in Algorithm 3.1 assumes $\text{diag}(\Theta)$ to be known and recursively applies Equation (3.17) across all Cartesian squares of nodal subsets inscribed within O , specifically all sets $V_k \times V_k$, for $k = 1, \dots, K$, where $O = \cup_{k=1}^K V_k \times V_k$, allowing us to identify a set \mathcal{S}_ξ containing edges in O^c :

ALGORITHM 3.1 (**RECURSIVE COMPLEMENT – $\text{diag}(\Theta)$ KNOWN**).

Input: Sets $V_1, \dots, V_K \subset V$ s.t. $O = \cup_{k=1}^K (V_k \times V_k)$, $\text{diag}(\Theta)$, $\tilde{\Theta} > 0$, and $\xi \in \mathbb{R}$.

1. Compute $\tilde{\Theta}^{(1)}, \dots, \tilde{\Theta}^{(K)}$, where

$$(3.18) \quad \tilde{\Theta}^{(k)} = \tilde{\Theta}_{V_k V_k} - \tilde{\Theta}_{V_k V_k^c} \tilde{\Theta}_{V_k^c V_k^c}^{-1} \tilde{\Theta}_{V_k^c V_k}$$

2. Compute $\tilde{\Theta}_{11}, \dots, \tilde{\Theta}_{pp}$, where

$$(3.19) \quad \tilde{\Theta}_{ii} = \max_{k: i \in V_k} \tilde{\Theta}_{i_k i_k}^{(k)}$$

and $i \in V$ is the i_k -th element of V_k .

3. Obtain

$$(3.20) \quad \mathcal{D}_\xi = \{i \in V : \tilde{\Theta}_{ii} < \Theta_{ii} + \xi\}.$$

Output: Set

$$(3.21) \quad \mathcal{S}_\xi = \check{O}^c \cap (\mathcal{D}_\xi \times \mathcal{D}_\xi),$$

where $\check{O}^c = \{(i, j) \in O^c : i < j\}$.

The RECO Algorithm 3.1 takes V_1, \dots, V_K , $\text{diag}(\Theta)$, and $\tilde{\Theta}$ as inputs and produces the set \mathcal{S}_ξ in Equation (3.21) as output. For $\xi > 0$ we have $\mathcal{S}_\xi = \check{O}^c$ because $\tilde{\Theta}_{ii} \leq \Theta_{ii}, \forall i \in V$. For $\xi = 0$ we have a striking result: the RECO Algorithm 3.1 produces the set $\mathcal{S} := \mathcal{S}_0$, which is a nontrivial *superset* of the edges connecting the variable pairs in O^c . The following theorem precisely states the properties of this superset:

THEOREM 3.4 (SUPERSET OF EDGES IN O^c - $\text{diag}(\Theta)$ KNOWN). *Let*

$$(3.22) \quad \mathcal{S} := \mathcal{S}_0,$$

where \mathcal{S}_ξ is the output of the RECO Algorithm 3.1 in Equation (3.21). Then

- (i). \mathcal{S} is a superset of edges in O^c .
- (ii). \mathcal{S} contains at least

$$(3.23) \quad M = \max_{t=1,2} |\text{proj}_t(\Omega)|$$

true edges of O^c , where

$$(3.24) \quad \Omega = \check{O}^c \cap (\tilde{\mathcal{D}} \times \tilde{\mathcal{D}}),$$

$$(3.25) \quad \tilde{\mathcal{D}} = \{i \in \mathcal{D}_0 : \exists k, i \in V_k, \{i\} \times V_k^c \subseteq O^c\},$$

\mathcal{D}_ξ is given in Equation (3.20), and $\text{proj}_t(\{z_{1j}, z_{2j}\}_{j=1}^K) = \{z_{tj}\}_{j=1}^K$.

Theorem 3.4 (i) establishes that all edges connecting the pairs in O^c are included in the edge set \mathcal{S} obtained via the RECO Algorithm 3.1. On the other hand, we also have $\Theta_{O^c \cap \mathcal{S}^c} = 0$, that is there is no true edge in O^c outside of \mathcal{S} . Thus the RECO Algorithm 3.1 allows us to identify all pairs in O^c that *are connected*, but also several pairs of nodes that *cannot be connected*. Hence, an upper bound to the number of edges in O^c is $|\mathcal{S}|$. On the other hand, part (ii) of the theorem states that at least M edges in \mathcal{S} are true. This number M is therefore a lower bound to the number of edges connecting the unobserved node pairs in O^c . In Section 3.2.4 we will see that the RECO Algorithm 3.1 greatly simplifies when $K = 2$. In light of this, one may wonder whether we could just enlarge $O^c = (\cup_{k=1}^K (V_k \times V_k))^c$ into a Cartesian product $W \times W \supseteq O^c$ and exploit the easier procedure for the case $K = 2$ rather than Algorithm 3.1. Proposition B.1 in Appendix B discusses the possibility of reducing a case $K > 2$ to a case $K = 2$, but explains why such approach

is not desirable because it is not always applicable and would only produce a larger superset \mathcal{S} than the one produced via Algorithm 3.1.

Figure 2 illustrates an example where the K observed subsets of nodes V_1, \dots, V_K are chained, i.e. $V_i \cap V_{i+1} \neq \emptyset, \forall i = 1, \dots, K-1$. In Figure 2(E) we display the recovered graph, where we can see that all edges in O^c have been retrieved thanks to the RECO algorithm. However, the sets V_1, \dots, V_K do not need to be chained to have the RECO procedure succeed; in fact, the procedure would work even if, for some k , $V_k \cap (\cup_{j \neq k} V_j) = \emptyset$, as long as $\cup_i V_i = V$, that is even if some set V_k does not overlap with any other. Thus, in Figure 3 we present another example where the sets V_1, \dots, V_K are random. Indeed, also in this case, the set \mathcal{S} in Figure 3(E) successfully contains all true edges in E_{O^c} .

3.2.2. *Assuming $\text{diag}(\Theta)$ unknown.* The set \mathcal{S} in Equation (3.21) could be viewed as an oracle superset that, however, is likely infeasible because assuming $\text{diag}(\Theta)$ to be known can be highly impractical. Thus, we provide more practical schemes for the identification of edges in O^c . The following Algorithm 3.2 is a variant of Algorithm 3.1 that does not require any knowledge of $\text{diag}(\Theta)$, while only two nonnegative scalars ξ_1, ξ_2 are involved:

ALGORITHM 3.2 (RECURSIVE COMPLEMENT - $\text{diag}(\Theta)$ UNKNOWN).

Input: Sets $V_1, \dots, V_K \subset V$ s.t. $O = \cup_{k=1}^K (V_k \times V_k)$, $\tilde{\Theta} \succ 0$, and $\xi_1, \xi_2 \in \mathbb{R}_+$.

1. Compute $\tilde{\Theta}^{(1)}, \dots, \tilde{\Theta}^{(K)}$, where

$$(3.26) \quad \tilde{\Theta}^{(k)} = \tilde{\Theta}_{V_k V_k} - \tilde{\Theta}_{V_k V_k^c} \tilde{\Theta}_{V_k^c V_k}^{-1} \tilde{\Theta}_{V_k^c V_k}$$

2. Obtain

$$(3.27) \quad \mathcal{H}_{\xi_1, \xi_2} = \left\{ i \in V : \forall k \text{ s.t. } i \in V_k, \exists j \neq i, \xi_1 < |\tilde{\Theta}_{i_k j_k}^{(k)}| < \xi_2 \right\}.$$

where $i, j \in V$ are, respectively, the i_k -th and j_k -th elements of V_k .

Output: Set

$$(3.28) \quad \mathcal{U}_{\xi_1, \xi_2} = \check{O}^c \cap \left[(\mathcal{H}_{\xi_1, \xi_2} \times V) \cup (V \times \mathcal{H}_{\xi_1, \xi_2}) \right].$$

We can see that, while the RECO Algorithm 3.1 identifies discrepancies between the diagonals of $\tilde{\Theta}^{(k)}$ (Equation (3.18)) and the corresponding diagonals of Θ , the RECO Algorithm 3.2 instead searches for the nonzero off-diagonal entries of $\tilde{\Theta}^{(k)}$ which have too small a magnitude. Specifically, as established in the next proposition, setting $\xi_1 = 0$ and $\xi_2 = \nu$ (Equation (3.3)) lets us find the entries of $\tilde{\Theta}^{(k)}$

that cannot be equal to the corresponding ones in Θ simply because, by definition of ν , no entry in Θ has magnitude in $(0, \nu)$. Indeed, if a discrepancy is found for an entry $\tilde{\Theta}_{i_k j_k}^{(k)}$, then Lemma 3.1 implies $\Theta_{i V_k^c} \neq 0$ and $\Theta_{j V_k^c} \neq 0$, i.e. at least one edge must be on row i and row j . The following proposition establishes the theoretical guarantees of the RECO Algorithm 3.2 as a recovery strategy of the edges in O^c when $\text{diag}(\Theta)$ is unknown:

PROPOSITION 3.1 (**EDGE RECOVERY IN O^c - $\text{diag}(\Theta)$ UNKNOWN**). *Let*

$$(3.29) \quad \mathcal{U} := \mathcal{U}_{0, \nu},$$

where $\mathcal{U}_{\xi_1, \xi_2}$ is the output of the RECO Algorithm 3.2 in Equation (3.28) and ν is the smallest magnitude of the nonzero entries of Θ_O (Equation (3.3)). The set \mathcal{U} contains at least

$$(3.30) \quad N = \max_{t=1,2} |\text{proj}_t(\tilde{O}^c \cap (\tilde{\mathcal{H}}_{0, \nu} \times \tilde{\mathcal{H}}_{0, \nu}))|$$

true edges of O^c , where $\tilde{\mathcal{H}}_{0, \nu} = \{i \in \mathcal{H}_{0, \nu} : \exists k, i \in V_k, \{i\} \times V_k^c \subseteq O^c\}$, and $\mathcal{H}_{\xi_1, \xi_2}$ is given in Equation (3.27).

Proposition 3.1 provides a lower bound N to the number of true edges of O^c contained in the edge set \mathcal{U} (Equation (3.29)) obtained via the RECO Algorithm 3.2. In Figures 2(F) and 3(F) we show that, in these specific examples, all the edges in O^c have been recovered by \mathcal{U} . Yet, in general, there is no guarantee \mathcal{U} contains all the edges in O^c , whereas the set \mathcal{S} obtained through Algorithm 3.1 is a superset of E_{O^c} (Theorem 3.4). However, the set \mathcal{U} is more realistically feasible than \mathcal{S} because knowing the diagonals of Θ is too strong an assumption, while knowledge about ν may be easier to assume. Indeed, as better discussed in Section 4.1, in practice knowledge about ν might be inherited from prior studies, or its value might be easily constrained based on very interpretable assumptions about, for instance, the general level of sparsity of Θ_O or node degrees. Furthermore, the RECO Algorithm 3.2 can be modified to operate on the scale of partial correlations: simply replace the matrix $\tilde{\Theta}^{(k)}$ in Equation (3.27) by its standardized version $\tilde{R}^{(k)} = -\text{diag}(\tilde{\Theta}^{(k)})^{-\frac{1}{2}} \tilde{\Theta}^{(k)} \text{diag}(\tilde{\Theta}^{(k)})^{-\frac{1}{2}}$. This may have great advantages in practice because partial correlations are easier to interpret – they are all on the same scale, while the entries of the precision matrix may be arbitrary. Setting $\xi_1 = 0$ and $\xi_2 = \nu_{\text{pcor}}$ (Equation (3.5)) would finally produce a set analogous to \mathcal{U} , say $\mathcal{U}^{\text{pcor}}$, which enjoys the properties guaranteed by Proposition 3.1.

As the reader may have noted, the set $\mathcal{U}_{\xi_1, \xi_2}$ in Equation (3.28) does not involve the simple Cartesian product of two node sets as the set \mathcal{S}_ξ in Equation (3.21),

but rather the union of two Cartesian products. This is because, by construction, $\mathcal{H}_{0,v} \subseteq \mathcal{D}_v$ (Equation (3.20)), and the alternate formulation of \mathcal{U} given by $\mathcal{U}^{\text{alt}} = \check{O}^c \cap (\mathcal{H}_{0,v} \times \mathcal{H}_{0,v})$ would not be guaranteed to contain any true edge. We give an example of such scenario at the end of Section 3.2.4.

3.2.3. *Final recovered graphs.* By combining the theorem on the exact graph recovery in O (Theorem 3.2) with the theorem on the superset of edges in O^c when $\text{diag}(\Theta)$ is known (Theorem 3.4) and the proposition for the recovery of edges in O^c when $\text{diag}(\Theta)$ is unknown (Proposition 3.1), we can specify the following two possible final graph recoveries:

$$(3.31) \quad \mathcal{E}_S = \{(i, j) : |\tilde{\Theta}_{ij}| > v/2\} \cup \mathcal{S} \quad (\text{DIAG}(\Theta) \text{ KNOWN})$$

and

$$(3.32) \quad \mathcal{E}_U = \{(i, j) : |\tilde{\Theta}_{ij}| > v/2\} \cup \mathcal{U} \quad (\text{DIAG}(\Theta) \text{ UNKNOWN})$$

The variant of \mathcal{E}_U based on partial correlations is given by

$$\mathcal{E}_U^{\text{pcor}} = \{(i, j) : |\tilde{R}_{ij}| > v_{\text{pcor}}/2\} \cup \mathcal{U}^{\text{pcor}},$$

where v_{pcor} is the smallest of the nonzero magnitudes of the true partial correlations (Equation (3.5)), and $\mathcal{U}^{\text{pcor}}$ is obtained, as described earlier, by simply replacing the matrix $\tilde{\Theta}^{(k)}$ in Equation (3.27) of the RECO Algorithm 3.2 by its standardized version $\tilde{R}^{(k)} = -\text{diag}(\tilde{\Theta}^{(k)})^{-\frac{1}{2}} \tilde{\Theta}^{(k)} \text{diag}(\tilde{\Theta}^{(k)})^{-\frac{1}{2}}$, and setting $\xi_1 = 0$ and $\xi_2 = v_{\text{pcor}}$. Finite sample counterparts of \mathcal{E}_S and \mathcal{E}_U will be specified in Section 4.1.

3.2.4. *Special case $K = 2$.* To provide more insight into the results on the graph recovery in O^c , consider the special case with $K = 2$ in Equation (2.3), which can be defined by $V_1 = A \cup B$ and $V_2 = B \cup C$, where A, B, C is a partition of V so that $O^c = (A \times C) \cup (C \times A)$ (Equation (3.7)). The following theorem is a special case of Theorem 3.4, but also provides additional results about the number of possible true graph structures in O^c :

THEOREM 3.5 (Superset of edges in O^c - $\text{diag}(\Theta)$ known ($K = 2$)). *Suppose $V_1 = A \cup B$ and $V_2 = B \cup C$, where A, B, C is a partition of V , and B may be the empty set. Let*

$$(3.33) \quad \mathcal{S} = \underbrace{\{i \in A : \tilde{\Theta}_{ii} < \Theta_{ii}\}}_{A^*} \times \underbrace{\{j \in C : \tilde{\Theta}_{jj} < \Theta_{jj}\}}_{C^*}$$

and let $m = \min\{|A^*|, |C^*|\}$ and $M = \max\{|A^*|, |C^*|\}$. Then

- (i). \mathcal{S} is a superset of E_{AC} .
- (ii). \mathcal{S} contains at least M true edges and, for $M \leq \kappa \leq mM$, it allows for up to

$$(3.34) \quad \xi_\kappa \leq \varphi_\kappa := \binom{|A||C|}{\kappa}$$

possible true graph structures of κ edges in AC . If $m = 1$, then $\mathcal{S} = E_{AC}$.

- (iii). \mathcal{S} is minimal in the sense that no graph structure included in \mathcal{S} may induce more distortions than those observed in the diagonals of $\tilde{\Theta}_{AA}$ and $\tilde{\Theta}_{CC}$.

Theorem 3.5 is a special case of Theorem 3.4 and, indeed the superset derived from the RECO Algorithm 3.1 for the general case $K > 1$ in Equation (3.22) reduces to Equation (3.33) for $K = 2$. However, Theorem 3.5 can be proved in an easier way because in this special case $K = 2$ the superset \mathcal{S} of the edges in Θ_{AC} is simply based on the distortions on the diagonals of $\tilde{\Theta}$ with respect to Θ as per Lemma B.7a in Appendix B. Part (ii) of the theorem shows that there are at least $M = \max\{|A^*|, |C^*|\}$ true edges in \mathcal{S} , that is M is a lower bound to the number of edges in Θ_{AC} . Indeed, M is the smallest number of nonzero entries in Θ_{AC} that could have induced the distortions found in the diagonals of $\tilde{\Theta}_{AA}$ and $\tilde{\Theta}_{CC}$. On the other hand, we have no more than mM edges in Θ_{AC} because that is the cardinality of the superset \mathcal{S} . Equation (3.34) states that the number of possible true graph structures of κ edges in O^c given that all of these are guaranteed to be inside \mathcal{S} , is smaller than the number φ_κ of all possible graph structures of κ edges connecting nodes in A to nodes in C . For instance, if $|A| = 3$, $|C| = 4$, $m = M = 2$, then $\xi_2 = 2 < \varphi_2 = 66$. Another example: if $|A| = |C| = 7$, $m = 4$ and $M = 5$, then $\xi_5 = 240 < \varphi_5 = 1,906,884$. This phenomenon happens first of all because $m \leq M \leq |A|, |C|$. Moreover, every row and column of \mathcal{S} is guaranteed to contain at least one true edge, and this constraint substantially reduces the number of possible graphical structures. A simple metric that quantifies the usefulness of the superset identification is $\chi_\kappa = (1 - \xi_\kappa / \varphi_\kappa) \in (0, 1]$, where $\chi_\kappa \approx 1$ indicates high informative power. Indeed, when χ_κ is large, it is much more likely to guess the true graph structure in O^c by randomly picking one of the possible graphs in \mathcal{S} than from the full set O^c . If $m = 1$, we have that the superset perfectly matches the full set of edges in O^c . This is the case where only one node in A is connected to C and/or only one node in C is connected with A . Lemma B.11 in Appendix B describes another, although very restrictive, special case where E_{AC} can be recovered exactly. Finally, part (iii) remarks that \mathcal{S} is optimal as it is the smallest possible superset of the edges in E_{AC} given the distortions found in the diagonals of $\tilde{\Theta}_{AA}$ and $\tilde{\Theta}_{CC}$. This property is reassuring as it excludes \mathcal{S} from being a trivial superset.

The following proposition restates Proposition 3.1 for the recovery of the edges in O^c when $\text{diag}(\Theta)$ is unknown in the special case $K = 2$:

PROPOSITION 3.2. *Suppose $V_1 = A \cup B$ and $V_2 = B \cup C$, where A, B, C is a partition of V . The set*

$$(3.35) \quad \mathcal{U} = (A_v \times C) \cup (A \times C_v),$$

where

$$(3.36) \quad A_v = \{i \in A : \exists j \neq i, 0 < |\tilde{\Theta}_{ij}| < v\},$$

$$(3.37) \quad C_v = \{j \in C : \exists i \neq j, 0 < |\tilde{\Theta}_{ij}| < v\},$$

contains at least $\max\{|A_v|, |C_v|\}$ true edges of O^c .

A version of \mathcal{U} based on partial correlation distortions, $\mathcal{U}^{\text{pcor}}$, can be obtained by simply replacing $\tilde{\Theta}_{ij}$ with $\tilde{R}_{ij} = -\tilde{\Theta}_{ij}(\tilde{\Theta}_{ii}\tilde{\Theta}_{jj})^{-1/2}$ and v with v_{pcor} in the equations above; $\mathcal{U}^{\text{pcor}}$ enjoys analogous properties stated by Proposition 3.2. As explained in the previous section, \mathcal{U} is more realistically feasible than $\mathcal{S} = A^* \times C^*$ in Equation (3.33), since identifying the distortions over all the diagonals of $\tilde{\Theta}$ requires too strong assumptions, while assumptions about v may be easier to formulate. Proposition 3.2 exploits Lemma B.7b in Appendix B, which states that there can be a distortion on a off-diagonal entry (i, j) of $\tilde{\Theta}_O$ only if the corresponding diagonals (i, i) and (j, j) are distorted. Unfortunately the converse is not true, meaning that $A_v \subseteq A^*$ and $C_v \subseteq C^*$ so that \mathcal{U} is not guaranteed to be a superset of E_{AC} since $\mathcal{S} = A^* \times C^*$ is minimal (Theorem 3.5 (iii)). For these reasons, the set \mathcal{U} is not defined as a simple Cartesian product. Indeed the alternate formulation $\mathcal{U}^{\text{alt}} = A_v \times C_v$ would not be guaranteed to contain any true edge. For instance, suppose $p = 15$, $A = \{1, \dots, 5\}$, $C = \{11, \dots, 15\}$, with $E_{AC} = \{(1, 11), (5, 15)\}$. Suppose $A_v = \{5\}$ and $C_v = \{11\}$. Then, while it is certain that $\mathcal{S} = \{1, 5\} \times \{11, 15\} \supseteq E_{AC}$, and that $\mathcal{U} = (\{5\} \times \{11, \dots, 15\}) \cup (\{1, \dots, 5\} \times \{11\})$ contains at least $\max\{|A_v|, |C_v|\} = 1$ true edge of O^c (in this case, it contains all of them!), $\mathcal{U}^{\text{alt}} = \{(5, 11)\}$ contains no true edge.

4. Graph recovery: finite sample analysis. In the previous section we investigated the graph quilting problem at the population level where we aim at recovering Θ and G from an incomplete true covariance matrix Σ_O . In this section we investigate the graph quilting problem in the *finite sample setting*, where the population quantity Σ_O is replaced by an *empirical estimate* $\hat{\Sigma}_O$. The finite sample setting differs substantially from the population level fundamentally for two

reasons. First, $\widehat{\Sigma}_O$ is a random quantity, so any recovered graph based on $\widehat{\Sigma}_O$ is a random object whose stochasticity and related graph recovery accuracy depend on multiple factors, primarily sample size n and number of node variables p ; such dependences need to be carefully studied, especially in high-dimensions when p can be very large compared with n . Second, $\widehat{\Sigma}_O$ is not guaranteed to be completable to a positive definite matrix, especially in high-dimensions. Indeed, the MAD_{GQ} optimization problem in Equation (2.6) based on such empirical estimate $\widehat{\Sigma}_O$ is not guaranteed to have any solution, or one with desirable statistical properties. Correspondingly, the max determinant matrix completion in Equation (2.7) based on $\widehat{\Sigma}_O$ is not guaranteed to produce any properly reconstructed sample covariance matrix, say $\widetilde{\Sigma}$. Therefore, the simple two-step procedure where $\widetilde{\Sigma}$ is first computed via Equation (2.7) and then plugged into a regularized estimation as in Equation (2.2), e.g. the graphical lasso (Yuan and Lin, 2007), would not constitute a solid approach to deal with the graph quilting estimation, especially in high-dimensions.

To deal with the graph quilting problem in finite sample settings we propose the $\text{MAD}_{GQ\text{lasso}}$, an ℓ_1 -regularized variant of the MAD_{GQ} that simultaneously performs precision matrix reconstruction and regularized estimation based on the empirical estimate $\widehat{\Sigma}_O$. The $\text{MAD}_{GQ\text{lasso}}$ estimate $\widehat{\Theta}$ is well defined in high-dimensions and converges to the MAD_{GQ} solution $\widetilde{\Theta}$ (Equation (2.6)) with rates of convergence similar to the graphical lasso (Ravikumar et al., 2011). All properties of MAD_{GQ} at the population level are inherited by $\text{MAD}_{GQ\text{lasso}}$ in the finite sample settings with high-probability whenever the sample size is sufficiently large relatively to the number of nodes. Specifically, we obtain graph estimators based on the $\text{MAD}_{GQ\text{lasso}}$ analogous to the graph recoveries based on the MAD_{GQ} specified in Section 3.2.3, and demonstrate that, for a sufficiently large sample size, these have same properties as their population counterparts. In Section 4.1 we define the various precision matrix and graph estimators. In Section 4.2 we establish the statistical properties of the estimators.

4.1. Estimators. Suppose we observe a collection of datasets $\mathbf{X}_1, \dots, \mathbf{X}_K$, where $\mathbf{X}_k \in \mathbb{R}^{n_k \times |V_k|}$ contains $n_k > 1$ joint observations about nodes $V_k \subset V$, $V_k \neq V_l, \forall k \neq l$, and $\bigcup_k V_k = V$. Note that, in the population analysis of Section 3 the case where $V_k \subset V_l$ for some $k \neq l$ was considered a trivial situation because $O = \bigcup_{j \in \{1, \dots, K\}} V_j \times V_j = \bigcup_{j \in \{1, \dots, K\} \setminus \{k\}} V_j \times V_j$. In finite sample settings we allow for these situations because they indeed affect the sample sizes of the sample covariances. We define the observed sample covariance matrix where the covariance between a pair (i, j) of variables is computed by using all available joint observations across the K datasets:

DEFINITION 4.1 (OBSERVED SAMPLE COVARIANCE). Let $X^{(1)}, \dots, X^{(n)}$ be n i.i.d. samples of a p -dimensional random vector $X^{(r)} = (X_1^{(r)}, \dots, X_p^{(r)})^T$. Let $I = [I_{ri}] \in R^{n \times p}$ be a matrix of indicators where $I_{ri} = 1$ if $X_i^{(r)}$ is observed, and $I_{ri} = 0$ otherwise. Let O be the set of pairs (i, j) that have joint sample size $n_{ij} := \sum_{r=1}^n I_{ri} I_{rj} > 1$. The observed sample covariance of X_i and X_j is

$$(4.1) \quad \widehat{\Sigma}_{ij} = \begin{cases} \widehat{m}_{ij} - \widehat{m}_i \widehat{m}_j, & (i, j) \in O \\ \mathbb{A}, & \text{otherwise,} \end{cases}$$

where

$$(4.2) \quad \widehat{m}_{ij} = \frac{\sum_{r=1}^n X_i^{(r)} X_j^{(r)} I_{ri} I_{rj}}{\sum_{r=1}^n I_{ri} I_{rj}}, \quad \widehat{m}_i = \frac{\sum_{r=1}^n X_i^{(r)} I_{ri}}{\sum_{r=1}^n I_{ri}},$$

or $\widehat{m}_i \equiv \mu_i$ if $\mathbb{E}[X_i^{(r)}] = \mu_i$ is known.

The observed sample covariance $\widehat{\Sigma}_O$ defined in Equation (4.1) is a consistent estimator of Σ_O as $n_{ij} \rightarrow \infty, \forall (i, j) \in O$. Yet, for finite n , $\widehat{\Sigma}_O$ is not guaranteed to have all principal minors positive, in which case it would not yield a proper MAD_{GQ} solution if simply plugged in Equation (2.6) in place of the population quantity Σ_O . We use regularization to overcome this problem and to further improve estimation accuracy in high-dimensions. We propose the $\text{MAD}_{GQ\text{lasso}}$, a regularized variant of the MAD_{GQ} optimization problem (Equation (2.6)) that enjoys desirable statistical properties in high-dimensions thanks to ℓ_1 penalization:

DEFINITION 4.2 (MAD_{GQlasso}). The MAD graph quilting lasso is the solution of the ℓ_1 -penalized optimization problem

$$(4.3) \quad \widehat{\Theta} = \underset{\Theta > 0, \Theta_{O^c} = 0}{\text{argmax}} \log \det \Theta - \sum_{(i,j) \in O} \Theta_{ij} \widehat{\Sigma}_{ij} - \|\Lambda \odot \Theta\|_{1,\text{off}} \quad (\text{MAD}_{GQ\text{lasso}})$$

where $\widehat{\Sigma}_{ij}$ is the observed sample covariance defined in Equation (4.1), $\|M\|_{1,\text{off}} = \sum_{i \neq j} |M_{ij}|$ is the ℓ_1 matrix norm computed only over the off-diagonals of the matrix M , $\Lambda = [\lambda_{ij}]$ is a matrix of nonnegative penalty parameters, and \odot denotes the Hadamard entrywise matrix product.

We can see that the $\text{MAD}_{GQ\text{lasso}}$ optimization problem (Equation (4.3)) combines the MAD_{GQ} problem (Equation (2.6)) with an ℓ_1 penalty over the off-diagonal entries of Θ , and imposes $\Theta_{ij} = 0$ wherever $n_{ij} < 2$. The following lemma shows that the ℓ_1 penalty guarantees Equation (4.3) to have a solution that is unique as long as the diagonals of $\widehat{\Sigma}_O$ are positive, without requiring the principal minors of $\widehat{\Sigma}_O$ to be all positive:

LEMMA 4.1. *The $MAD_{GQlasso}$ optimization problem in Equation (4.3) has a unique solution if $\|\widehat{\Sigma}_O\|_\infty < \infty$, and $\widehat{\Sigma}_{ii} > 0$ and $\lambda_{ij} > 0$, for all $i, j \in V$.*

Also the graphical lasso estimator (Yuan and Lin, 2007)

$$(4.4) \quad \widehat{\Theta}_{\text{glasso}} = \underset{\Theta > 0}{\operatorname{argmax}} \log \det \Theta - \sum_{i,j=1}^p \Theta_{ij} \widehat{\Sigma}_{ij} - \lambda \|\Theta\|_{1,\text{off}},$$

imposes an ℓ_1 penalty which enforces sparse solutions, but it assumes $O \equiv V \times V$ and $n_{ij} \equiv n \geq 2$ for any (i, j) . Therefore, the $MAD_{GQlasso}$ framework is more general than the graphical lasso, although it is an estimator of $\widetilde{\Theta}$, rather than Θ . The study of the statistical properties of the $MAD_{GQlasso}$ will prove to be more challenging than in the full data samples case of the graphical lasso. Theorem 4.1 in Section 4.2 determines the statistical behavior of the $MAD_{GQlasso}$ in high-dimensions.

In the following definition we specify two graph structure estimators, which are finite sample versions of the graph structure recoveries \mathcal{E}_S and \mathcal{E}_U defined in Section 3.2.3:

DEFINITION 4.3 (**GRAPH STRUCTURE ESTIMATORS**). *Let $\widehat{\Theta}$ be the $MAD_{GQlasso}$ estimator (Equation 4.3) based on the observed empirical covariance matrix $\widehat{\Sigma}_O$ (Equation 4.1). Let $\widehat{\mathcal{F}}_\xi$ and $\widehat{\mathcal{U}}_{\xi_1, \xi_2}$ be equal to, respectively, the outputs of the RECO Algorithm 3.1 ($\operatorname{diag}(\Theta)$ known) and the RECO Algorithm 3.2 ($\operatorname{diag}(\Theta)$ unknown) using $\widehat{\Theta}$ in place of Θ , and let $\tau, \xi, \xi_1, \xi_2 \in \mathbb{R}$ be hyperparameters. We define the following graph structure estimators:*

$$(4.5) \quad \widehat{\mathcal{E}}_S^{\tau, \xi} = \left\{ (i, j) \in O : |\widehat{\Theta}| > \tau \right\} \cup \widehat{\mathcal{F}}_\xi \quad (\text{DIAG}(\Theta) \text{ KNOWN})$$

and

$$(4.6) \quad \widehat{\mathcal{E}}_U^{\tau, \xi_1, \xi_2} = \left\{ (i, j) \in O : |\widehat{\Theta}| > \tau \right\} \cup \widehat{\mathcal{U}}_{\xi_1, \xi_2} \quad (\text{DIAG}(\Theta) \text{ UNKNOWN})$$

Of course, a variant of $\widehat{\mathcal{E}}_U^{\tau, \xi_1, \xi_2}$ based on partial correlations, say $\widehat{\mathcal{E}}_U^{\text{pcor}, \tau, \xi_1, \xi_2}$, can also be obtained analogously to $\mathcal{U}_U^{\text{pcor}}$ in Section 3.2.3. The statistical properties of these estimators are established in Theorems 4.2 and 4.3 in Section 4.2.2. Each graph estimator requires the penalty parameter Λ and a parameter τ to obtain an estimate of E_O . The optimal parameter Λ is given by Theorem 4.1 and, in practice, it may be chosen using cross-validation or stability (Fan et al., 2009; Liu et al., 2010). Under the assumptions of Theorem 4.2 the oracle parameter of τ is $\tau = \nu/2$ (Equation (3.3)) for $\widehat{\mathcal{E}}_S^{\tau, \xi}$ and $\widehat{\mathcal{E}}_U^{\tau, \xi_1, \xi_2}$, and $\tau = \nu_{\text{pcor}}/2$ (Equation (3.5)) for $\widehat{\mathcal{E}}_U^{\text{pcor}, \tau, \xi_1, \xi_2}$. In

practice, whenever some basic knowledge about the graph is available, it may be possible to reasonably approximate the threshold τ for any estimator. For instance, suppose it is safe to assume that the proportion of edges in O is approximately equal to $\pi_O \in [0, 1]$. Then, perhaps, the parameter τ may be chosen so that the estimate of E_O , say $\widehat{E}_O^\tau := \widehat{\mathcal{E}}_{S,O}^{\tau,\xi} = \widehat{\mathcal{E}}_{U,O}^{\tau,\xi_1,\xi_2}$, contains no more than a proportion π_O of edges, that is

$$\tau^* = \min \{t : |\widehat{E}_O^t| \leq \pi_O \times |O|\}$$

Analogous argument can be done in terms of τ_{pcor} in relation to $\widehat{\mathcal{E}}_U^{\text{pcor},\tau,\xi_1,\xi_2}$.

While $\widehat{\mathcal{E}}_S^{\tau,\xi}$ requires $\text{diag}(\Theta)$ and ξ to produce an estimate of the superset \mathcal{S} , the estimator $\widehat{\mathcal{E}}_U^{\tau,\xi_1,\xi_2}$ only needs two parameters ξ_1 and ξ_2 . Thus, it is reasonable to conclude that $\widehat{\mathcal{E}}_U^{\tau,\xi_1,\xi_2}$ is more realistically feasible than $\widehat{\mathcal{E}}_S^{\tau,\xi}$ because knowledge of $\text{diag}(\Theta)$ is very unrealistic. Theorem 4.3 provides the oracle parameters for ξ_1 and ξ_2 for the exact recovery of the set \mathcal{U} with high-probability. In order to choose ξ_1 and ξ_2 in practice, at least two options are possible: (i) we simply set $\xi_1 = 0$ and $\xi_2 = \tau$ and accept the possibility of detecting several false distortions, which in turn may lead to too large a set $\widehat{\mathcal{U}}$ containing many false positives; (ii) we use the bootstrap to approximate the standard deviation sd_{ijk} of $|\widehat{\Theta}_{ijk}^{(k)}|$ – the finite sample counterpart of Equation (3.26) based on the $\text{MAD}_{GQlasso}$ estimator $\widehat{\Theta}$ – for all i, j, k , and then set $\xi_1 = 2 \max_{ijk} \text{sd}_{ijk}$ and $\xi_2 = \nu - 2 \max_{ijk} \text{sd}_{ijk}$. However, the accurate theoretical study of all these possible solutions is beyond the scope of this paper, and it is left to our future research.

4.2. Statistical properties of the estimators. In this section we establish the statistical guarantees for the estimators proposed in Section 4.1. We first specify the statistical framework of analysis by stating some assumptions (Assumptions 4.1). We then state three theorems: Theorem 4.1, which establishes the rates of convergence of the $\text{MAD}_{GQlasso}$ $\widehat{\Theta}$ (Equation 4.3) as an estimator of the MAD_{GQ} recovered precision matrix Θ (Equation 2.6), and Theorems 4.2 and 4.3, which establish, respectively, the high-dimensional graph structure recovery guarantees of $\widehat{\mathcal{E}}_S^{\tau,\xi}$ (Equation (4.5)) and of $\widehat{\mathcal{E}}_U^{\tau,\xi_1,\xi_2}$ (Equation (4.6)).

4.2.1. Assumptions. To investigate the statistical behavior of the $\text{MAD}_{GQlasso}$ in high-dimensions and the related graph structure estimators $\widehat{\mathcal{E}}_S^{\tau,\xi}$ and $\widehat{\mathcal{E}}_U^{\tau,\xi_1,\xi_2}$, we first need to impose some assumptions to put the problem into a sufficiently general but manageable framework. Several of our assumptions match those of Ravikumar et al. (2011), who proved that the graphical lasso estimator (Equation (4.4)) is sparse-consistent for Θ – graph structure consistency – and concentrates about Θ in elemen-

twice ℓ_∞ -norm with rates expressed in terms of tail conditions on the probability concentration inequalities of the empirical covariances. The results of Ravikumar et al. (2011) are quite general as they do not require the data to be Gaussian, but that the aforementioned tail conditions are of exponential or polynomial type; in the special case of Gaussian data the convergence rate of the graphical lasso can be expressed as $\mathcal{O}(\sqrt{\log p/n})$. However, our situation is quite different in several aspects, so we need to depart from Ravikumar et al. (2011) in several aspects. Indeed, the $\text{MAD}_{GQlasso}$ estimator $\widehat{\Theta}$ (Equation (4.3)) is based on a partially observed sample covariance matrix $\widehat{\Sigma}_O$, whereas the graphical lasso uses a fully observed sample covariance matrix. This requires us to make assumptions about the observed pairs set O and the heterogeneous sample sizes across the entries of $\widehat{\Sigma}_O$. Moreover, our graph estimators $\widehat{\mathcal{E}}_S^{r,\xi}$ and $\widehat{\mathcal{E}}_U^{r,\xi_1,\xi_2}$ involve several additional matrix manipulations, such as thresholding and the RECO algorithms 3.1 and 3.2. The ensemble of all those operations makes the study of the graph estimation performance more intricate, requiring a delicate assessment of uncertainty propagation.

We make the following assumptions:

ASSUMPTIONS 4.1. *Let $n_{ij} = \sum_{r=1}^n I_{ri}I_{rj}$ be the joint sample size for node pair (i, j) (Definition 4.1), and let $O = \{(i, j) : n_{ij} > 1\}$ be the observed set of node pairs with minimum joint sample size $\bar{n} = \min_{(i,j) \in O} n_{ij}$. Let $\widetilde{\Theta}$ be the MAD_{GQ} precision matrix (Equation 2.6) based on the observed portion of the population covariance matrix Σ_O (Equation (2.6)), and let $\widetilde{\Sigma} = \widetilde{\Theta}^{-1}$ and $\widetilde{E} = \{(i, j) : \widetilde{\Theta}_{ij} \neq 0\}$. Let*

$$(4.7) \quad \omega = \min_{i: \widetilde{\Theta}_{ii} < \Theta_{ii}} |\Theta_{ii} - \widetilde{\Theta}_{ii}|,$$

where $\widetilde{\Theta}_{ii}$ is defined in Equation (3.19) of the RECO Algorithm 3.1. Moreover, let $\sigma(n, \epsilon) = \max_{(i,j) \in O} \sigma_{ij}(n, \epsilon)$, where

$$(4.8) \quad \sigma_{ij}(n, \epsilon) = \inf\{\sigma \geq 0 : P(|\widehat{\Sigma}_{ij,n} - \Sigma_{ij}| > \sigma) \leq \epsilon^{-1}\}$$

specifies the tail condition of the empirical covariance $\widehat{\Sigma}_{ij,n} := \widehat{\Sigma}_{ij}$ with sample size $n_{ij} = n$ (Equation (4.1)). We assume

- A1. For all $i \in V$, $n_{ii} > 1$.
- A2. For any p , $|O^c| = \lceil \eta p^2 \rceil$, for some $\eta < 1$.
- A3. $\exists \alpha \in (0, 1]$ such that $\max_{e \in \widetilde{E}^c} \|\Gamma_{e\widetilde{E}}(\Gamma_{\widetilde{E}\widetilde{E}})^{-1}\|_1 \leq 1 - \alpha$, where $\Gamma = \widetilde{\Sigma} \otimes \widetilde{\Sigma}$.
- A4. $\sigma(n, \epsilon)$ is nonincreasing with n and nondecreasing with $\epsilon \in (1, \infty)$.
- A5. The maximum node degree is $d := \max_{i=1,\dots,p} \|\Theta_{i, V \setminus \{i\}}\|_0 \geq 1$.

Assumption A1 guarantees that $(i, i) \in O, \forall i \in V$, so that all diagonals of Σ and $\widehat{\Sigma}$ are included in Σ_O and $\widehat{\Sigma}_O$, respectively. Assumption A2 introduces the parameter η , which measures the relative size of O^c . We will see that, even though a smaller η means more observed node pairs, a larger η also implies a higher probability of concentration of $\widehat{\Theta}$ about $\widetilde{\Theta}$. Indeed, a smaller set O translates into less parameters to estimate as a larger portion Θ_{O^c} is set to zero in Equation (4.3). Assumption A3 is the same mutual incoherence condition in Ravikumar et al. (2011), except that it is imposed on $\widetilde{\Theta}$ rather than Θ . The mutual incoherence condition limits the influence of the pairs of disconnected nodes on the pairs of connected nodes. Assumption A4 guarantees that the observed sample covariances concentrate around their target values as the sample size increases. Finally, A5 specifies the node degree of the graph.

4.2.2. *Main theorems.* The following theorem establishes the rate of convergence of $\widehat{\Theta}$ as an estimator of $\widetilde{\Theta}$:

THEOREM 4.1 (CONVERGENCE RATE OF $\text{MAD}_{\text{GQlasso}}$). *Suppose Assumptions 4.1 hold, and let $\Lambda_{ij} = \lambda_{p, \bar{n}} = \frac{\beta}{\alpha} \sigma(\bar{n}, p^\gamma)$ with $\gamma > 2$, for all $(i, j) \in O$. There exist a minimal sample size \bar{n}^* (Equation (A.2)) and a scalar $C > 0$ depending on α and Γ defined in A3, such that for any $\bar{n} \geq \bar{n}^*$*

$$(4.9) \quad \|\widehat{\Theta} - \widetilde{\Theta}\|_\infty \leq C\sigma(\bar{n}, p^\gamma)$$

with probability larger than $1 - (1 - \eta)p^{2-\gamma}$, where $\|*\|_\infty$ is the elementwise ℓ_∞ norm.

Equation (4.9) induces a hyper-cubic region centered at the target parameter $\widetilde{\Theta}$. For a fixed parameter $\gamma > 2$, the estimator $\widehat{\Theta}$ lies in this region with probability larger than $1 - (1 - \eta)p^{2-\gamma}$. The size of this region decreases as the minimal sample size \bar{n} increases, and increases with the number of nodes p according to the tail condition on the empirical covariance estimator (Equation (4.8)). A larger γ systematically yields a larger hyper-cube and, correspondingly, a larger guaranteed probability of concentration for any given \bar{n} and p . Also, a larger η , which measures the relative size of O^c , yields a larger probability of concentration. The latter is an important aspect of the $\text{MAD}_{\text{GQlasso}}$: while the rate of convergence in Equation (4.9) matches the one of the graphical lasso (Ravikumar et al., 2011), the guaranteed probability of concentration of $\widehat{\Theta}$ around $\widetilde{\Theta}$, i.e. $1 - (1 - \eta)p^{2-\gamma}$, is larger than the probability of concentration of the graphical lasso about Θ with full sample covariances, i.e. $1 - p^{2-\gamma}$. Indeed, this is because $\widehat{\Theta}$ has less parameters to

estimate, as $\widehat{\Theta}_{O^c}$ has been constrained to be zero, which is beneficial since, by definition, $\widetilde{\Theta}_{O^c} = 0$. The proof of Theorem 4.1 in Appendix A builds upon the one of Theorem 1 in Ravikumar et al. (2011) for the convergence rates of the graphical lasso, but it departs from it in several aspects because of the additional constraint $\Theta_{O^c} = 0$ of the $\text{MAD}_{GQlasso}$ (Equation (4.3)) and the diverse sample sizes across the entries of the partially observed empirical covariance matrix $\widehat{\Sigma}_O$.

For the special case of Gaussian data, the rate of convergence established by Theorem 4.1 takes the explicit form given in the following corollary:

COROLLARY 4.1 (CONVERGENCE RATE IN THE GAUSSIAN CASE). *Suppose the conditions of Theorem 4.1 hold. If the data are i.i.d. multivariate Gaussian, then there exists a scalar $C > 0$ depending on α , Γ , and γ such that Equation (4.9) reduces to*

$$(4.10) \quad \|\widehat{\Theta} - \widetilde{\Theta}\|_\infty \leq C \sqrt{\frac{\log p}{\bar{n}}}$$

This corollary shows that with Gaussian data the minimal sample size \bar{n} needs to scale with the logarithm of the number of nodes p in order to guarantee concentration of $\widehat{\Theta}$ about $\widetilde{\Theta}$.

Although it is also possible to show that the $\text{MAD}_{GQlasso}$ estimator (Equation (4.3)) is sparsistent for $\widetilde{\Theta}$ (that is, under some conditions, $\widehat{\Theta}$ has same graphical structure as $\widetilde{\Theta}$ with high probability), because we build the graph estimators $\widehat{\mathcal{E}}_S^{\tau, \xi}$ and $\widehat{\mathcal{E}}_U^{\tau, \xi_1, \xi_2}$ (Definition 4.3) via thresholding strategies and the application of the RECO algorithms (3.1 and 3.2), such sparsistency result is not necessary. In fact, we only need to exploit the bound in Equation (4.9) to show that, whenever $\widehat{\Theta}$ gets sufficiently close to $\widetilde{\Theta}$, the graph estimators $\widehat{\mathcal{E}}_S^{\tau, \xi}$ and $\widehat{\mathcal{E}}_U^{\tau, \xi_1, \xi_2}$ (with appropriate choice of parameters τ, ξ, ξ_1, ξ_2) match their population level counterparts \mathcal{E}_S and \mathcal{E}_U (Section 3.2.3) with high probability. We establish the statistical guarantees of the two graph structure estimators separately in two theorems, Theorem 4.2 and Theorem 4.3. In these two theorems, while the statements about the recovery in O are identical, the properties of the recovered edges of O^c differ as they are based on the two different RECO Algorithms 3.1 and 3.2, where the first assumes $\text{diag}(\Theta)$ known and the second does not.

In the following theorem we establish the high-dimensional graph structure recovery guarantees provided by the graph structure estimator $\widehat{\mathcal{E}}_S^{\tau, \xi}$ when $\text{diag}(\Theta)$ is known (Equation (4.5)):

THEOREM 4.2 (FINITE SAMPLE GRAPH RECOVERY – $\text{diag}(\Theta)$ KNOWN).
 Suppose Assumptions 4.1 hold, and further assume $\delta < \nu/2$ (Equations (3.2) and (3.3)). Moreover, let $\Lambda_{ij} = \lambda_{p,\bar{n}} = \frac{8}{\alpha} \sigma(\bar{n}, p^\gamma)$ with $\gamma > 2$ for all $(i, j) \in O$, and let $\widehat{\mathcal{E}}_S \equiv \widehat{\mathcal{E}}_S^{\nu/2, -\omega/2}$ be as in Equation (4.5) where we set $\tau = \nu/2$ and $\xi = -\omega/2$ (Equation (4.7)). Then

(i). EXACT GRAPH RECOVERY IN O .

For $\bar{n} > \bar{n}_O^* = \max\{\bar{n}^*, \min\{n : C\sigma(n, p^\gamma) \leq \nu/2 - \delta\}\}$, where C is a scalar depending on α and Γ , with probability larger than $1 - (1 - \eta)p^{2-\gamma}$ we have

$$(4.11) \quad \widehat{\mathcal{E}}_{S,O} = E_O$$

(ii). NO FALSE NEGATIVES IN O^c .

For $\bar{n} > \bar{n}_{\mathcal{S}}^* = \max\{\bar{n}^*, \min\{n : D\sqrt{d}p\sigma(n, p^\gamma) \leq \omega/2\}\}$, where D is a scalar depending on α and Γ , with probability larger than $1 - (1 - \eta)p^{2-\gamma}$ we have

$$(4.12) \quad \widehat{\mathcal{E}}_{S,O^c} = \mathcal{S} \supseteq E_{O^c},$$

where \mathcal{S} is the superset of edges of O^c (Equation (3.22)).

Theorem 4.2 states the conditions under which, with high probability, the graph structure estimator $\widehat{\mathcal{E}}_S$ exactly recovers the true graph structure in O (E_O) and the superset of edges in O^c ($\mathcal{S} \supseteq E_{O^c}$, Equation (3.22)) obtained via the RECO Algorithm 3.1. Specifically, part (i) of the theorem combines the theorem on the exact graph recovery in O (Theorem 3.2) with the theorem on the rate of convergence of the $\text{MAD}_{\text{GQlasso}}$ (Theorem 4.1), thereby identifying the conditions that guarantee $\widehat{\Theta}$ to be sufficiently close to $\widetilde{\Theta}$ to let us threshold it appropriately as per Theorem 3.2. Part (ii) of the theorem combines the theorem on the superset of edges in O^c (Theorem 3.4) with the theorem on the rate of convergence of the $\text{MAD}_{\text{GQlasso}}$ (Theorem 4.1), demonstrating that also in the finite sample setting it is possible to recover all the edges in O^c with high probability. We can see that, in both parts of the theorem, the required sample sizes \bar{n}_O^* and $\bar{n}_{\mathcal{S}}^*$ decrease with $\nu/2 - \delta$ (positive by assumption) and with ω (Equation (4.7)). This is reasonable because: (a) $\nu/2 - \delta$ is the maximum distortion allowed between $\widehat{\Theta}$ and $\widetilde{\Theta}$ to guarantee $\widehat{\delta} := \max_{(i,j) \in O, i \neq j} |\Theta_{ij} - \widehat{\Theta}_{ij}| \leq \nu/2$, allowing us to apply Theorem 3.2 on $\widehat{\Theta}$ rather than on $\widetilde{\Theta}$ for the exact recovery of E_O with high-probability; (b) ω is the smallest of the nonzero distances $|\widetilde{\Theta}_{ii} - \Theta_{ii}|$, $i = 1, \dots, p$, where $\widetilde{\Theta}_{ii}$ and Θ_{ii} are key quantities of the RECO Algorithm 3.1 as it is built upon the detection of instances where $\widetilde{\Theta}_{ii} < \Theta_{ii}$ – the tighter the inequality is, the more difficult it is to verify it accurately. Hence, in both cases, a larger minimal sample size is required when

$v/2 - \delta$ or ω are smaller because the distinction between signal and noise becomes subtler. Corollary 4.2 provides more explicit expressions of the minimal required sample sizes \bar{n}_O^* and $\bar{n}_{\mathcal{O}}^*$ for the case of Gaussian data.

In the following theorem we establish the high-dimensional graph structure recovery guarantees provided by the graph structure estimator $\widehat{\mathcal{E}}_U^{\tau, \xi_1, \xi_2}$ when $\text{diag}(\Theta)$ is unknown (Equation (4.6)):

THEOREM 4.3 (FINITE SAMPLE GRAPH RECOVERY – $\text{diag}(\Theta)$ UNKNOWN). *Suppose Assumptions 4.1 hold, and further assume $\delta < v/2$ (Equations (3.2) and (3.3)) and let $\Lambda_{ij} = \lambda_{p, \bar{n}} = \frac{\alpha}{\alpha} \sigma(\bar{n}, p^\gamma)$ with $\gamma > 2$ for all $(i, j) \in O$. Moreover, let $\widehat{\mathcal{E}}_U \equiv \widehat{\mathcal{E}}_U^{v/2, \psi_1, v - \psi_2}$ be as in Equation (4.5) where we set $\tau = v/2$ and $\xi_1 = \psi_1$ and $\xi_2 = v - \psi_2$ with*

$$(4.13) \quad \psi_1 = \min_{0 < \widetilde{\Theta}_{ijk}^{(k)} < v} |\widetilde{\Theta}_{ijk}^{(k)}|/2 \quad \text{and} \quad \psi_2 = \left(v - \max_{0 < \widetilde{\Theta}_{ijk}^{(k)} < v} |\widetilde{\Theta}_{ijk}^{(k)}| \right)/2$$

where $\widetilde{\Theta}_{ijk}^{(k)}$ is defined in Equation (3.27) of Algorithm 3.2. Then

(i). EXACT GRAPH RECOVERY IN O .

For $\bar{n} > \bar{n}_O^* = \max\{\bar{n}^*, \min\{n : C\sigma(n, p^\gamma) \leq v/2 - \delta\}\}$, where C is a scalar depending on α and Γ , with probability larger than $1 - (1 - \eta)p^{2-\gamma}$ we have

$$(4.14) \quad \widehat{\mathcal{E}}_{U, O} = E_O$$

(ii). MINIMAL EDGE RECOVERY IN O^c .

For $\bar{n} > \bar{n}_{\mathcal{O}}^* = \max\{\bar{n}^*, \min[n : D\sqrt{d}p\sigma(n, p^\gamma) \leq \min(\psi_1, \psi_2)]\}$, where D is a scalar depending on α and Γ , with probability larger than $1 - (1 - \eta)p^{2-\gamma}$ we have

$$(4.15) \quad \widehat{\mathcal{E}}_{U, O^c} = \mathcal{U},$$

where \mathcal{U} is the set in Equation (3.29) containing at least N edges of O^c (Equation (3.30)).

Theorem 4.2 states the conditions under which, with high probability, the graph structure estimator $\widehat{\mathcal{E}}_U$ exactly recovers the true graph structure in O (E_O) and the set \mathcal{U} in Equation (3.29) containing at least N edges of O^c (Equation (3.30)). The condition $\bar{n} > \bar{n}_{\mathcal{O}}^*$ guarantees that, with probability larger than $1 - (1 - \eta)p^{2-\gamma}$, the estimator $\widehat{\Theta}_{ijk}^{(k)}$ is sufficiently close to $\widetilde{\Theta}_{ijk}^{(k)}$ so that, for any i, j, k , the condition $\psi_1 < |\widehat{\Theta}_{ijk}^{(k)}| < v - \psi_2$ is equivalent to $0 < |\widetilde{\Theta}_{ijk}^{(k)}| < v$, which is the condition used

in Equation (3.27) of the RECO Algorithm 3.2 with $\xi_1 = 0, \xi_2 = \nu$. Theorem 4.3 may also be restated in terms of $\widehat{\mathcal{E}}_U^{\text{pcor}}$ by replacing $\widetilde{\Theta}^{(k)}$ by its standardized version $\widetilde{R}^{(k)} = -\text{diag}(\widetilde{\Theta}^{(k)})^{-\frac{1}{2}} \widetilde{\Theta}^{(k)} \text{diag}(\widetilde{\Theta}^{(k)})^{-\frac{1}{2}}$, and ν by ν_{pcor} .

The following corollary provides more explicit expressions of the minimal sample sizes $\bar{n}_O^*, \bar{n}_{\mathcal{S}}^*, \bar{n}_{\mathcal{U}}^*$ used in Theorems 4.2 and 4.3 for the case of Gaussian data:

COROLLARY 4.2 (SAMPLE COMPLEXITY IN THE GAUSSIAN CASE). *Suppose the conditions of Theorem 4.1 hold. If the data are i.i.d. multivariate Gaussian then the minimal joint sample sizes $\bar{n}_O^*, \bar{n}_{\mathcal{S}}^*$, and $\bar{n}_{\mathcal{U}}^*$ required in Theorems 4.2 and 4.3 are*

$$(4.16) \quad \bar{n}_O^* = \max \left\{ \bar{n}^*, C_O \frac{\log p}{(\nu/2 - \delta)^2} \right\} \quad (\text{GRAPH IN } O)$$

$$(4.17) \quad \bar{n}_{\mathcal{S}}^* = \max \left\{ \bar{n}^*, C_{\mathcal{S}} \frac{dp \log p}{\omega^2} \right\} \quad (\text{GRAPH IN } O^c - \text{DIAG}(\Theta) \text{ KNOWN})$$

$$(4.18) \quad \bar{n}_{\mathcal{U}}^* = \max \left\{ \bar{n}^*, C_{\mathcal{U}} \frac{dp \log p}{\min(\psi_1, \psi_2)^2} \right\} \quad (\text{GRAPH IN } O^c - \text{DIAG}(\Theta) \text{ UNKNOWN})$$

where $C_O, C_{\mathcal{S}}$, and $C_{\mathcal{U}}$ are scalars depending on α, Γ , and γ .

We can see that the minimum theoretical sample sizes to achieve graph structure recovery as per Theorems 4.2 and 4.3 depend on the parameters δ, ν, ω , and ψ_i . The smaller the quantities $\nu/2 - \delta, \omega$, and $\min\{\psi_1, \psi_2\}$ are, the subtler the distinction between signal and noise becomes, and therefore a larger sample size is required to achieve exact recovery of E_O, \mathcal{S} or \mathcal{U} .

5. Simulations. We now illustrate the statistical properties of the $\text{MAD}_{GQ\text{lasso}}$ with an extensive simulation study. We generate Gaussian data with various choices of number of nodes p , nodal degree d , sample size n , relative size of O^c measured by $\eta = |O^c|/p^2 \in [0, 1)$ (see Assumptions 4.1), and with graph G belonging to one of the following classes illustrated in Figure 4(A):

- (i) *Chain* ($d = 2$).
- (ii) *Loop* ($d = 2$).
- (iii) *Star* ($1 \leq d \leq p$).
- (iv) *Tree* (binary case, $d = 3$).

- (v) *Spatial model* $S(p, w, r)$, where nodes have spatial positions $w = \{w_1, \dots, w_p\}$, and nodes (i, j) are connected if their distance $D_{ij} = \|w_i - w_j\|_2$ is below r .
- (vi) *Erdős-Rényi model* $ER(p, \pi)$ (Erdős and Rényi, 1959), where the edges are randomly assigned to node pairs independently with probability π . The expected node degree is equal to $p\pi$.
- (vii) *Barabási-Albert model* $BA(p, p_0)$ (Albert and Barabási, 2002), where $p_0 < p$ is the initial number of connected nodes, and the other $p - p_0$ nodes are sequentially added to the network by connecting each of them to an existing node i of degree d_i with probability proportional to $d_i / \sum_k d_k$.
- (viii) *Spatial-Random model* $SR(p, w, f)$, where nodes have spatial positions $w = \{w_1, \dots, w_p\}$, and a pair (i, j) is connected with probability $\pi_{ij} = f(D_{ij})$, where f is a decreasing function of the distance $D_{ij} = \|w_i - w_j\|_2$, e.g. $f(x) = e^{-ax}$, $a > 0$. This model produces networks that reflect the spatial neuronal functional connectivity structure observed in some brain cortical areas (Vinci et al., 2018a,b), where two neurons are more likely to be conditionally independent when physically farther apart (D_{ij} large).

In Section 5.1 we verify the rates of convergence postulated by Theorem 4.1, while in Section 5.2 we assess the graph recovery performance based on the graph estimators in Definition 4.3. Throughout these sections we set $\lambda_{ij} \equiv \lambda, \forall i \neq j$ in Equation (4.3), denoting the $\text{MAD}_{GQ\text{lasso}}$ estimator by $\widehat{\Theta}(\lambda)$, and, to avoid our conclusions depend on a specific tuning selection criterion, in several occasions we pick $\lambda^* = \arg \min_{\lambda \geq 0} \|\widehat{\Theta}(\lambda) - \widetilde{\Theta}\|_\infty$, which produces the oracle $\text{MAD}_{GQ\text{lasso}}$ denoted by $\widehat{\Theta}(\lambda^*)$. This oracle quantity may be viewed as the best possible evaluation of $\widehat{\Theta}(\lambda)$ as an estimator of $\widetilde{\Theta}$ that could ever be achieved with any penalty parameter selection criterion that aims at minimizing the ℓ_∞ distortion between $\widehat{\Theta}(\lambda)$ and $\widetilde{\Theta}$. Similarly, we denote the oracle graphical lasso (Equation (4.4)) by $\widehat{\Theta}(\lambda^{**})$, where $\lambda^{**} = \arg \min_{\lambda \geq 0} \|\widehat{\Theta}(\lambda) - \Theta\|_\infty$. All ground truth precision matrices used here have diagonals equal to 1, while the nonzero off-diagonals have magnitude p^{-1} , 25% of which are positive and 75% are negative (correspondingly, 75% of nonzero partial correlations are positive). We ensure all matrices satisfy Assumptions 4.1. We create graph quilting scenarios by assuming the observed nodal sets $V_1, \dots, V_K \subset V$ to be given by

$$(5.1) \quad V_k = \left\{ 1 + \left\lfloor \frac{k-1}{K-1} (p - q_0) \right\rfloor, \dots, q_0 + \left\lceil \frac{k-1}{K-1} (p - q_0) \right\rceil \right\},$$

where $p/K < q_0 < p$ so that $|V_k| \approx q_0, \forall k = 1, \dots, K$, and a smaller q_0 implies a larger η , and vice versa. To avoid this specific observational scheme causes any loss of generality, all precision matrices built as described above have their rows

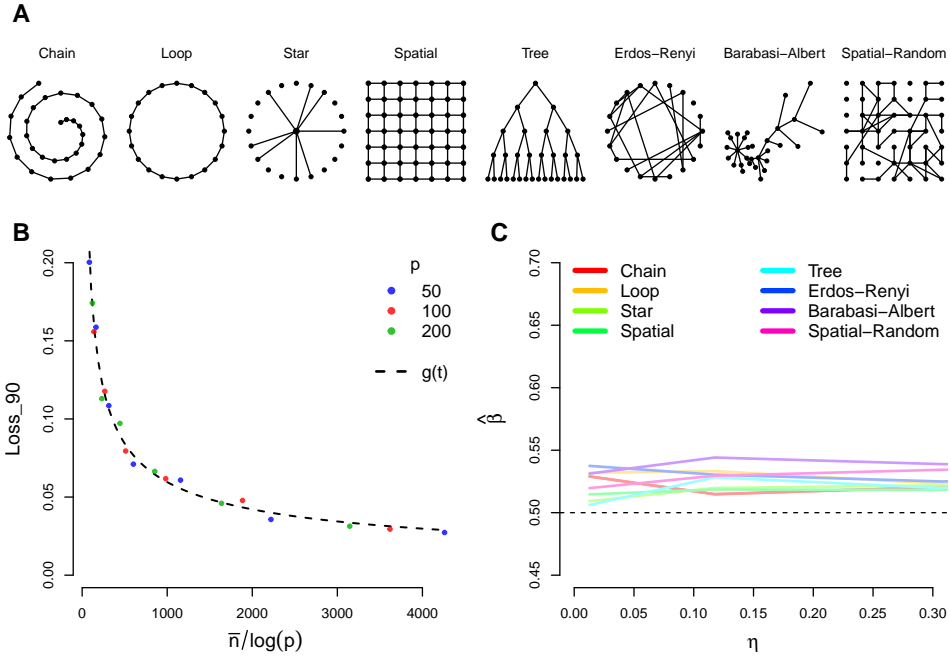


FIG 4. Convergence rate of $MAD_{GQlasso}$. (A) Classes of graphs used in simulations. (B) $LOSS_{90}$ for chain graphs of various number p of nodes plotted versus the rescaled minimum sample size $\bar{n}/\log p$. All curves concentrate about $g(t) = Ct^{-\beta}$, with $\beta = 1/2$ and some constant $C > 0$ (dashed curve fitted using least squares), in agreement with Equation (4.10). (C) Fitted $\hat{\beta}$ versus η for various graph structures. In all cases $\hat{\beta} \geq 1/2$.

and columns finally randomly permuted so that the set O^c approximately contains $\eta \times 100\%$ of the total edges.

5.1. *Simulation 1 – Rates of convergence.* Given a $p \times p$ precision matrix Θ with graph belonging to one of the classes (i)-(viii) listed above, we generate $N = 100$ datasets of n Gaussian random vectors $X^{(1)}, \dots, X^{(n)} \stackrel{i.i.d.}{\sim} N(0, \Theta^{-1})$. Then, for a given observational scheme as per Equation (5.1) with $K = 3$ and missingness proportion η , we compute the N corresponding oracle $MAD_{GQlasso}$ estimates $\hat{\Theta}(\lambda^*)$, and the related ℓ_1 distortions $\|\hat{\Theta}(\lambda^*) - \tilde{\Theta}\|_\infty$. In Figure 4(A) we illustrate the results for the case of a chain graph and missingness proportion $\eta = .1$. We compute the 90th empirical quantile of the N computed ℓ_1 distortions ($LOSS_{90}$) and plot it versus the scaled minimum joint sample size $\bar{n}/\log p$ for $p \in \{50, 100, 200\}$ and $500 \leq n \leq 50000$. This graph shows that the ℓ_1 distortion $\|\hat{\Theta}(\lambda^*) - \tilde{\Theta}\|_\infty$ at a given scaled sample size $\bar{n}/\log p$ is below the displayed curves with probability at least 0.9. All curves concentrate about the function $g(t) = Ct^{-\beta}$ (dashed curve),

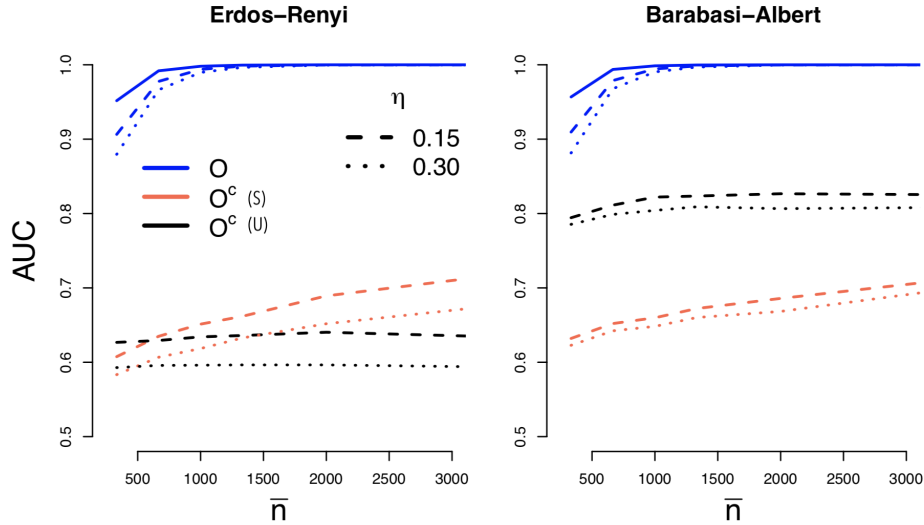


FIG 5. Performance of the graph estimators $\widehat{\mathcal{G}}_S^{\tau, \xi}$, $\widehat{\mathcal{G}}_U^{\tau, \xi_1, \xi_2}$ (Definition 4.3). We display the AUC in O (blue curves) and O^c (black and red curves) as functions of the minimal joint sample size \bar{n} and relative size of O^c given by η for two graph types with $p = 100$ nodes: Erdős-Rényi $ER(p = 100, \pi = 0.05)$ and Barabási-Albert $BA(p = 100, p_0 = 1)$. The AUC in O degrades with η but steadily increases with \bar{n} converging to 1 for any η . On the other hand, the AUC in O^c is based either on the set $\widehat{\mathcal{G}}_{S, O^c} = \widehat{\mathcal{F}}_\xi$ (red curve) or the set $\widehat{\mathcal{G}}_{U, O^c} = \widehat{\mathcal{U}}_{\xi_1, \xi_2}$ (black curve); the likely presence of false positives can produce a low specificity explaining the systematically lower AUC that, however, stays well above the level 0.5 of random edge assignment.

where $\beta = 1/2$ and $C > 0$ is a constant. This result confirms the rate of convergence established in Equation (4.10). We further repeat the simulation in (A) for several other graph structures and proportions of missingness $\eta \in (0, .3]$. For each case, we regress LOSS_{90} on $t = \bar{n} / \log p$ assuming the regression form $g(t) = Ct^{-\beta}$. In Figure 4(B) we plot the fitted $\widehat{\beta}$ versus η . We can see that for any η the estimated β is slightly larger than $1/2$, indeed confirming an even slightly faster rate of convergence than in Equation (4.10).

5.2. *Simulation 2 – Graph recovery performance.* We now investigate the graph recovery performance of the graph structure estimators $\widehat{\mathcal{G}}_S^{\tau, \xi}$ and $\widehat{\mathcal{G}}_U^{\tau, \xi_1, \xi_2}$ in Definition 4.3. We consider several scenarios with various values of minimal joint sample size \bar{n} and relative size of O^c given by η , for the estimation of the graph models (vi)-(viii) with $p = 100$ nodes: Erdős-Rényi $ER(p = 100, \pi = 0.05)$ and Barabási-Albert $BA(p = 100, p_0 = 1)$. We quantify the graph performance in terms of the area under the ROC curve (AUC), which summarizes the sensitivity and specificity across changes of the penalty parameter λ and the hyperparameters τ , ξ , ξ_1 and ξ_2

(Definition 4.3). Figure 5 displays the AUC in O (blue curves) and O^c (black and red curves) as functions of the minimal joint sample size \bar{n} and relative size of O^c given by η for the two graph types. The AUC in O degrades with η but steadily increases with \bar{n} converging to 1 for any η . On the other hand, the AUC in O^c is based either on the set $\widehat{\mathcal{E}}_{S,O^c} = \widehat{\mathcal{F}}_{\xi}$ (red curve) or the set $\widehat{\mathcal{E}}_{U,O^c} = \widehat{\mathcal{U}}_{\xi_1, \xi_2}$ (black curve); the likely presence of false positives can produce a low specificity explaining the systematically lower AUC that, however, stays well above the level 0.5 of random edge assignment.

6. Neuronal functional connectivity estimation from nonsimultaneous calcium imaging recordings. As explained in Section 1.2, neuronal functional connectivity is the statistical dependence structure of neurons’ activities. Estimating functional connectivity from *in vivo* neuronal recordings helps us understand how neurons interact with one another while they process information under different stimuli and other experimental conditions. The study of functional connectivity enables us to understand the functions, and potentially the structure, of neuronal circuits, but also the causes of their dysfunction that characterize various brain disorders (Baggio and Junqué, 2019; Engels et al., 2018; Cai et al., 2018). The functional connectivity of p neurons can be described by means of a conditional dependence graph, where p nodes represent the neurons, and an edge connects two nodes if and only if the activities of the corresponding neurons are dependent conditionally on the activity of all the other cells and input sources. Gaussian graphical models have been successfully applied to several neuronal data recordings to infer the functional connectivity of hundreds of neurons (Vinci et al., 2018a,b; Yatsenko et al., 2015).

New ambitious neuroscience projects involve the recording of the activities of tens of thousands of neurons in 3-dimensional portions of brain through calcium imaging technology (Pnevmatikakis et al., 2016; Pachitariu et al., 2016; Stringer et al., 2019). For instance, consider the massive publicly available data set of Stringer et al. (2019) consisting of calcium activity traces of about 10,000 neurons in a cubic portion of mouse visual cortex (70–385 μ m depth). These neurons were simultaneously recorded *in vivo* using 2-photon imaging of GCaMP6s with 2.5Hz scan rate (Pachitariu et al., 2016), while the animal was free to run on an air-floating ball in complete darkness for about 105 minutes. In Figure 6(A) we display the neurons’ spatial positions occupying a 1mm \times 1mm \times .5mm 3-dimensional space, and the functional connections recovered with the graphical lasso (Glasso) based on the full data (we display 6000 edges for illustration).

The large scale recordings allowed by calcium imaging technologies certainly

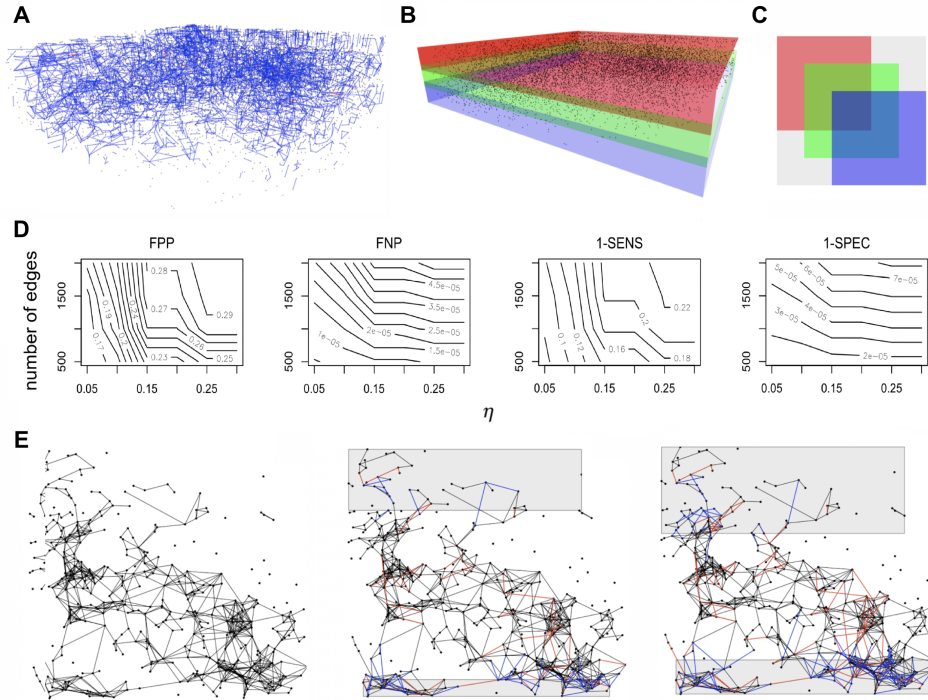


FIG 6. (A) Brain cube functional connectivity network of 9136 neurons (mouse visual cortex) estimated from full data for a given number of edges equal to 6000. (B) Example of nonsimultaneously recorded subsets of the brain cube. (C) Jointly observed pairs of neurons given scheme in B ($\eta \approx .2$). (D) Graph divergence of $\widehat{\mathcal{G}}_{\mathcal{U}}^{\tau, \xi_1, \xi_2}$ from Glasso as a function of η and total number of edges in the graph. (E) Graphical lasso network estimate based on simultaneous neuronal recordings of the most superficial cortical layer of (A), and network recovery assuming neurons in top shaded areas are never recorded simultaneously with neurons in bottom shaded areas (two cases: $\eta = .2$ and $\eta = .4$). $\widehat{\mathcal{G}}_{\mathcal{U}}^{\tau, \xi_1, \xi_2}$ largely recovers the network structure, with a few comparative false positives highlighted in red and comparative false negatives highlighted in blue.

poses the statistical challenge of extreme high-dimensionality, since the length of the experiments, and thereby the sample size, cannot be increased likewise that much. However, this is not the only challenge. A fundamental trade-off between temporal and spatial resolution characterizes calcium imaging technologies: the more neurons we aim to record from simultaneously, the coarser the time resolution is. Since important neuronal activity patterns happen on very short time scales, it is often preferred to record the activities of a subset of neurons at once with a fine temporal resolution rather than recording the activities of the entire neuronal population simultaneously with a coarse time resolution. This is particularly necessary when a 1mm^3 portion of brain, containing about 100,000 neurons, has to be

recorded. In Figure 6(B) we illustrate a possible observational scheme over a brain portion where three subsets of neurons are recorded with a fine temporal resolution over separate experimental sessions, i.e. *nonsimultaneously*. Yet, if these subsets of the neuronal population are recorded *nonsimultaneously*, only a subset O of all possible pairs of neurons may have joint observations, while the rest (O^c) remain unobserved with no empirical covariance (Figure 6(C)). Hence, the graph quilting problem arises.

Assuming the observational scheme in (C), we drop data from the 105 minutes recordings (the data used in (A)) in a way that each of the three subsets of neurons is roughly recorded 105/3 minutes, and compute $\hat{\Theta}_U^{\tau, \xi_1, \xi_2}$ (tuned to have same number of edges as Glasso estimate) for different numbers of edges and values of η (by varying size of each neuronal subset), and assessed the divergence of $\hat{\Theta}_U^{\tau, \xi_1, \xi_2}$ from Glasso in terms of false positive proportion (FPP), false negative proportion (FNP), sensitivity (SENS) and specificity (SPEC). Figure 6(D) shows that these divergences increase with the number of edges and, as expected, with η . However, we can see that FNP and 1-SPEC are particularly low. This result is in line with Theorem 3.1, which guarantees that, at the population level, the MAD_{GQ} contains false negatives only in situations that are Lebesgue measure negligible. This property is inherited by the $\text{MAD}_{GQ\text{lasso}}$ with high probability. Finally, to provide more insight, in Figure 6(E) we show the graphical lasso network estimate based on simultaneous neuronal recordings of the most superficial cortical layer of (A), and network recoveries assuming that neurons in top shaded areas are never recorded simultaneously with neurons in bottom shaded areas (two cases: $\eta = .2$ and $\eta = .4$). $\hat{\Theta}_U^{\tau, \xi_1, \xi_2}$ largely recovers the network structure, with a few comparative false positives highlighted in red and comparative false negatives highlighted in blue.

7. Discussion. We introduced and investigated the *graph quilting* problem in Gaussian graphical models. This problem asks for the retrieval of the precision matrix Θ and the associated graph $G = \{V, E\}$, where $E = \{(i, j) : \Theta_{ij} \neq 0\}$, given a partially observed covariance matrix $\Sigma_O = \{\Sigma_{ij} : (i, j) \in O\}$ for some subset of indices O . We extended this to the estimation of Θ and G from an incomplete set of empirical covariances $\hat{\Sigma}_O$. We first demonstrated that, with no additional assumptions, it is impossible to recover Θ and G from Σ_O alone since there is no one-to-one mapping between Σ_O and Θ . On the other hand, as a first step, we demonstrated that a simple maximum determinant (MAD_{GQ}) estimator $\tilde{\Theta}$ can be shown to be close to the true Θ under certain conditions. In general, the graph induced by $\tilde{\Theta}$ given by $\tilde{E} = \{(i, j) : \tilde{\Theta}_{ij} \neq 0\}$ can be quite different from the true graph E . In order to deal with this, we proposed a thresholding strategy targeted at eliminating only the spurious edges in $\tilde{\Theta}$; we show that under certain conditions, this procedure

removes any edge (i, j) of \tilde{E} wherever $\Theta_{ij} = 0$ and yields perfect graph recovery in O . Furthermore, we devised an algorithm that we dub Recursive Complement (RECO) to recover edges in O^c by exploiting the positions of the detected “distortions” in $\tilde{\Theta}$. When the diagonals of Θ are known, then it is possible to use the RECO algorithm to obtain a nontrivial superset of all edges in O^c ; otherwise, it is possible to recover at least a minimum number of edges in O^c . In the finite sample setting, we conduct the aforementioned graph recoveries with an ℓ_1 regularized version of MAD_{GQ} , the $\text{MAD}_{GQ\text{lasso}}$, based on an incomplete sample covariance matrix. We established the statistical properties of two graph estimators based on $\text{MAD}_{GQ\text{lasso}}$. We also verified the theoretical results via simulations and illustrated the use of the methods with the analysis of real calcium imaging data.

The graph quilting framework and the proposed algorithms are novel, and several extensions are possible. We expect graph quilting, in the forms presented in this paper or others, to play an important role in the analysis of data from disparate fields where observations are structurally missing, such as neuroscience, genomics, analysis of medical records, proteomics, and finance.

Acknowledgements. Giuseppe Vinci was supported by NeuroNex (NSF), Rice Academy Postdoctoral Fellows, and Dan L. Duncan Foundation.

SUPPLEMENTARY MATERIAL

Supplement to “Graph Quilting: Graphical model selection from partially observed covariances”: Appendix

()

References.

- AHRENS, M. B., ORGER, M. B., ROBSON, D. N., LI, J. M., & KELLER, P. J. (2013). Whole-brain functional imaging at cellular resolution using light-sheet microscopy. *Nature methods*, 10(5), 413-420.
- ALIVISATOS, A. P., ANDREWS, A. M., BOYDEN, E. S., CHUN, M., CHURCH, G. M., DEISSEROTH, K., ET AL. (2013). Nanotools for neuroscience and brain activity mapping.
- ALLEN, G. I., & LIU, Z. (2013). A local poisson graphical model for inferring networks from sequencing data. *IEEE transactions on nanobioscience*, 12(3), 189-198.
- ALBERT, R., & BARABÁSI, A. L. (2002). Statistical mechanics of complex networks. *Reviews of modern physics*, 74(1), 47.
- BAGGIO, H. C., & JUNQUÉ, C. (2019). Functional MRI in Parkinson’s Disease Cognitive Impairment. *International review of neurobiology*, 144, 29-58.
- BAKONYI, M., & WOERDEMAN, H. J. (1995). Maximum entropy elements in the intersection of an affine space and the cone of positive definite matrices. *SIAM Journal on Matrix Analysis and Applications*, 16(2), 369-376.
- BANERJEE, S., and GHOSAL, S. (2015). Bayesian structure learning in graphical models. *J. Multivariate Anal.* **136** 147-162.

- BICKEL, P. J., RITOV, Y. A., & TSYBAKOV, A. B. (2009). Simultaneous analysis of Lasso and Dantzig selector. *The Annals of Statistics*, 37(4), 1705–1732.
- BISHOP, W. E., & YU, B. M. (2014). Deterministic symmetric positive semidefinite matrix completion. In *Advances in Neural Information Processing Systems* (pp. 2762–2770).
- BROWN, E. N., KASS, R. E., & MITRA, P. P. (2004). Multiple neural spike train data analysis: state-of-the-art and future challenges. *Nature neuroscience*, 7(5), 456–461.
- CAI, T., LIU, W., & LUO, X. (2011). A constrained ℓ_1 minimization approach to sparse precision matrix estimation. *Journal of the American Statistical Association*, 106(494), 594–607.
- CAI, J., LIU, A., MI, T., GARG, S., TRAPPE, W., MCKEOWN, M. J., & WANG, Z. J. (2018). Dynamic Graph Theoretical Analysis of Functional Connectivity in Parkinson’s Disease: The Importance of Fiedler Value. *IEEE journal of biomedical and health informatics*.
- CANDES, E. J., & PLAN, Y. (2010). Matrix completion with noise. *Proceedings of the IEEE*, 98(6), 925–936.
- CANDÁLS, E. J., & RECHT, B. (2009). Exact matrix completion via convex optimization. *Foundations of Computational mathematics*, 9(6), 717.
- CANDES, E., & TAO, T. (2007). The Dantzig selector: Statistical estimation when p is much larger than n . *The annals of Statistics*, 35(6), 2313–2351.
- CHANDRASEKARAN, V., PARRILO, P. A., and WILLSKY, A. S. (2012). Latent variable graphical model selection via convex optimization. *Ann. Statist.* **40** 1935–1967.
- COHEN, M. R., & KOHN, A. (2011). Measuring and interpreting neuronal correlations. *Nature neuroscience*, 14(7), 811–819.
- COHEN, M. R., AND MAUNSELL, J. H. (2009). Attention improves performance primarily by reducing interneuronal correlations. *Nature neuroscience*, 12(12), 1594–1600.
- CUNNINGHAM, J. P., & YU, B. M. (2014). Dimensionality reduction for large-scale neural recordings. *Nature neuroscience*, 17(11), 1500–1509.
- DEMPSTER, A. P. (1972). Covariance selection. *Biometrics*, 157–175.
- DOBRA, A., HANS, C., JONES, B., NEVINS, J. R., YAO, G., & WEST, M. (2004). Sparse graphical models for exploring gene expression data. *Journal of Multivariate Analysis*, 90(1), 196–212.
- EFRON, B., TIBSHIRANI, R., STOREY, J. D., AND TUSHER, V. (2001). Empirical Bayes analysis of a microarray experiment. *Journal of the American statistical association*, 96(456), 1151–1160.
- ENGELS, G., VLAAR, A., MCCOY, B., SCHERDER, E., & DOUW, L. (2018). Dynamic functional connectivity and symptoms of Parkinson’s disease: a resting-state fMRI study. *Frontiers in aging neuroscience*, 10, 388.
- ERDŐS, P., & RÉNYI, A. (1959). On Random Graphs I *Publicationes Mathematicae*. 6: 290–297.
- FAN, J., FENG, Y., & WU, Y. (2009). Network exploration via the adaptive LASSO and SCAD penalties. *The annals of applied statistics*, 3(2), 521.
- FRIEDMAN, N. (2004). Inferring cellular networks using probabilistic graphical models. *Science*, 303(5659), 799–805.
- FRIEDMAN, J., HASTIE, T., and TIBSHIRANI, R. (2008). Sparse inverse covariance estimation with the graphical lasso. *Biostatistics* **9** 432–441.
- GALLOPIN, M., RAU, A., & JAFFRÁL’ZIC, F. (2013). A hierarchical Poisson log-normal model for network inference from RNA sequencing data. *PloS one*, 8(10), e77503.
- GAWAD, C., KOH, W., & QUAKE, S. R. (2016). Single-cell genome sequencing: current state of the science. *Nature Reviews Genetics*, 17(3), 175.
- GERLINGER, M., ROWAN, A. J., HORSWELL, S., LARKIN, J., ENDESFELDER, D., GRONROOS, E., ... & VARELA, I. (2012). Intratumor heterogeneity and branched evolution revealed by multi-region sequencing. *New England journal of medicine*, 366(10), 883–892.

- GONG, W., KWAK, I. Y., POTA, P., KOYANO-NAKAGAWA, N., & GARRY, D. J. (2018). DrImpute: imputing dropout events in single cell RNA sequencing data. *BMC bioinformatics*, 19(1), 220.
- GORIS, R. L., MOVSHON, J. A., AND SIMONCELLI, E. P. (2014). Partitioning neuronal variability. *Nature neuroscience*, 17(6), 858-865.
- GRONE, R., JOHNSON, C. R., SÁ, E. M., AND WOLKOWICZ, H. (1984). Positive definite completions of partial Hermitian matrices. *Linear algebra and its applications*, 58, 109-124.
- HARTEMINK, A. J., GIFFORD, D. K., JAAKKOLA, T. S., & YOUNG, R. A. (2000). Using graphical models and genomic expression data to statistically validate models of genetic regulatory networks. In *Biocomputing 2001* (pp. 422-433).
- HENG, T. S., PAINTER, M. W., ELPEK, K., LUKACS-KORNEK, V., MAUERMANN, N., TURLEY, S. J., ... & DAVIS, S. (2008). The Immunological Genome Project: networks of gene expression in immune cells. *Nature immunology*, 9(10), 1091.
- HSIEH, C. J., DHILLON, I. S., RAVIKUMAR, P. K., & SUSTIK, M. A. (2011). Sparse inverse covariance matrix estimation using quadratic approximation. In *Advances in neural information processing systems* (pp. 2330-2338).
- KELLY, R. C., SMITH, M. A., SAMONDS, J. M., KOHN, A., BONDS, A. B., MOVSHON, J. A., & LEE, T. S. (2007). Comparison of recordings from microelectrode arrays and single electrodes in the visual cortex. *Journal of Neuroscience*, 27(2), 261-264.
- KELLY, R. C., SMITH, M. A., KASS, R. E., & LEE, T. S. (2010). Local field potentials indicate network state and account for neuronal response variability. *Journal of computational neuroscience*, 29(3), 567-579.
- KELLY, R. C., & KASS, R. E. (2012). A framework for evaluating pairwise and multiway synchrony among stimulus-driven neurons. *Neural computation*, 24(8), 2007-2032.
- KERR, J. N., & DENK, W. (2008). Imaging in vivo: watching the brain in action. *Nature Reviews Neuroscience*, 9(3), 195-205.
- KIPKE, D. R., SHAIN, W., BUZSÁKI, G., FETZ, E., HENDERSON, J. M., HETKE, J. F., & SCHALK, G. (2008). Advanced neurotechnologies for chronic neural interfaces: new horizons and clinical opportunities. *Journal of Neuroscience*, 28(46), 11830-11838.
- KISELEV, V. Y., ANDREWS, T. S., & HEMBERG, M. (2019). Challenges in unsupervised clustering of single-cell RNA-seq data. *Nature Reviews Genetics*, 20(5), 273-282.
- KLEIN, A. M., MAZUTIS, L., AKARTUNA, I., TALLAPRAGADA, N., VERES, A., LI, V., ... & KIRSCHNER, M. W. (2015). Droplet barcoding for single-cell transcriptomics applied to embryonic stem cells. *Cell*, 161(5), 1187-1201.
- KOLAR, M., & XING, E. P. (2012). Estimating sparse precision matrices from data with missing values. In *Proceedings of the 29th International Conference on Machine Learning*, Edinburgh, Scotland, UK.
- KRÄMER, N., SCHÄFER, J., & BOULESTEIX, A. L. (2009). Regularized estimation of large-scale gene association networks using graphical Gaussian models. *BMC bioinformatics*, 10(1), 384.
- KRUMSIEK, J., SUHRE, K., ILLIG, T., ADAMSKI, J., & THEIS, F. J. (2011). Gaussian graphical modeling reconstructs pathway reactions from high-throughput metabolomics data. *BMC systems biology*, 5(1), 21.
- LAURENT, M. (2009). Matrix completion problems. *Encyclopedia of Optimization*, 1967-1975.
- LI, W. V., & LI, J. J. (2018). An accurate and robust imputation method scImpute for single-cell RNA-seq data. *Nature communications*, 9(1), 997.
- LIU, H., HAN, F., YUAN, M., LAFFERTY, J., & WASSERMAN, L. (2012). High-dimensional semi-parametric Gaussian copula graphical models. *The Annals of Statistics*, 40(4), 2293-2326.
- LIU, H., ROEDER, K., & WASSERMAN, L. (2010). Stability approach to regularization selection

- (stars) for high dimensional graphical models. In *Advances in neural information processing systems* (pp. 1432-1440).
- LOH, PO-LING; WAINWRIGHT, MARTIN J. (2012). High-dimensional regression with noisy and missing data: Provable guarantees with nonconvexity. *Ann. Statist.* 40 (2012), no. 3, 1637–1664.
- MACOSKO, E. Z., BASU, A., SATIJA, R., NEMESH, J., SHEKHAR, K., GOLDMAN, M., ... & TROMBETTA, J. J. (2015). Highly parallel genome-wide expression profiling of individual cells using nanoliter droplets. *Cell*, 161(5), 1202-1214.
- MAUNSELL, J. H. (2015). Neuronal mechanisms of visual attention. *Annual Review of Vision Science*, 1, 373-391.
- MEINSHAUSEN, N., & BÜHLMANN, P. (2006). High-dimensional graphs and variable selection with the lasso. *The annals of statistics*, 34(3), 1436–1462.
- MITCHELL, J. F., SUNDBERG, K. A., AND REYNOLDS, J. H. (2009). Spatial attention decorrelates intrinsic activity fluctuations in macaque area V4. *Neuron*, 63(6), 879-888.
- PACHITARIU, M., STRINGER, C., SCHRÄUDER, S., DIPOPPA, M., ROSSI, L. F., CARANDINI, M., & HARRIS, K. D. (2016). Suite2p: beyond 10,000 neurons with standard two-photon microscopy. *Biorxiv*, 061507.
- PFAU, D., PNEVMATIKAKIS, E. A., & PANINSKI, L. (2013). Robust learning of low-dimensional dynamics from large neural ensembles. In *Advances in neural information processing systems* (pp. 2391–2399).
- PNEVMATIKAKIS, E. A., SOUDRY, D., GAO, Y., MACHADO, T. A., MEREL, J., PFAU, D., REARDON, T., MU, Y., LACEFIELD, C., YANG, W., & AHRENS, M. (2016). Simultaneous denoising, deconvolution, and demixing of calcium imaging data. *Neuron*, 89(2), 285–299.
- RAVIKUMAR, P., WAINWRIGHT, M. J., RASKUTTI, G., & YU, B. (2011). High-dimensional covariance estimation by minimizing ℓ_1 -penalized log-determinant divergence. *Electronic Journal of Statistics*, 5, 935–980.
- SHADLEN, M. N., & NEWSOME, W. T. (1998). The variable discharge of cortical neurons: implications for connectivity, computation, and information coding. *Journal of neuroscience*, 18(10), 3870-3896.
- SMITH, R. L. (2008). The positive definite completion problem revisited. *Linear Algebra and Its Applications*, 429(7), 1442–1452.
- SMITH, M. A., & KOHN, A. (2008). Spatial and temporal scales of neuronal correlation in primary visual cortex. *Journal of Neuroscience*, 28(48), 12591-12603.
- SMITH, M. A., & SOMMER, M. A. (2013). Spatial and temporal scales of neuronal correlation in visual area V4. *Journal of Neuroscience*, 33(12), 5422–5432.
- SMITH, M. A., JIA, X., ZANDVAKILI, A., & KOHN, A. (2013). Laminar dependence of neuronal correlations in visual cortex. *Journal of neurophysiology*, 109(4), 940–947.
- SONG, D., WANG, H., TU, C. Y., MARMARELIS, V. Z., HAMPSON, R. E., DEADWYLER, S. A., & BERGER, T. W. (2013). Identification of sparse neural functional connectivity using penalized likelihood estimation and basis functions. *Journal of computational neuroscience*, 35(3), 335-357.
- SOUDRY, D., KESHRI, S., STINSON, P., OH, M. H., IYENGAR, G., & PANINSKI, L. (2015). Efficient “shotgun” inference of neural connectivity from highly sub-sampled activity data. *PLoS computational biology*, 11(10), e1004464.
- STÄDLER, N., & BÜHLMANN, P. (2012). Missing values: sparse inverse covariance estimation and an extension to sparse regression. *Statistics and Computing*, 22(1), 219-235.
- STEGLE, O., TEICHMANN, S. A., & MARIONI, J. C. (2015). Computational and analytical challenges in single-cell transcriptomics. *Nature Reviews Genetics*, 16(3), 133-145.
- STEVENSON, I. H., & KORDING, K. P. (2011). How advances in neural recording affect data anal-

- ysis. *Nature neuroscience*, 14(2), 139-142.
- STRINGER, C., PACHITARIU, M., STEINMETZ, N., REDDY, C. B., CARANDINI, M., & HARRIS, K. D. (2019). Spontaneous behaviors drive multidimensional, brainwide activity. *Science*, 364(6437), 255-255.
- STUART, J. M., SEGAL, E., KOLLER, D., & KIM, S. K. (2003). A gene-coexpression network for global discovery of conserved genetic modules. *science*, 302(5643), 249-255.
- TURAGA, S., BUESING, L., PACKER, A. M., DALGLEISH, H., PETTIT, N., HAUSSER, M., & MACKE, J. H. (2013). Inferring neural population dynamics from multiple partial recordings of the same neural circuit. In *Advances in Neural Information Processing Systems* (pp. 539-547).
- VAN DIJK, D., NAINYS, J., SHARMA, R., KATHAIL, P., CARR, A. J., MOON, K. R., ... & PE'ER, D. (2017). MAGIC: A diffusion-based imputation method reveals gene-gene interactions in single-cell RNA-sequencing data. *BioRxiv*, 111591.
- VANDENBERGHE, L., BOYD, S., & WU, S. P. (1998). Determinant maximization with linear matrix inequality constraints. *SIAM journal on matrix analysis and applications*, 19(2), 499-533.
- VINCI, G., VENTURA, V., SMITH, M. A., & KASS, R. E. (2016). Separating spike count correlation from firing rate correlation. *Neural computation*, 28(5), 849-881.
- VINCI, G., VENTURA, V., SMITH, M. A., & KASS, R. E. (2018a). Adjusted regularization of cortical covariance. *Journal of computational neuroscience*, 45(2), 83-101.
- VINCI, G., VENTURA, V., SMITH, M. A., & KASS, R. E. (2018b). Adjusted regularization in latent graphical models: Application to multiple-neuron spike count data. *The Annals of Applied Statistics*, 12(2), 1068-1095.
- WANG, Y. R., & HUANG, H. (2014). Review on statistical methods for gene network reconstruction using expression data. *Journal of theoretical biology*, 362, 53-61.
- WATTS, D. J., & STROGATZ, S. H. (1998). Collective dynamics of "small-world" networks. *Nature*, 393(6684), 440.
- WOHRER, A., ROMO, R., & MACHENS, C. K. (2010). Linear readout from a neural population with partial correlation data. In *Advances in Neural Information Processing Systems* (pp. 2469-2477).
- YATSENKO, D., JOSIĆ, K., ECKER, A. S., FROUDARAKIS, E., COTTON, R. J., AND TOLIAS, A. S. (2015). Improved estimation and interpretation of correlations in neural circuits. *PLoS Comput Biol*, 11(3), e1004083.
- YIN, J., & LI, H. (2011). A sparse conditional gaussian graphical model for analysis of genetical genomics data. *The annals of applied statistics*, 5(4), 2630.
- YU, B. M., CUNNINGHAM, J.P, SANTHANAM, G., RYU, S.I., SHENOY, K.V., AND SAHANI, M. (2009). Gaussian-process factor analysis for low-dimensional single-trial analysis of neural population activity. In *Advances in neural information processing systems*, 1881-1888.
- YUAN, M. (2010). High dimensional inverse covariance matrix estimation via linear programming. *Journal of Machine Learning Research*, 11(Aug), 2261-2286.
- YUAN, M. (2012). Discussion: Latent variable graphical model selection via convex optimization. *Ann. Statist.* **40** 1968-1972.
- YUAN, M., & LIN, Y. (2007). Model selection and estimation in the Gaussian graphical model. *Biometrika*, 94(1), 19-35.
- ZHANG, B. & HORVATH, S. (2005). A general framework for weighted gene co-expression network analysis. *Statistical applications in genetics and molecular biology*
- ZHANG, L., & ZHANG, S. (2018). Comparison of computational methods for imputing single-cell RNA-sequencing data. *IEEE/ACM transactions on computational biology and bioinformatics*.
- ZOU, H., and HASTIE, T. (2005). Regularization and variable selection via the elastic net. *J. Roy. Statist. Soc. Ser. B* **67** 301-320.

Supplemental Materials.

APPENDIX A: PROOFS OF MAIN RESULTS

PROOF OF THEOREM 2.1. A positive definite completion of Σ_O exists since Σ is positive definite. Thus, the max-determinant completion of Σ_O (Equation (2.7)) has a unique solution $\tilde{\Sigma} = \tilde{\Theta}^{-1}$ where $\tilde{\Theta}_{O^c} \equiv 0$ and $[\tilde{\Theta}^{-1}]_O = \Sigma_O$. On the other hand $[\Theta^{-1}]_O = \Sigma_O$, and since $E \subseteq O$, we also have $\Theta_{O^c} \equiv 0$. Therefore $\tilde{\Theta} = \Theta$. \square

PROOF OF LEMMA 2.1. The solution $\tilde{\Theta} = \tilde{\Sigma}^{-1}$ to Equation (2.6) is uniquely identified by the constraints $\det \tilde{\Theta} > 0 \Leftrightarrow \det \tilde{\Sigma} > 0$ and $\tilde{\Theta}_{O^c} = [\tilde{\Sigma}^{-1}]_{O^c} = 0$, and by its first order condition $[\tilde{\Theta}^{-1}]_O - \Sigma_O = 0 \Leftrightarrow \tilde{\Sigma}_O = \Sigma_O$. The solution $\tilde{\Sigma}$ to Equation (2.7) is uniquely identified by the constraints $\det \tilde{\Sigma} > 0$ and $\tilde{\Sigma}_O = \Sigma_O$, and by its first order condition $[\tilde{\Sigma}^{-1}]_{O^c} = 0$. Hence, Equations (2.6) and (2.7) are equivalent. \square

PROOF OF THEOREM 3.1. Let ν be the Lebesgue measure restricted to the positive definite cone \mathcal{S}_p^{++} of $p \times p$ positive definite matrices. Define the function $F_O : \mathcal{S}_p^{++} \rightarrow \mathcal{S}_p^{++}$ as $F_O(\Theta) = \tilde{\Theta}$, where $\tilde{\Theta}$ is the MAD_{GQ} solution based on $\Sigma_O = [\Theta^{-1}]_O$. Since F is a continuous function of Σ_O (Lemma B.4), we have that $\nu(\{\Theta \in \mathcal{S}_p^{++} : F_O(\Theta)_{ij} = 0\}) = 0$ for any $(i, j) \in O$. Thus,

$$\nu\left(\cup_{(i,j) \in O} \{\Theta \in \mathcal{S}_p^{++} : F_O(\Theta)_{ij} = 0\}\right) \leq \sum_{(i,j) \in O} \nu\left(\{\Theta \in \mathcal{S}_p^{++} : F_O(\Theta)_{ij} = 0\}\right) = 0$$

Therefore, given Θ_O , the set of positive definite matrices that have a MAD_{GQ} completion containing false nondiscoveries in O occupies a subset of the positive definite cone of null hyper-volume. \square

PROOF OF THEOREM 3.2. For $\|\Theta_{O^c}\|_\infty$ sufficiently small, we have $\delta < \nu/2$, since $\tilde{\Theta}_O$ is a continuous function of Θ_{O^c} for fixed Θ_O (Lemma B.4), and $\tilde{\Theta}_O = \Theta_O$ at $\Theta_{O^c} = 0$. Then for any $(i, j) \in O$,

$$\tilde{\Theta}_{ij} \in [\Theta_{ij} - \delta, \Theta_{ij} + \delta] \subset (\Theta_{ij} - \nu/2, \Theta_{ij} + \nu/2)$$

The latter interval overlaps with $[-\nu/2, \nu/2]$ if and only if $\Theta_{ij} = 0$, because $|\Theta_{ij}| > 0 \Leftrightarrow |\Theta_{ij}| \geq \nu$. Hence, $\tilde{\Theta}_{ij} > \nu/2 \Leftrightarrow \Theta_{ij} > 0$, and $\tilde{\Theta}_{ij} < -\nu/2 \Leftrightarrow \Theta_{ij} < 0$. \square

PROOF OF THEOREM 3.3. The first part of the statement of this lemma is a simplified version of Lemma B.6, therefore its proof is straightforward. Moreover, Let $\gamma_{EF} = \|\Theta_{EF}\|_\infty$ and $\gamma_{EE} = \|\Theta_{EE}^{-1}\|_\infty$. The proof of the second part of the lemma

follows from a direct application of Lemmas B.1, B.2, and B.3 to the blocks of the matrix $\Theta - \tilde{\Theta}$ in

$$\|\Theta - \tilde{\Theta}\|_\infty = \max_{(D,E) \in \{A,B,C\}} \|\Theta_{DE} - \tilde{\Theta}_{DE}\|_\infty,$$

and

$$\|\Theta - \tilde{\Theta}\|_0 = \sum_{(D,E) \in \{A,B,C\}} \|\Theta_{DE} - \tilde{\Theta}_{DE}\|_0$$

where all addends satisfy the functional form given in the statement. \square

PROOF OF LEMMA 3.1. Let $\Theta \in \mathcal{S}_p^{++}$ be a positive definite matrix with inverse $\Sigma = \Theta^{-1}$. The Schur complement implies that for any $U \subset V = \{1, \dots, p\}$

$$\Sigma_{UU} = (\Theta_{UU} - \Theta_{UU^c} \Theta_{U^c U^c}^{-1} \Theta_{U^c U})^{-1}$$

Thus, if $\tilde{\Theta} \in \mathcal{S}_p^{++}$ has inverse $\tilde{\Sigma} = \tilde{\Theta}^{-1}$ such that $\Sigma_O = \tilde{\Sigma}_O$, where $O = \cup_{k=1}^K V_k \times V_k$, with $V_k \subset V = \{1, \dots, p\}$, then

$$\Theta_{UU} - \Theta_{UU^c} \Theta_{U^c U^c}^{-1} \Theta_{U^c U} = \tilde{\Theta}_{UU} - \tilde{\Theta}_{UU^c} \tilde{\Theta}_{U^c U^c}^{-1} \tilde{\Theta}_{U^c U}$$

for any $U \subset V$ such that $U \times U \subseteq O$. \square

PROOF OF THEOREM 3.4. The Schur complements of $\Theta_{V_k^c V_k^c}$ and $\tilde{\Theta}_{V_k^c V_k^c}$ are entangled by $\Sigma_{V_k V_k}$ through Equation (3.18). Since $\Theta_{V_k^c V_k^c} > 0$, then

$$w^T \Theta_{V_k^c V_k^c}^{-1} w > 0 \iff w \neq 0.$$

Thus, for any $k \in 1, \dots, K$ and any $i \in V_k$,

$$(A.1) \quad \tilde{\Theta}_{i_k i_k}^{(k)} < [\Theta_{V_k V_k}]_{i_k i_k} \iff [\Theta_{V_k V_k}]_{i_k^*} \neq 0,$$

where $[\Theta_{V_k V_k}]_{i_k i_k} \equiv \Theta_{ii}$, and M_{j^*} is the j -th row of matrix M . For every $i \in V$ we need the inequality in Equation (A.1) to be satisfied for all k such that $i \in V_k$. Hence, requiring $\tilde{\Theta}_{ii} < \Theta_{ii}$ in Equation (3.20) ensures $E_{O^c} \subseteq \mathcal{S}$; this proves part (i). To prove (ii), note that the set $\tilde{\mathcal{D}}$ contains all elements of \mathcal{D} that identify rows falling in \tilde{O}^c that surely contain at least one true edge; this is because the condition $V_k \times V_k^c \subseteq O^c$ guarantees that the distortions on the diagonals of $\tilde{\Theta}_{V_k V_k}$ are incontrovertibly due to edges in O^c . \square

PROOF OF PROPOSITION 3.1. The set $\tilde{\mathcal{H}}_{0,v}$ contains all elements of $\mathcal{H}_{0,v}$ that identify rows falling in \tilde{O}^c that surely contain at least one true edge. Taking projections of $\tilde{O}^c \cap (\tilde{\mathcal{H}}_{0,v} \times \tilde{\mathcal{H}}_{0,v})$ lets us identify the minimum number of true edges in \mathcal{U} , in a similar fashion as in Theorem 3.4. \square

PROOF OF THEOREM 3.5. (i) Lemma B.7 guarantees that if $\tilde{\Theta}_{ii} < \Theta_{ii}$ with $i \in A$, then there must be a nonzero entry on row i in Θ_{AC} . Moreover, if $\tilde{\Theta}_{jj} < \Theta_{jj}$ with $j \in C$, then there must be a nonzero entry on column j in Θ_{AC} . On the other hand, if $\tilde{\Theta}_{ii} = \Theta_{ii}$ with $i \in A$, then $\Theta_{iC} = 0$, and if $\tilde{\Theta}_{jj} = \Theta_{jj}$ with $j \in C$, then $\Theta_{Aj} = 0$. Therefore the set \mathcal{S} in Equation (3.33) contains all pairs of nodes in $A \times C$ that are connected. (ii) The set \mathcal{S} is a Cartesian product where every row and every column contains at least one edge. Thus, the minimum number of true edges in \mathcal{S} is M , while the maximum number of edges is mM , that is the cardinality of \mathcal{S} . (iii) Finally, from the same reasoning used in (i), the existence of any edge in \mathcal{S} would have at least one but no more than the distortions observed in the diagonals of $\tilde{\Theta}_{AA}$ and $\tilde{\Theta}_{CC}$. \square

PROOF OF PROPOSITION 3.2. The second part of Lemma B.7 guarantees that if a distortion is found in the off-diagonal entries in $A \times (A \cup B)$ and $(B \cup C) \times C$, then it is possible to identify rows and columns of Θ_{AC} that are nonzero, as in Theorem 3.5. However, off-diagonal distortions are not necessary to diagonal distortions, and there might be more distortions beyond those entries where $|\tilde{\Theta}_{ij}| < \nu$. But, by construction, \mathcal{U} contains at least $\max\{|A_\nu|, |C_\nu|\}$ true edges. \square

PROOF OF LEMMA 4.1. The maximum in Equation (4.3), if it exists, is unique because the objective function is strictly concave as its log-determinant component is strictly concave. To see that the maximum is achieved, first note that, for $\lambda_{ij} > 0, \forall (i, j) \in O$, Lagrangian duality lets us rewrite Equation (4.3) as

$$\hat{\Theta} = \underset{\Theta > 0, \Theta_{O^c} = 0, \|\Lambda \otimes \Theta\|_{1, \text{off}} \leq C(\Lambda)}{\operatorname{argmax}} \log \det \Theta - \sum_{(i,j) \in O} \Theta_{ij} \hat{\Sigma}_{ij},$$

for some $C(\Lambda) < \infty$. This representation shows that the off-diagonal elements of Θ are bounded within the weighted ℓ_1 -ball, meaning that only $\{\Theta_{ii}\}_{i \in V}$ might potentially diverge to infinity, and thereby the objective function. However, we have

$$\begin{aligned} \log \det \Theta - \sum_{(i,j) \in O} \Theta_{ij} \hat{\Sigma}_{ij} &\leq \log \det \Theta - \sum_{i \in V} \Theta_{ii} \hat{\Sigma}_{ii} + \text{const} \\ &\leq \sum_{i \in V} (\log \Theta_{ii} - \Theta_{ii} \hat{\Sigma}_{ii}) + \text{const} \\ &=: -h(\Theta_{11}, \dots, \Theta_{pp}), \end{aligned}$$

where the first inequality holds because the off-diagonals of Θ are bounded in the ℓ_1 -ball and $\|\hat{\Sigma}_O\|_\infty < \infty$, while the second inequality is an application of Hadamard's inequality for positive definite matrices. The function h is a coercive function of $\{\Theta_{ii}\}_{i \in V}$ since it diverges to ∞ for any sequence $\|(\Theta_{11}^t, \dots, \Theta_{pp}^t)\|_2 \rightarrow +\infty$, as long

as $\widehat{\Sigma}_{ii} > 0, \forall i \in V$. Therefore, the maximum of the objective function of Equation (4.3) is attained. Finally, a matrix $\widehat{\Theta} > 0$ is optimal for Equation (4.3) if and only if there exists \widehat{Z} in the sub-differential $\partial \| * \|_{1, \text{off}}$ evaluated at $\widehat{\Theta}$ satisfying the first order condition $\widehat{\Sigma}_O - [\widehat{\Theta}^{-1}]_O + \Lambda_O \odot \widehat{Z}_O = 0$. \square

PROOF OF THEOREM 4.1. Let $S = \{(i, j) : \widetilde{\Theta}_{ij} \neq 0\}$. Since $\widetilde{\Theta}_{O^c} = 0$, we have $S \subseteq O$, $O^c \subseteq S^c$, and $S \cup (S^c \setminus O^c) = O$. Let $\widehat{\Theta}^S$ be a more constrained version of the $\text{MAD}_{GQlasso}$ in Equation (4.3) where the constraint $\Theta_{O^c} = 0$ is replaced by $\Theta_{S^c} = 0$. Define

$$\begin{aligned} W_O &= \widehat{\Sigma}_O - \Sigma_O, \\ \Delta &= \widehat{\Theta}^S - \widetilde{\Theta}, \\ R(\Delta) &= (\widehat{\Theta}^S)^{-1} - \widetilde{\Sigma} + \widetilde{\Sigma} \Delta \widetilde{\Sigma}, \\ \Gamma &= \widetilde{\Sigma} \otimes \widetilde{\Sigma}, \\ \kappa_\Sigma &= \|\widetilde{\Sigma}\|_\infty = \max_j \sum_{k=1}^p |\widetilde{\Sigma}_{jk}|, \\ \kappa_\Gamma &= \|(\Gamma_{SS})^{-1}\|_\infty \end{aligned}$$

The following proof exploits the results B1, B2, and B3 of Lemma B.8. Let $\lambda_{\bar{n}} = \frac{8}{\alpha} \sigma(\bar{n}, p^\gamma)$, and suppose

- (i) $\|W_O\|_\infty \leq \sigma(\bar{n}, p^\gamma)$
- (ii) $\bar{n} \geq \bar{n}^*$ where

$$(A.2) \quad \bar{n}^* = \min \left\{ n : \sigma(n, p^\gamma) \leq \left[2 \left(1 + \frac{8}{\alpha} \right)^2 3d \max\{\kappa_\Sigma \kappa_\Gamma, \kappa_\Sigma^3 \kappa_\Gamma^2\} \right]^{-1} \right\}$$

1. First, note that

$$\begin{aligned} \|W_O\|_\infty + \lambda_{\bar{n}} &\leq \sigma(\bar{n}, p^\gamma) + \frac{8}{\alpha} \sigma(\bar{n}, p^\gamma) \\ &= \left(1 + \frac{8}{\alpha} \right) \sigma(\bar{n}, p^\gamma) \\ &\leq \left(1 + \frac{8}{\alpha} \right) \left[2 \left(1 + \frac{8}{\alpha} \right)^2 3d \max\{\kappa_\Sigma \kappa_\Gamma, \kappa_\Sigma^3 \kappa_\Gamma^2\} \right]^{-1} \quad [\text{using (ii)}] \\ &\leq [2\kappa_\Gamma]^{-1} \min\{(3\kappa_\Sigma d)^{-1}, (3\kappa_\Sigma^3 \kappa_\Gamma d)^{-1}\} \underbrace{\left(1 + \frac{8}{\alpha} \right)^{-1}}_{\leq 1} \\ &\leq [2\kappa_\Gamma]^{-1} \min\{(3\kappa_\Sigma d)^{-1}, (3\kappa_\Sigma^3 \kappa_\Gamma d)^{-1}\} \end{aligned}$$

so that B3 implies $\|\Delta\|_\infty \leq 2\kappa_\Gamma (\|W_O\|_\infty + \lambda_{\bar{n}})$. Thus, this implies two useful facts:

- (a) $\|\Delta\|_\infty \leq (3\kappa_\Sigma d)^{-1}$;

$$(b) \|\Delta\|_\infty \leq 2\kappa_\Gamma(1+8/\alpha)\sigma(\bar{n}, p^\gamma).$$

2. Inequality (a) lets B2 of Lemma B.8 hold, so that

$$\begin{aligned} \|R(\Delta)_O\|_\infty &\leq \|R(\Delta)\|_\infty \\ &\leq \frac{3}{2}d\|\Delta\|_\infty^2\kappa_\Sigma^3 \\ &\leq 6\kappa_\Sigma^3\kappa_\Gamma^2d(1+\frac{8}{\alpha})^2[\sigma(\bar{n}, p^\gamma)]^2 \quad [using (b)] \\ &= [6\kappa_\Sigma^3\kappa_\Gamma^2d(1+\frac{8}{\alpha})^2\sigma(\bar{n}, p^\gamma)]\frac{\alpha}{8}\lambda_{\bar{n}} \\ &\leq \left[6\kappa_\Sigma^3\kappa_\Gamma^2d(1+\frac{8}{\alpha})^2\left[2(1+\frac{8}{\alpha})^23d\max\{\kappa_\Sigma\kappa_\Gamma, \kappa_\Sigma^3\kappa_\Gamma^2\}\right]^{-1}\right]\frac{\alpha}{8}\lambda_{\bar{n}} \quad [using (ii)] \\ &\leq \frac{\alpha}{8}\lambda_{\bar{n}} \end{aligned}$$

3. Therefore, $\max\{\|W_O\|_\infty, \|R(\Delta)_O\|_\infty\} \leq \frac{\alpha}{8}\lambda_{\bar{n}}$, so B1 implies $\widehat{\Theta} = \widehat{\Theta}^S$, and consequently $\|\widehat{\Theta} - \widetilde{\Theta}\|_\infty = \|\widehat{\Theta}^S - \widetilde{\Theta}\|_\infty = \|\Delta\|_\infty \leq 2\kappa_\Gamma(1+8/\alpha)\sigma(\bar{n}, p^\gamma)$ (result (b) in step 1). Steps 1-2 hold if $\|W_O\|_\infty \leq \sigma(\bar{n}, p^\gamma)$, which does not happen with probability

$$\begin{aligned} P(\|W_O\|_\infty > \sigma(\bar{n}, p^\gamma)) &= P\left(\bigcup_{(i,j) \in O} \{|W_{ij}| > \sigma(\bar{n}, p^\gamma)\}\right) \\ &\leq \sum_{(i,j) \in O, i \leq j} P(|W_{ij}| > \sigma(\bar{n}, p^\gamma)) \\ &\leq \sum_{(i,j) \in O, i \leq j} P(|W_{ij}| > \sigma(n_{ij}, p^\gamma)) \\ &\leq \sum_{(i,j) \in O, i \leq j} P(|W_{ij}| > \sigma_{ij}(n_{ij}, p^\gamma)) \\ &\leq \frac{|O|+p}{2}p^{-\gamma} \\ &\leq |O|p^{-\gamma} \\ &\leq (p^2 - |O^c|)p^{-\gamma} \\ &= (p^2 - \lceil \eta p^2 \rceil)p^{-\gamma} \\ &\leq (1-\eta)p^{2-\gamma} \end{aligned}$$

where we used A4 (Assumption 4.1).

□

PROOF OF THEOREM 4.2. If $\bar{n} \geq \bar{n}_O^*$, then Theorem 4.1 implies that, with probability larger than $1 - (1-\eta)p^{2-\tau}$,

$$\|\widehat{\Theta} - \widetilde{\Theta}\|_\infty \leq C\sigma(\bar{n}, p^\tau) \leq \nu/2 - \delta,$$

which implies

$$\begin{aligned}
\tilde{\delta} &:= \max_{(i,j) \in O, i \neq j} |\hat{\Theta} - \Theta_{ij}| \\
&\leq \max_{(i,j) \in O, i \neq j} |\hat{\Theta} - \tilde{\Theta}_{ij}| + \max_{(i,j) \in O, i \neq j} |\tilde{\Theta}_{ij} - \Theta_{ij}| \\
&\leq \|\hat{\Theta} - \tilde{\Theta}\|_\infty + \max_{(i,j) \in O, i \neq j} |\tilde{\Theta}_{ij} - \Theta_{ij}| \\
&< \nu/2 - \delta + \delta \\
&< \nu/2
\end{aligned}$$

Since $\tilde{\delta} < \nu/2$, Theorem 3.2 implies $|\hat{\Theta}_{ij}| > \nu/2 \Leftrightarrow \Theta_{ij} \neq 0$ with $\text{sign}(\hat{\Theta}_{ij}) = \text{sign}(\Theta_{ij})$, $\forall (i, j) \in O, i \neq j$. This proves part (i) of the theorem. For part (ii), first note that Lemma B.9 implies that

$$\|\hat{\Theta} - \tilde{\Theta}\|_\infty \leq t \Rightarrow |\hat{\Theta}_{i_k i_k}^{(k)} - \tilde{\Theta}_{i_k i_k}^{(k)}| = \mathcal{O}(\sqrt{dpt})$$

for any $i \in V$ and any $k = 1, \dots, K$. Lemma B.10 further implies

$$|\hat{\Theta}_{ii} - \tilde{\Theta}_{ii}| = |\max_k \hat{\Theta}_{i_k i_k}^{(k)} - \max_k \tilde{\Theta}_{i_k i_k}^{(k)}| \leq \max_{k=1, \dots, K} |\hat{\Theta}_{i_k i_k}^{(k)} - \tilde{\Theta}_{i_k i_k}^{(k)}| = \mathcal{O}(\sqrt{dpt}).$$

Under the assumptions of Theorem 4.1, for $\bar{n} \geq \bar{n}^*$ with probability larger than $1 - (1 - \eta)p^{2-\gamma}$, the inequality above holds with $t = C\sigma(\bar{n}, p^\gamma)$, and so

$$\max_{i \in V} |\hat{\Theta}_{ii} - \tilde{\Theta}_{ii}| \leq D\sqrt{dps}(n, p^\gamma)$$

for some scalar D depending on α and Γ . Thus, if $\bar{n} \geq \bar{n}_{\mathcal{S}}^* \geq \bar{n}^*$ we have, with probability larger than $1 - (1 - \eta)p^{2-\gamma}$,

$$\max_{i \in V} |\hat{\Theta}_{ii} - \tilde{\Theta}_{ii}| \leq \omega/2$$

which, finally, implies

$$\hat{\Theta}_{ii} < \Theta_{ii} - \omega/2 \Leftrightarrow \tilde{\Theta}_{ii} < \Theta_{ii}, \quad \forall i \in V,$$

yielding

$$\widehat{\mathcal{F}}_{-\omega/2} = \mathcal{S} \supseteq E_{O^c}.$$

□

PROOF OF THEOREM 4.3. The part (i) of the theorem is equivalent to part (i) of Theorem 4.2, so we only need to prove part (ii). Lemma B.9 implies

$$\|\widehat{\Theta} - \widetilde{\Theta}\|_\infty \leq t \Rightarrow \|\widehat{\Theta}^{(k)} - \widetilde{\Theta}^{(k)}\|_\infty = \mathcal{O}(\sqrt{dpt})$$

for all $k = 1, \dots, K$. Under the assumptions of Theorem 4.1, for $\bar{n} \geq \bar{n}^*$ with probability larger than $1 - (1 - \eta)p^{2-\gamma}$, the inequality above holds with $t = C\sigma(\bar{n}, p^\gamma)$, and so

$$\max_{i,j,k} |\widehat{\Theta}_{i_k j_k}^{(k)} - \widetilde{\Theta}_{i_k j_k}^{(k)}| \leq D\sqrt{dpt}\sigma(n, p^\gamma)$$

for some scalar D depending on α and Γ . Thus, if $\bar{n} \geq \bar{n}_{\mathcal{U}}^* \geq \bar{n}^*$ we have, with probability larger than $1 - (1 - \eta)p^{2-\gamma}$,

$$\max_{i,j,k} |\widehat{\Theta}_{i_k j_k}^{(k)} - \widetilde{\Theta}_{i_k j_k}^{(k)}| \leq \min\{\psi_1, \psi_2\}$$

which implies

$$\psi_1 < |\widehat{\Theta}_{i_k j_k}^{(k)}| < v - \psi_2 \Leftrightarrow 0 < |\widetilde{\Theta}_{i_k j_k}^{(k)}| < v, \text{ for any } i, j, k,$$

yielding

$$\widehat{\mathcal{U}}_{\psi_1, v-\psi_2} = \mathcal{U}$$

□

APPENDIX B: AUXILIARY RESULTS

LEMMA B.1. *Let U , D , and V be matrices of dimensions $m \times d$, $d \times s$, and $s \times q$, respectively. Let m_0 be the number of nonzero rows of U and q_0 be the number of nonzero columns of V . Let $\text{rd}(M)$ and $\text{cd}(M)$ be maximum row-degree and maximum column-degree of a matrix M , respectively. Then*

$$\begin{aligned} \|UDV\|_0 &\leq \min [m_0 \min\{q_0, \min(s, \text{rd}(U)\text{rd}(D))\text{rd}(V)\}, \\ &\quad q_0 \min\{m_0, \min(d, \text{cd}(V)\text{cd}(D))\text{cd}(U)\}] \\ &\leq \min [m_0 \min\{q_0, \min(s, \text{rd}(U)\|D\|_0)\text{rd}(V)\}, \\ &\quad q_0 \min\{m_0, \min(d, \text{cd}(V)\|D\|_0)\text{cd}(U)\}] \\ &\leq \min [m_0 \min\{q_0, s \text{rd}(V)\}, q_0 \min\{m_0, d \text{cd}(U)\}] \\ &\leq m_0 q_0 \\ &\leq \min\{m, \|U\|_0\} \min\{q, \|V\|_0\} \end{aligned}$$

If D is a $d \times d$ symmetric matrix and $V = U^T$, then

$$\begin{aligned} \|UDU^T\|_0 &\leq m_0 \min\{m_0, \min(d, \text{rd}(U)\text{rd}(D))\text{cd}(U)\} \\ &\leq m_0 \min\{m_0, d \text{cd}(U)\} \\ &\leq m_0^2 \\ &\leq \min\{m, \|U\|_0\}^2 \end{aligned}$$

LEMMA B.2. *Let M be a $p \times p$ positive definite matrix, and let $k = (\|M\|_0 - p)/2$. Then*

$$(B.1) \quad \|M^{-1}\|_0 \leq \min\{p^2, k^2 + k + p\}$$

LEMMA B.3. *Let $M \in R^{d \times q}$, $P \in R^{q \times p}$, and $Q \in R^{p \times r}$. Then*

$$\|MP\|_\infty \leq \min\{\text{rd}(M), \text{cd}(P)\} \|M\|_\infty \|P\|_\infty \leq q \|M\|_\infty \|P\|_\infty$$

and

$$\begin{aligned} \|MPQ\|_\infty &\leq \min\{\text{rd}(M), \text{cd}(P)\} \text{cd}(Q) \|M\|_\infty \|P\|_\infty \|Q\|_\infty \\ &\leq qp \|M\|_\infty \|P\|_\infty \|Q\|_\infty \end{aligned}$$

If $p = q$ and M and Q are diagonal matrices, then

$$\|MPQ\|_\infty \leq \|M\|_\infty \|P\|_\infty \|Q\|_\infty$$

If S is positive definite diagonalizable as $S = V\Lambda V^T$, then

$$(B.2) \quad \|S^{-1}\|_\infty \leq \lambda_{\min}^{-1} \text{rd}(V) \|V\|_\infty^2 \leq \lambda_{\min}^{-1} q \|V\|_\infty^2$$

LEMMA B.4 (MAD_{GQ} continuity). *Let $\mathcal{D}_{M_O} = \{M_{O^c} : M \succ 0\}$ be the set of portions M_{O^c} that complete M_O into a positive definite matrix M , and let $\mathcal{F}_p = \{M_O : \mathcal{D}_{M_O} \neq \emptyset\}$ be the set of positive completable partial matrices. Let $\tilde{\Theta}$ be the MAD_{GQ} solution in Equation (2.6). Then*

1. $\tilde{\Theta}$ is a continuous function of $\Sigma_O \in \mathcal{F}_p$.
2. For fixed Θ_O , $\tilde{\Theta}$ is a continuous function of $\Theta_{O^c} \in \mathcal{D}_{\Theta_O}$.

LEMMA B.5 (MAD_{GQ} as a function of Θ). *Assume Equation (3.7). The MAD_{GQ} solution $\tilde{\Theta}$ in Equation (2.6) has components $\tilde{\Theta}_{AC} = 0$, and*

$$\tilde{\Theta}_{AA} = \Theta_{AA} - \Theta_{AC} \Theta_{CC}^{-1} \Theta_{CA}, \quad \tilde{\Theta}_{AB} = \Theta_{AB} - \Theta_{AC} \Theta_{CC}^{-1} \Theta_{CB},$$

$$\begin{aligned}\tilde{\Theta}_{BC} &= \Theta_{BC} - \Theta_{BA}\Theta_{AA}^{-1}\Theta_{AC}, & \tilde{\Theta}_{CC} &= \Theta_{CC} - \Theta_{CA}\Theta_{AA}^{-1}\Theta_{AC}, \\ \tilde{\Theta}_{BB} &= \Theta_{BB} - \Theta_{BC}\Theta_{CC}^{-1}\Theta_{CB} + \tilde{\Theta}_{BC}\tilde{\Theta}_{CC}^{-1}\tilde{\Theta}_{CB} \\ &= \Theta_{BB} - \Theta_{BA}\Theta_{AA}^{-1}\Theta_{AB} + \tilde{\Theta}_{BA}\tilde{\Theta}_{AA}^{-1}\tilde{\Theta}_{AB}\end{aligned}$$

Clearly, if $\Theta_{AC} = 0$, we obtain $\tilde{\Theta} \equiv \Theta$. The distortion $\tilde{\Theta}_{BB} - \Theta_{BB}$ is due to B being forced to be a separator of A and C . Note that $\tilde{\Theta}_{ii} \leq \Theta_{ii}, \forall i \in A \cup C$.

LEMMA B.6. Let m_{EF} be the number of nonzero rows in Θ_{EF} , $\text{rd}_{EF} = \text{rd}(\Theta_{EF})$, and $\tilde{\text{rd}}_{EE} = \text{rd}(\tilde{\Theta}_{EE}^{-1})$, where $\text{rd}(\cdot)$ is defined in Lemma B.1. Moreover, let $\kappa = \|\Theta_{AC}\|_0$ and $\gamma = \|\Theta_{AC}\|_\infty$. Under the conditions of Lemma B.5 we have

1. The ℓ_0 distortion between Θ and $\tilde{\Theta}$ has components

$$\begin{aligned}\|\Theta_{AC} - \tilde{\Theta}_{AC}\|_0 &= \kappa \\ \|\Theta_{AA} - \tilde{\Theta}_{AA}\|_0 &\leq m_{AC} \min\{m_{AC}, \min\{|C|, \text{rd}_{AC}\tilde{\text{rd}}_{CC}\}\text{rd}_{CA}\} \\ \|\Theta_{BB} - \tilde{\Theta}_{BB}\|_0 &\leq \min\{m_{BC} \min\{m_{BC}, \min\{|C|, \text{rd}_{BC}\tilde{\text{rd}}_{CC}\}\text{rd}_{CB}\} \\ &\quad + m_{\overline{BC}} \min\{m_{\overline{BC}}, \min\{|C|, \text{rd}_{\overline{BC}}\tilde{\text{rd}}_{\overline{CC}}\}\text{rd}_{\overline{CB}}\}, \\ &\quad m_{BA} \min\{m_{BA}, \min\{|A|, \text{rd}_{BA}\tilde{\text{rd}}_{AA}\}\text{rd}_{AB}\} \\ &\quad + m_{\overline{BA}} \min\{m_{\overline{BA}}, \min\{|A|, \text{rd}_{\overline{BA}}\tilde{\text{rd}}_{\overline{AA}}\}\text{rd}_{\overline{AB}}\}\} \\ \|\Theta_{CC} - \tilde{\Theta}_{CC}\|_0 &\leq m_{CA} \min\{m_{CA}, \min\{|A|, \text{rd}_{CA}\tilde{\text{rd}}_{AA}\}\text{rd}_{AC}\} \\ \|\Theta_{AB} - \tilde{\Theta}_{AB}\|_0 &\leq \min\{m_{AC} \min\{m_{BC}, \min\{|C|, \text{rd}_{AC}\tilde{\text{rd}}_{CC}\}\text{rd}_{CB}\}, \\ &\quad m_{BC} \min\{m_{AC}, \min\{|C|, \text{rd}_{BC}\tilde{\text{rd}}_{CC}\}\text{rd}_{CA}\}\} \\ \|\Theta_{BC} - \tilde{\Theta}_{BC}\|_0 &\leq \min\{m_{BA} \min\{m_{AC}, \min\{|A|, \text{rd}_{BA}\tilde{\text{rd}}_{AA}\}\text{rd}_{AC}\}, \\ &\quad m_{AC} \min\{m_{BC}, \min\{|C|, \text{rd}_{CA}\tilde{\text{rd}}_{AA}\}\text{rd}_{AB}\}\}\end{aligned}$$

2. The ℓ_∞ distortion between Θ and $\tilde{\Theta}$ has components

$$\begin{aligned}\|\Theta_{AC} - \tilde{\Theta}_{AC}\|_\infty &= \gamma \\ \|\Theta_{AA} - \tilde{\Theta}_{AA}\|_\infty &\leq \min\{\text{rd}_{AC}, \tilde{\text{rd}}_{CC}\}\text{rd}_{AC}\tilde{\gamma}_{CC}\gamma^2 \\ \|\Theta_{BB} - \tilde{\Theta}_{BB}\|_\infty &\leq I(\gamma > 0) \min\{\min\{\text{rd}_{BC}, \tilde{\text{rd}}_{CC}\}\text{rd}_{BC}\gamma_{BC}^2\tilde{\gamma}_{CC} \\ &\quad + \min\{|B|, |C|\}|B|(\gamma_{BC} + \min\{\text{rd}_{BA}, \tilde{\text{rd}}_{AA}\}\text{rd}_{CA}\gamma_{AB}\tilde{\gamma}_{AA}\gamma)^2\eta_1, \\ &\quad \min\{\text{rd}_{BA}, \tilde{\text{rd}}_{AA}\}\text{rd}_{BA}\gamma_{BA}^2\tilde{\gamma}_{AA} \\ &\quad + \min\{|A|, |B|\}|B|(\gamma_{BA} + \min\{\text{rd}_{BC}, \tilde{\text{rd}}_{CC}\}\text{rd}_{AC}\gamma_{CB}\tilde{\gamma}_{CC}\gamma)^2\eta_2\} \\ \|\Theta_{CC} - \tilde{\Theta}_{CC}\|_\infty &\leq \min\{\text{rd}_{CA}, \tilde{\text{rd}}_{AA}\}\text{rd}_{CA}\tilde{\gamma}_{AA}\gamma^2 \\ \|\Theta_{AB} - \tilde{\Theta}_{AB}\|_\infty &\leq \min\{\text{rd}_{AC}, \tilde{\text{rd}}_{CC}\}\text{rd}_{BC}\tilde{\gamma}_{CC}\gamma_{BC}\gamma \\ \|\Theta_{BC} - \tilde{\Theta}_{BC}\|_\infty &\leq \min\{\text{rd}_{BA}, \tilde{\text{rd}}_{AA}\}\text{rd}_{CA}\tilde{\gamma}_{AA}\gamma_{AB}\gamma\end{aligned}$$

where

$$\begin{aligned}\eta_1 &= \sup_{\Theta_{AC}, \text{ s.t. } \Theta > 0} \|(\Theta_{CC} - \Theta_{CA}\Theta_{AA}^{-1}\Theta_{AC})^{-1}\|_\infty < \infty \\ \eta_2 &= \sup_{\Theta_{AC}, \text{ s.t. } \Theta > 0} \|(\Theta_{AA} - \Theta_{AC}\Theta_{CC}^{-1}\Theta_{CA})^{-1}\|_\infty < \infty\end{aligned}$$

LEMMA B.7. *Assume Equation (3.7) holds. Then,*

- (a). *For $i \in A$, $\tilde{\Theta}_{ii} < \Theta_{ii} \Leftrightarrow \Theta_{iC} \neq 0$, and for $j \in C$, $\tilde{\Theta}_{jj} < \Theta_{jj} \Leftrightarrow \Theta_{jA} \neq 0$, that is if a distortion is found on a diagonal entry $\tilde{\Theta}_{ss}$ with $s \in A$ or $s \in C$, then there must be a nonzero entry in the corresponding row or column, respectively, of Θ_{AC} .*
- (b). *For $(i, j) \in A \times (A \cup B)$, $\tilde{\Theta}_{ij} \neq \Theta_{ij} \Rightarrow \tilde{\Theta}_{ii} < \Theta_{ii}$, and for $(i, j) \in (B \cup C) \times C$, $\tilde{\Theta}_{ij} \neq \Theta_{ij} \Rightarrow \tilde{\Theta}_{jj} < \Theta_{jj}$. Hence, distortions in the off-diagonals of $\tilde{\Theta}_O$ imply distortions on the corresponding diagonals entries, which in turn let us identify nonzero rows or columns in Θ_{AC} as described above.*

LEMMA B.8. *Under assumptions A1-A5:*

- B1. *If $\max\{\|W_O\|_\infty, \|R(\Delta)_O\|_\infty\} \leq \frac{\alpha}{8}\lambda$, then $\hat{\Theta} = \hat{\Theta}^S$.*
- B2. *If $\|\Delta\|_\infty \leq (3\kappa_\Sigma d)^{-1}$, then $\|R(\Delta)_O\|_\infty \leq \|R(\Delta)\|_\infty \leq \frac{3}{2}d\|\Delta\|_\infty^2\kappa_\Sigma^3$.*
- B3. *If $r := 2\kappa_\Gamma(\|W_O\|_\infty + \lambda) \leq \min\{(3\kappa_\Sigma d)^{-1}, (3\kappa_\Sigma^3\kappa_\Gamma d)^{-1}\}$, then $\|\Delta\|_\infty \leq r$.*

LEMMA B.9. *Let $X, Y \in \mathbb{R}^{p \times p}$ be positive definite matrices with row-degree smaller than d . Then, for any set $A \subset \{1, \dots, p\}$,*

$$(B.3) \quad \|X/X_{AA} - Y/Y_{AA}\|_\infty \leq C\sqrt{dp}\|X - Y\|_\infty$$

LEMMA B.10. *Let $(x_1, y_1), \dots, (x_K, y_K) \in \mathbb{R}^2$. Then*

$$(B.4) \quad \left| \max_{k=1, \dots, K} x_k - \max_{j=1, \dots, K} y_j \right| \leq \max_{k=1, \dots, K} |x_k - y_k|$$

LEMMA B.11 (Exact graph recovery in O^c in a special case). *If Θ_{CC} is diagonal, then there is an edge connecting $(i, j) \in AC$ if $\exists k \in B$ s.t. $\Theta_{jk} \neq 0$, $\Theta_{-j,k} = 0$ and $\tilde{\Theta}_{ik} \neq \Theta_{ik}$. Similarly, if Θ_{AA} is diagonal, then there is an edge $(i, j) \in AC$ if $\exists k \in B$ s.t. $\Theta_{ik} \neq 0$, $\Theta_{-i,k} = 0$ and $\tilde{\Theta}_{jk} \neq \Theta_{jk}$.*

PROPOSITION B.1 (Reduction to $K = 2$). *Let $\bar{U}_1 = \{i \in V : \exists j > i : (i, j) \in O^c\}$ and $\bar{U}_2 = \{j \in V : \exists i < j : (i, j) \in O^c\}$. If $\bar{U}_1 \cap \bar{U}_2 = \emptyset$, then a $K > 2$ case may be*

transformed into a $K = 2$ case by using Σ_{O_2} instead of Σ_O , where $O_2^\varepsilon = \bar{U}_1 \times \bar{U}_2 \supseteq O^\varepsilon$. The superset given by Equation (3.33) with $A = \bar{U}_1$ and $C = \bar{U}_2$ contains \mathcal{S} in Equation (3.21).

APPENDIX C: PROOFS OF AUXILIARY RESULTS

PROOF OF LEMMA B.1. First of all, $\text{rd}(UD) \leq \min\{s, \text{rd}(U)\text{rd}(D)\}$, and similarly $\text{rd}(UDV) \leq \min\{q_0, \min\{s, \text{rd}(U)\text{rd}(D)\}\text{rd}(V)\}$. Thus, we obtain

$$\|UDV\|_0 \leq m_0 \min\{q_0, \min(s, \text{rd}(U)\text{rd}(D))\text{rd}(V)\}.$$

On the other hand, we further have $\|UDV\|_0 \leq q_0 \text{cd}(UDV) = q_0 \text{rd}(V^T D^T U^T)$, where $\text{rd}(M^T) \equiv \text{cd}(M)$. This proves the first inequality; the other ones are trivial. To prove the last of each group of inequalities, we can alternatively see the following. The matrix UD is zero on the same rows where U is zero. Similarly, $V^T(D^T U^T)$ is zero on the same rows where V^T is zero. Hence, UDV is zero on the rows where U is zero and columns where V is zero. \square

PROOF OF LEMMA B.2. The maximum number of either directly or indirectly connected pairs of nodes through k edges can be attained in a chain graph connecting $m = \min\{p, k + 1\}$ nodes; we give a proof of this at the end. If M is a precision matrix with k non-zero upper-diagonal entries, then the pairwise covariances in M^{-1} of these m connected nodes are all potentially non-zero, while covariances with disconnected nodes are zero. Thus, the number of non-zero entries in M^{-1} can be as large as m^2 plus the number of diagonals relative to the $p - m$ disconnected nodes.

Suppose a graph \mathcal{G}_1 is made of q disconnected chain subgraphs $\{\mathcal{C}_i\}$, and $e_i \geq 2$ is the number of nodes in \mathcal{C}_i . The number of nonzero covariances under $\{\mathcal{C}_i\}$ is $\sum_{i=1}^q e_i^2$. Let \mathcal{G}_2 be a graph obtained by rearranging the edges in \mathcal{G}_1 , and is made of a unique chain graph \mathcal{C} , which contains at least $\sum_{i=1}^q e_i - (q - 1)$ nodes, and $(q - 1)$

disconnected nodes. The number of nonzero covariances under \mathcal{G}_2 is at least

$$\begin{aligned}
\left(\sum_{i=1}^q e_i - (q-1)\right)^2 + (q-1) &= \left(\sum_{i=1}^q e_i\right)^2 + (q-1)^2 - 2(q-1)\sum_{i=1}^q e_i + (q-1) \\
&= \sum_{i=1}^q e_i^2 + \sum_{i=1}^q e_i \sum_{j \neq i} e_j + q^2 - q - 2(q-1)\sum_{i=1}^q e_i \\
&\geq \sum_{i=1}^q e_i^2 + q^2 - q \\
&\geq \sum_{i=1}^q e_i^2
\end{aligned}$$

where the first inequality holds because $\sum_{j \in \{1, \dots, q\} \setminus \{i\}} e_j \geq 2(q-1)$, for any fixed i . \square

PROOF OF LEMMA B.3. Each entry of MP is the inner product of two vectors of length q where one has at most $\text{rd}(M) \leq q$ non-zero entries of maximum magnitude $\|M\|_\infty$, and the other one has at most $\text{cd}(P) \leq q$ non-zero entries of maximum magnitude $\|P\|_\infty$. \square

PROOF OF LEMMA B.4. The objective function in Equation (2.6)

$$f(\Theta_O, \Sigma_O) = \log \det \Theta - \sum_{(i,j) \in O} \Theta_{ij} \Sigma_{ij},$$

for $\Theta_{O^c} = 0$, is a continuous real-valued function of $(\Theta_O, \Sigma_O) \in \mathcal{F}_p \times \mathcal{F}_p$. Equation (2.6) can be rewritten as

$$(C.1) \quad \tilde{\Theta} := F(\Sigma_O) = \operatorname{argmax}_{\Theta \in \mathcal{A}(\Sigma_O)} f(\Theta_O, \Sigma_O),$$

where $\mathcal{A}(\Sigma_O)$ is a continuous compact-valued correspondence. By Berge's Maximum Theorem, $F(\Sigma_O)$ is an upper hemicontinuous correspondence with nonempty and compact values. On the other hand, since Σ_O is completable to a positive definite matrix, the max determinant problem has a unique solution, i.e. $F(\Sigma_O)$ is single-valued. Therefore, $\tilde{\Theta}$ is a continuous function of Σ_O . Thus, the first statement is proved. For the second statement, note that $\Sigma = G(\Theta) := \Theta^{-1}$, where $G: \mathcal{S}^{++} \rightarrow \mathcal{S}^{++}$ is a continuous function, and \mathcal{S}^{++} is the cone of $p \times p$ positive definite matrices. For a fixed positive completable Θ_O , we have that $\Sigma = G_{\Theta_O}(\Theta_{O^c})$ and thereby $\Sigma_O = [G_{\Theta_O}(\Theta_{O^c})]_O$ are continuous functions of $\Theta_{O^c} \in \mathcal{D}_{\Theta_O}$. For a fixed Θ_O , the chain of mappings $\Theta_{O^c} \mapsto \Sigma_O \mapsto \tilde{\Theta}$ defines the composite function $\tilde{\Theta} = H(\Theta_{O^c}) = F([G_{\Theta_O}(\Theta_{O^c})]_O)$ where $F(\Sigma_O)$ is given in Equation (C.1). Since $\mathcal{A}([G_{\Theta_O}(\Theta_{O^c})]_O)$ is

a continuous compact-valued correspondence of Θ_{O^c} , Berge's Maximum Theorem applies and therefore $\tilde{\Theta}$ is a continuous function of $\Theta_{O^c} \in \mathcal{D}_{\Theta_0}$. \square

PROOF OF LEMMA B.5. Let

$$\begin{aligned} \Sigma_1 &= \begin{bmatrix} \Sigma_{AA} & \Sigma_{AB} \\ \Sigma_{BA} & \Sigma_{BB} \end{bmatrix}, & \Sigma_2 &= \begin{bmatrix} \Sigma_{BB} & \Sigma_{BC} \\ \Sigma_{CB} & \Sigma_{CC} \end{bmatrix} \\ \Theta_1 &= \begin{bmatrix} \Theta_{AA} & \Theta_{AB} \\ \Theta_{BA} & \Theta_{BB} \end{bmatrix}, & \Theta_2 &= \begin{bmatrix} \Theta_{BB} & \Theta_{BC} \\ \Theta_{CB} & \Theta_{CC} \end{bmatrix}, \\ \Theta_{1,C} &= \begin{bmatrix} \Theta_{AC} \\ \Theta_{BC} \end{bmatrix}, & \Theta_{2,A} &= \begin{bmatrix} \Theta_{BA} \\ \Theta_{CA} \end{bmatrix}, \end{aligned}$$

and $\Theta_{C,1} = \Theta_{1,C}^T$ and $\Theta_{A,2} = \Theta_{2,A}^T$. The Schur complement gives

$$\begin{aligned} \Sigma_1^{-1} &= \Theta_1 - \Theta_{1,C} \Theta_{CC}^{-1} \Theta_{C,1} \\ (C.2) \quad &= \begin{bmatrix} \Theta_{AA} - \Theta_{AC} \Theta_{CC}^{-1} \Theta_{CA}, & \Theta_{AB} - \Theta_{AC} \Theta_{CC}^{-1} \Theta_{CB} \\ \Theta_{BA} - \Theta_{BC} \Theta_{CC}^{-1} \Theta_{CA}, & \Theta_{BB} - \Theta_{BC} \Theta_{CC}^{-1} \Theta_{CB} \end{bmatrix} \end{aligned}$$

and

$$\begin{aligned} \Sigma_2^{-1} &= \Theta_2 - \Theta_{2,A} \Theta_{AA}^{-1} \Theta_{A,2} \\ (C.3) \quad &= \begin{bmatrix} \Theta_{BB} - \Theta_{BA} \Theta_{AA}^{-1} \Theta_{AB}, & \Theta_{BC} - \Theta_{BA} \Theta_{AA}^{-1} \Theta_{AC} \\ \Theta_{CB} - \Theta_{CA} \Theta_{AA}^{-1} \Theta_{AB}, & \Theta_{CC} - \Theta_{CA} \Theta_{AA}^{-1} \Theta_{AC} \end{bmatrix}. \end{aligned}$$

If $\Theta_{AC} = 0$ then

$$(C.4) \quad \Sigma_1^{-1} = \begin{bmatrix} \Theta_{AA}, & \Theta_{AB} \\ \Theta_{BA}, & \Theta_{BB} - \Theta_{BC} \Theta_{CC}^{-1} \Theta_{CB} \end{bmatrix}$$

$$(C.5) \quad \Sigma_2^{-1} = \begin{bmatrix} \Theta_{BB} - \Theta_{BA} \Theta_{AA}^{-1} \Theta_{AB}, & \Theta_{BC} \\ \Theta_{CB}, & \Theta_{CC} \end{bmatrix}$$

and solving (C.4) and (C.5) for each block of Θ gives

$$(C.6) \quad \tilde{\Theta} = \tilde{\Sigma}^{-1} = \begin{bmatrix} [\Sigma_1^{-1}]_{AA} & [\Sigma_1^{-1}]_{AB} & 0 \\ [\Sigma_1^{-1}]_{BA} & \tilde{\Theta}_{BB} & [\Sigma_2^{-1}]_{BC} \\ 0 & [\Sigma_2^{-1}]_{CB} & [\Sigma_2^{-1}]_{CC} \end{bmatrix}$$

where

$$(C.7) \quad \tilde{\Theta}_{BB} = [\Sigma_1^{-1}]_{BB} + [\Sigma_2^{-1}]_{BC} [\Sigma_2^{-1}]_{CC}^{-1} [\Sigma_2^{-1}]_{CB}$$

$$(C.8) \quad = [\Sigma_2^{-1}]_{BB} + [\Sigma_1^{-1}]_{BA} [\Sigma_1^{-1}]_{AA}^{-1} [\Sigma_1^{-1}]_{AB}$$

Rewriting (C.6) in terms of Θ components using expressions in (C.2) and (C.3) completes the proof. \square

PROOF OF LEMMA B.6. The upper bounds given in this lemma are obtained by applying Lemma B.1. It is worth giving details about bounding $\|\Theta_{BB} - \tilde{\Theta}_{BB}\|_\infty \leq \|\Theta_{BC}\Theta_{CC}^{-1}\Theta_{CB}\|_\infty + \|\tilde{\Theta}_{BC}\tilde{\Theta}_{CC}^{-1}\tilde{\Theta}_{CB}\|_\infty$ where

$$\begin{aligned} \|\tilde{\Theta}_{BC}\tilde{\Theta}_{CC}^{-1}\tilde{\Theta}_{CB}\|_\infty &\leq \min\{\text{rd}_{\tilde{BC}}, \tilde{\text{rd}}_{\tilde{CC}}\} \text{rd}_{\tilde{BC}} \gamma_{\tilde{BC}}^2 \tilde{\gamma}_{\tilde{CC}} \\ &\leq \min\{|B|, |C|\} |B| (\gamma_{BC} + \|\Theta_{BA}\Theta_{AA}^{-1}\Theta_{AC}\|_\infty)^2 \eta_1 \\ &\leq \min\{|B|, |C|\} |B| (\gamma_{BC} + \min\{\text{rd}_{BA}, \tilde{\text{rd}}_{AA}\} \text{rd}_{CA} \gamma_{AB} \tilde{\gamma}_{AA} \gamma_{AC})^2 \eta_1 \end{aligned}$$

Similar steps can be done to bound

$$\|\Theta_{BB} - \tilde{\Theta}_{BB}\|_\infty \leq \|\Theta_{BA}\Theta_{AA}^{-1}\Theta_{AB}\|_\infty + \|\tilde{\Theta}_{BA}\tilde{\Theta}_{AA}^{-1}\tilde{\Theta}_{AB}\|_\infty.$$

\square

PROOF OF LEMMA B.7. Lemma B.5 implies

$$(C.9) \quad \Theta_{A(A \cup B)} - \tilde{\Theta}_{A(A \cup B)} = [\Theta_{AC}\Theta_{CC}^{-1}\Theta_{CA}, \Theta_{AC}\Theta_{CC}^{-1}\Theta_{CB}]$$

and

$$(C.10) \quad \Theta_{(B \cup C)C} - \tilde{\Theta}_{(B \cup C)C} = [\Theta_{CA}\Theta_{AA}^{-1}\Theta_{AB}, \Theta_{CA}\Theta_{AA}^{-1}\Theta_{AC}]^T.$$

Since Θ_{CC} is positive definite, given a vector w , we have $w^T \Theta_{CC}^{-1} w > 0$ if and only if $w \neq 0$, where $w \neq 0$ means that at least one entry of w is nonzero. Thus, for $i \in A$, $\Theta_{ii} > \tilde{\Theta}_{ii}$ if and only if $\Theta_{iC}\Theta_{CC}^{-1}\Theta_{Ci} > 0 \Leftrightarrow \Theta_{iC} \neq 0$. Similarly, Θ_{AA} is positive definite so that, for $j \in C$, $\Theta_{jj} > \tilde{\Theta}_{jj}$ if and only if $\Theta_{Aj} \neq 0$. Moreover, for $(i, j) \in A \times (A \cup B)$ and $i \neq j$, we have that $\Theta_{ij} \neq \tilde{\Theta}_{ij}$ only if $\Theta_{iC}\Theta_{CC}^{-1}\Theta_{Cj} \neq 0$, requiring $\Theta_{iC} \neq 0$; it is not a sufficient condition because $\Theta_{iC}\Theta_{CC}^{-1}\Theta_{Cj} = 0$ if $\Theta_{Cj} = 0$. Similarly, for $(i, j) \in (B \cup C) \times C$ and $i \neq j$, we have that $\Theta_{ij} \neq \tilde{\Theta}_{ij}$ only if $\Theta_{iA}\Theta_{AA}^{-1}\Theta_{Aj} \neq 0$, requiring $\Theta_{Aj} \neq 0$. \square

PROOF OF LEMMA B.8. B1 is proved in the same way as Lemma 4 of Ravikumar et al. (2011) where we only need to replace W_A or $R(\Delta)_A$ by $W_{A \cap O}$ and $R_{A \cap O}$,

for any set of entries A . B2 follows from Lemma 5 of Ravikumar et al. (2011) who proved $\|R(\Delta)\|_\infty \leq \frac{3}{2}d\|\Delta\|_\infty^2\kappa_{\Sigma^*}^3$. B3 can be proved by modifying the last part of the proof of Lemma 6 of Ravikumar et al. (2011) as follows: upperbounds to the quantities $\|T_1\|_\infty$ and $\|T_2\|_\infty$ can be established by replacing $\|W\|_\infty$ by $\|W_O\|_\infty$, and $\|R(\Delta)\|_\infty$ by $\|R(\Delta)_O\|_\infty$. \square

PROOF OF LEMMA B.9.

We will prove the equivalent statement: for any $p \times p$ positive definite matrices Σ and Ψ , and any set $A \subset \{1, \dots, p\}$

$$\|\Sigma_{AA}^{-1} - \Psi_{AA}^{-1}\|_\infty \leq C\sqrt{dp}\|\Sigma^{-1} - \Psi^{-1}\|_\infty$$

Notice that the following chain of (in)equalities are true

$$\begin{aligned} \|\Sigma_{AA}^{-1} - \Psi_{AA}^{-1}\|_\infty &\leq \|\Sigma_{AA}^{-1} - \Psi_{AA}^{-1}\|_2 \\ &= \|\Sigma_{AA}^{-1}(\Sigma_{AA} - \Psi_{AA})\Psi_{AA}^{-1}\|_2 \\ &\leq \|\Sigma_{AA}^{-1}\|_2 \|\Sigma_{AA} - \Psi_{AA}\|_2 \|\Psi_{AA}^{-1}\|_2 \\ &\leq \|\Sigma_{AA}^{-1}\|_2 \|\Sigma - \Psi\|_2 \|\Psi_{AA}^{-1}\|_2 \\ &\leq \|\Sigma_{AA}^{-1}\|_2 \|\Sigma\|_2 \|\Sigma^{-1} - \Psi^{-1}\|_2 \|\Psi\|_2 \|\Psi_{AA}^{-1}\|_2 \\ &\leq C\sqrt{dp} \|\Sigma^{-1} - \Psi^{-1}\|_\infty, \end{aligned}$$

where the third inequality comes from sub-multiplicativity of the matrix ℓ_2 -norm. The second and the penultimate step follows from observing that for any two square matrices X and Y , we can write $X^{-1} - Y^{-1} = Y^{-1}(Y - X)X^{-1}$. The fourth from the fact that the ℓ_2 -norm of a submatrix is smaller than the ℓ_2 -norm of the full matrix. In the last step, we use the standard relationship between the ℓ_2 -norm and the max-norm for a matrix with $\mathcal{O}(dp)$ non-zeros, and the constant C only depends on the condition numbers of the matrices in question. \square

PROOF OF LEMMA B.10. Suppose $\max_k x_k \leq \max_k y_k$, and let $k_y^* = \arg \max_k y_k$. Then

$$x_{k_y^*} \leq \max_k x_k \leq \max_k y_k = y_{k_y^*},$$

which implies

$$|\max_k x_k - \max_k y_k| \leq |y_{k_y^*} - x_{k_y^*}| \leq \max_{k=1, \dots, K} |x_k - y_k|.$$

Same inequality can be obtained for the case $\max_k x_k \geq \max_k y_k$. \square

PROOF OF PROPOSITION B.1. The proposition identifies conditions where the shape of O^c allows for a reduction of O into a $K = 2$ case. As the size of O^c increases, the number of true edges falling in O^c is nondecreasing, inducing a non-decreasing variation in the set of diagonal distortions in the portions $\tilde{\Theta}_{V_k V_k}$'s, and therefore a larger superset of edges in O_2^c , which includes the superset of edges in O^c . \square

RICE UNIVERSITY
DEPARTMENT OF STATISTICS
DUNCAN HALL
6100 MAIN ST
HOUSTON, 77005, TX, USA
E-MAIL: gv9@rice.edu

ARIZONA STATE UNIVERSITY
DEPARTMENT OF ELECTRICAL AND COMPUTER ENGINEERING
650 E. TYLER MALL
TEMPE 85281, USA
E-MAIL: gautamd@asu.edu

RICE UNIVERSITY
DEPARTMENT OF ELECTRICAL AND COMPUTER ENGINEERING
DUNCAN HALL
6100 MAIN ST
HOUSTON, 77005, TX, USA
E-MAIL: gallen@rice.edu